Universidade do Minho
Escola de Engenharia

Carolina Maria Clasen Soares de Sousa

Development of a Heat Exchanger for Exhaust Gas Energy Exploitation

dezembro de 2021

Development of a Heat Exchanger for Exhaust Gas Energy Exploitation

Carolina Sousa

UMinho | 2021

Universidade do Minho
Escola de Engenharia

Carolina Maria Clasen Soares de Sousa

Development of a Heat Exchanger for Exhaust Gas Energy Exploitation

Dissertação de Mestrado

Ciclo de Estudos Integrados Conducentes ao Grau de Mestre em Engenharia Mecânica

Trabalho efetuado sob a orientação do

Professor Francisco Carrusca Pimenta de Brito e do

Professor Jorge José Gomes Martins

dezembro de 2021

DECLARAÇÃO

Nome: Carolina Maria Clasen Soares de Sousa

Título da dissertação: Development of a Heat Exchanger for Exhaust Gas Energy Exploitation

Orientadores:

Professor Doutor Francisco Carrusca Pimenta de Brito

Professor Doutor Jorge José Gomes Martins

Ano de conclusão: 2021

Mestrado Integrado em Engenharia Mecânica

Universidade do Minho, _____/_____/_____

Assinatura:

Aos meus pais.

Acknowledgements

Agradeço aos Professores Doutores Francisco Carrusca Pimenta de Brito e Jorge José Gomes Martins, do Departamento de Engenharias Mecânica da Escola de Engenharia da Universidade do Minho, pelo conhecimento proporcionado, pelas enriquecedoras sugestões e pela sábia orientação. Agradeço o apoio, a disponibilidade, o acompanhamento incessante, a preocupação e a paciência demonstrados ao longo do trabalho.

Ao grupo LaMoTa pelo suporte técnico oferecido. À BorgWarner Emission Systems, Centro Técnico de Vigo, pelo fornecimento das wavy fins e suporte técnico para pesquisa em geradores termoelétricos de escape no LaMoTA. À AVL List GmbH, pelo o acesso à licença do AVL Suite através do AVL University Partnership Program (Platinum Partnership). AVL Cruise e AVL Boost foram utilizados nesta dissertação. Ao Projeto FCT PTDC/EME-TED/7801/2020 – COOLSPOT - Interfacial Cooling Strategies for high Power dissipation conversion Technologies. Esta dissertação foi elaborada com o apoio deste projeto, que visa desenvolver câmaras de vapor texturizadas a laser para serem utilizadas em conceitos como o avaliado na presente dissertação.

Aos meus pais, pelo encorajamento e incentivo, pelos conselhos e sacrifícios, pelo amparo e pelo amor. Sempre lutaram por mim para que hoje e ao longo da minha vida conseguisse alcançar tudo que tenho. São as pessoas que mais admiro e que mais admirarei.

Um obrigado especial ao Sérgio por ser o meu confidente, melhor amigo e pelo apoio e amor incondicional. Sem ele, não teria o mesmo ânimo para a superação desta importante etapa da minha vida.

Por fim quero agradecer aos meus amigos, muito obrigada por todo o companheirismo, amizade e pelas histórias vividas ao longo destes anos que ficarão memoráveis para toda a vida.

STATEMENT OF INTEGRITY

I hereby declare having conducted this academic work with integrity. I confirm that I have not used plagiarism or any form of undue use of information or falsification of results along the process leading to its elaboration.

I further declare that I have fully acknowledged the Code of Ethical Conduct of the Universidade do Minho.

_____, _____

(Location) (Date)

_____

(Carolina Maria Clasen Soares de Sousa)

Abstract

Development of a Heat Exchanger for Exhaust Gas Energy Exploitation

The road transport industry faces the need to develop its fleet for lower energy consumption, pollutants and CO_2 emissions. Waste heat recovery systems with Thermoelectric generators (TEGs) can directly convert the exhaust heat into electric energy, aiding the electrical needs of the vehicle, thus reducing its dependency on fuel energy. The present work assesses the optimization and evaluation of a LaMoTa Uminho temperature-controlled thermoelectric generator (TCTG) concept to be used in a commercial heavy-duty vehicle (HDV). The system consists of a heat exchanger (HE) with wavy fins (WFs) plates in an aluminium matrix along with vapour chambers (VC), machined directly into the matrix, that grant the thermal control. Above are the TEGs and cooling plates (CPs) for heat dissipation.

The TCTG concept behaviour was analysed under realistic driving conditions. With a 1D model (Matlab algorithm) of the system was possible to predict its thermal and thermoelectric performance along with the given driving cycles. An HDV with a 16 L Diesel engine was simulated in AVL software. Data regarding the exhaust gas temperature and mass flow were obtained for each point of two cycle runs, which were implemented in the 1D model. Additionally, a 2D heat transfers simulation in COMSOL provided the thermal resistances of the system which were added to the algorithm.

The developed system proved to have a good capacity for applications with volatile thermal loads since it was able to avoid the overheating of the TEGs by spreading the heat to areas with lower available thermal loads. It was predicted a maximum average electrical production of 2.4 kW, which resulted in fuel savings of about 2% and CO_2 emissions reduction of around 37 g/km.

Keywords: Heavy-duty vehicles, Thermal control, Thermoeletric generators, Vapour chambers, Waste heat recovery systems

Resumo

Desenvolvimento de um Permutador de Calor para o Aproveitamento da Energia dos Gases de Escape

A indústria de transportes rodoviários tem o dever de desenvolver a sua frota para diminuir o consumo de energia, poluentes e emissões de CO_2. Geradores termoeléctricos (TEGs) convertem diretamente o calor dos gases de escape em energia eléctrica, o que auxilia as necessidades eléctricas do veículo e reduz a dependência da energia do combustível. O presente estudo realiza a optimização e avaliação de um gerador termoeléctrico com controlo de temperatura (conceito LaMoTa Uminho) num veículo comercial pesado (HDV). O sistema consiste num permutador de calor com placas de alhetas ondulada numa matriz de alumínio juntamente com câmaras de vapor, maquinadas diretamente na matriz, que concedem o controlo térmico. Acima estão os TEGs e as placas de arrefecimento para dissipação de calor.

O sistema foi analisado em condições de condução reais. Com um modelo 1D (algoritmo Matlab) do sistema foi possível prever o seu desempenho térmico e termoeléctrico durante ciclos de condução. Um HDV com um motor Diesel de 16 L foi simulado no software AVL. Foram obtidos dados relativos à temperatura dos gases de escape e ao fluxo de massa para cada ponto de dois ciclos de condução, que foram implementados no modelo 1D. Uma simulação de transferência de calor 2D em COMSOL forneceu as resistências térmicas do sistema, que foram adicionadas ao algoritmo.

O sistema demonstrou ter boa capacidade para aplicações com cargas térmicas voláteis, dado que foi capaz de evitar o sobreaquecimento dos TEGs, espalhando o calor para áreas com cargas térmicas baixas. Preveu-se uma produção eléctrica média máxima de 2,4 kW, o que significa uma poupança de combustível de cerca de 2% e redução de emissões de CO2 de cerca de 37 g/km.

Palavras-chave: Câmaras de vapor, Controlo térmico, Geradores termoeléctricos, Sistemas de recuperação de calor residual, Veículos pesados

Contents

List of Figures

List of Tables

Acronyms

TEG	Thermoelectric Generator
VCHP	Variable Conductance Heat Pipes
HP	Heat Pipes
HD	Heavy-Duty
VC	Vapour Chamber
WF	Wavy Fins
WHVC	World Harmonized Vehicle Cycle
HDV	Heavy-Duty Vehicle
WHRS	Waste Heat Recovery System
RC	Rankine Cycle
HE	Heat Exchanger
TCTG	Temperature-Controlled Thermoelectric Generator
VCVC	Variable Conductance Vapour Chambers
LD	Light-Duty
WLTP	Worldwide Harmonized Ligh Duty Vehicles
GVWR	Gross Vehicle Weight Rating
TDC	Top Dead Center
BDC	Bottom Dead Center
AFR	Air-Fuel Ratio
ERG	Exhaust Gas Recirculation
EATS	Exhaust Aftertreatment Systems
DPF	Diesel Particulate Filter
SCR	Selective Catalytic Reduction
LDV	Light-Duty Vehicle
SI	Spark-Ignition
CI	Compression-Ignition

EFM	Electromotive Force
ZT	Thermoeletric Figure of Merit
TE	Thermoeletric
TEM	Thermometric Modules
CHE	Compact Heat Exchangers

Symbols

Latin Variables

$\dot{Q}$	Thermal power	W
h	Heat transfer coefficient	W/m^{2}K
A	Area	m^2
C_p	Specific heat capacity at constant pressure	J/kg K
p	Pressure	Pa
$\dot{m}$	Mass flow rate	kg/s
u	Velocity	m/s
De	Hydraulic diameter	m
f	Fanning friction factor	-
L	Length	m
j	Cold burn factor	-
Pr	Prandtl number	-
T	Temperature	°C
$\dot{V}$	Volume flow rate	m^3/s
Re	Reynolds number	-
B	Torque	N.m
R	Thermal resistance	K/W
N	Engine speed	rpm
H	Height	m

Greek Variables

α	Seebeck coefficient	V/K
λ	Thermal conductivity	W/m.K
η	Efficiency	-
μ	Dynamic viscosity	Pa.s

ρ	Density	kg/m3
δ, ϵ	Thickness	m

Subscripts

m	Material
h	Hot
c	Cold, section
TG	Thermoeletric power generation
p	Fin pitch
s	Fin spacing
f	Total finned surface, fuel
o	Total air side heat transfer surface
e	Engine
cd	Conduction
cv	Convection

Chapter 1

Contextualization

1.1 Presentation

Within the increasing demand of the transport sector comes the challenge of reducing its emissions. The road transport sector presents itself as the second-largest contributor to the increase of carbon dioxide emissions, being responsible for more than a third of the total energy consumption of the countries belonging to the European Union. According to the European scenario, it is expected that the passenger transport sector will increase by 40% and freight transport by 60% from 2010 to 2050, so this sector, which plays an important role in the European economy that still relies heavily on fossil fuels, faces the need to reduce its CO_2 emissions. Considering this need, the European Union has set several targets to control CO_2 emissions. For 2021, a CO_2 emission target of 95 gCO_2/km has been set for passenger transport. For heavy transportation, CO_2 emissions must show a 30% reduction by 2030, with an interim target of 15% in 2025. This is because much of the emissions come from heavy transports, preceded by light cars. In 2016 heavy transport accounted for 26.2% of emissions from road vehicles, Figure 1 shows a breakdown of emissions from each type of combustion engine transport in the year 2016 [1–3]. The goals set by the European Union not only embrace the rise of electric vehicles but also the development of automobiles towards the improvement of their efficiency, fuel consumption reduction, and consequently emissions. It should be noted that are considered as electric vehicles (EVs), battery electric vehicles (BEV), fuel cell hybrid electric vehicle (FCHEV), plug-in hybrid electric vehicles (PHEV), and hybrid electric vehicle (HEV) which are the two EVs with internal combustion engines. Thus, for the automotive evolution and on behalf of increasing its tank-to-wheel efficiency, heat recovery techniques should be adopted, making use of the thermal losses presented in vehicles with internal combustion engines and transforming them into electrical energy through thermoelectric modules (TEGs). It is a fact that electrical mobility has been rising

through the years, yet there are still major developments to be done so that this electrification becomes accessible in the Heavy Duty (HD) industry, complying with the high frequent long hauls on which these vehicles operate [4–6].

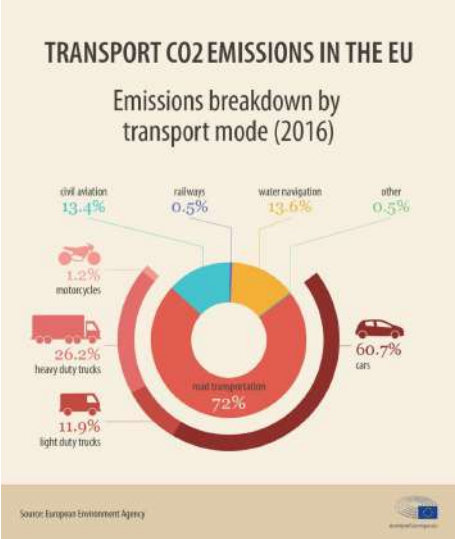

Figure 1: Breakdown of CO2 emissions by road transports in 2016 [7]

1.2 Motivation

Road vehicles with combustion engines have numerous constraints that result in the dissipation of fuel energy, jeopardizing their efficiency. There are several mechanisms by which the tank-to-wheel efficiency can be undermined. The paper [8] gather values appearing in the literature regarding the energy distribution of the global fleet of trucks shown in Figure 2. Around 50% of the fuel energy is wasted on direct losses such as thermal loads, where 30% of the fuel energy is lost into the exhaust gases in the form of heat and 20% through cooling, disappearing by conduction through the engine structure and the cooling radiator. While, in the other half, 3.1% goes to non-frictional auxiliary losses and about 47% of the fuel energy is converted into mechanical power. From these 47%, 13.5% are used to overcome the air drag as well as to the electrical and indoor cooling system, and only about 34% is used to overcome friction in any part of the vehicle, including brakes and tires, making the HDV move. It is possible to conclude that instead of the major percentage of thermal losses being dissipated into the environment, it can be used as an energy source. Hence, heat recovery will enable the reduction of fuel consumption and consequently increase the vehicle efficiency and decrease the emission of greenhouse gases [6, 8].

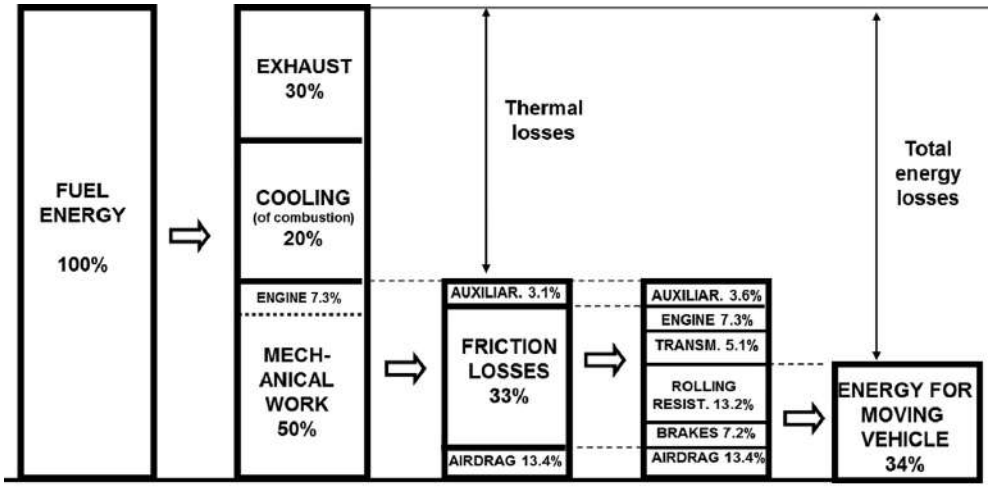

Figure 2: Breakdown of the average energy consumption in heavy duty vehicles [8]

Considering the thermal energy dissipated, mainly by the exhaust system, which has the most potential for recovery given its higher temperature than coolant temperature, it is imperative to explore means for waste heat recovery. This justifies the increasing interest in waste heat recovery systems (WHRSs) to generate electricity such as organic Rankine cycles and thermoelectric generators. By producing electricity from thermal energy, the engine´s mechanical load required by the alternator, or other electrical auxiliaries, such as air-conditioning, oil and water pumps or air compressor, will be reduced increasing the fuel economy. The Rankine Cycle (RC) enables the conversion of heat to mechanical work and then to electrical energy. Though safety aspects regarding the toxicity of the organic fluid at high temperatures, maximum operating pressure, flammability, and complex design and building, culminating in intense maintenance, which is troublesome in commercial vehicles due to the high cost and susceptibility for breakdowns [9]. Thermoelectric generators (TEGs) can quietly convert thermal energy directly into electrical energy by the Seebeck principle. These highly reliable devices, if carefully projected, have no moving parts, are small, require low maintenance, and can raise fuel efficiency up to 5%. TEGs include several connected semiconductors, positively doped (p-type) and negatively doped (n-type), which create thermoelectric junctions, the p-n couples. As a temperature gradient is created across the thermoelectric junctions an electromotive force is induced, enabling, by implementing an electrical load, the flow of electrical current to the vehicle. However, TEGs have limitations regarding the maximum tolerated temperature. Most commercially available TEGs with bismuth telluride modules can only support near 250°C and some developed materials like magnesium silicide can bear proximally 400°C. Once TEGs are to be integrated into the exhaust gas recirculation or in the exhaust after-treatment system, where exhaust gas temperature can reach 600°C or more, it is impossible to place these modules in direct contact with the heat source, so there is the need to apply a heat exchanger system allowing the thermal control of the temperature gradient flowing through the system [6, 9–11].

To fully exploit the TEGs efficiency, these must work at uniform temperatures and closest to the temperature limit, therefore the heat exchanger must be capable of maximizing the heat absorption as much as possible independently of the driving cycle, which can have high or low exhaust temperatures while ensuring that the temperature does not exceed the limit of the modules. This is a nearly impossible goal to achieve with conventional heat exchangers because a heat exchanger will be either optimized for maximum heat absorption being prone to overheating in high thermal load events, or it will be optimized for a narrow operating condition range, operating poorly for lower loads and needing to waste exhaust heat under high thermal loads. The Project Exhaust2Energy, carried out at the Engines Laboratory at the University of Minho, LaMoTa, has been developing several groundbreaking systems with a temperature-controlled thermoelectric generator (TCTG) concept. The concept, presented in Figure 3, allows to maximize the heat absorption while still providing temperature control, in a best-of-both-worlds strategy to simultaneously maximize electrical output and avoid overheating. This temperature control is achieved through the concept, proposed by the researchers, of heat spreading through a phase change. This consists of using a liquid/vapour phase change system embedded along the HE which has the role of absorbing the excess heat from overheated regions, keeping them below the maximum allowable temperature, and then spreading and delivering this heat to under-heated regions of the heat exchanger, optimizing temperature level in this region. The HE prototypes incorporate corrugated pipes that absorb exhaust heat and lead the thermal energy from the exhaust gas through the entire system, as they are embedded in a cast-aluminium matrix along with variable conductance heat pipes (VCHPs). The hot faces of the TEGs are attached to the aluminium blocks, while the cold face is attached to finned water-cooling plates. The VCHPs are responsible for the heat spreading effect explained above. They enable the control of the heat fraction that reaches the TEG, working as capillary-driven heat carriers/spreaders. In the VCHPs the exhaust heat is absorbed by an evaporator generating vapour, this vapour will carry thermal energy to the condensation region where the heat is released to the TEGs and the condensates return to the evaporator through the wick structure by the action of capillary pumping. Since the exhaust gas temperature is not constant, and the modules require uniform temperature, there is the need for a uniform phase change temperature inside the HPs irrespective of thermal load. This can only be obtained through variable conductance, which is implemented by filing part of the condenser with a non-condensable gas. This way, the vapour will fill a higher or lower portion depending on the available thermal energy, thus only a part of the condenser will be active and the rest, filled with the non-condensable gas, inactive. In the case of high exhaust temperatures, the heat transfer area in contact with the TEGs will be higher compared with lower exhaust temperatures [11].

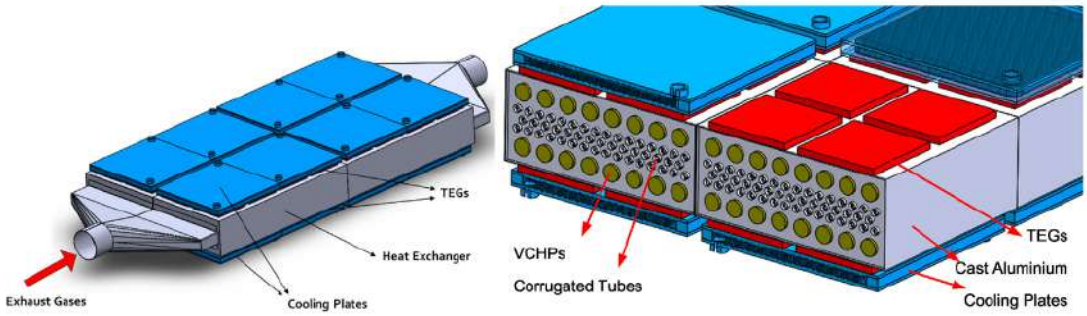

Figure 3: (a) global and (b) cut overview of temperature-controlled thermoelectric generator concept based on corrugated tubes and VCHPs [11]

Corrugated pipes embedded in aluminium, have issues regarding their conceivable minimum thickness on casting procedures, reducing the compactness factor and consequently the heat transfer effectiveness. VCHPs are expensive devices, usually made of copper, a poor pressure-resistant material, and prone to corrosion in casting. An alternative approach to the HE model above presented can be made by reformulating the two major elements, the component by which the exhaust heat is absorbed, the corrugated pipes, and the components through which the temperature control is implemented, VCHPs, also aiming at the best performance of the TEGs. There are several types of compact heat exchangers, that is, heat exchangers with a high heat-transfer area-to-volume ratio. These include plain, perforated, offset, or corrugated tubes, with the purpose to enhance heat transfer surface area and improve heat transfer coefficients. Wavy Fins (WFs) are notable due to their simplicity of manufacture and potential for thermal performance at a reasonably low-pressure drop. The wavy characteristic of the fin, while lengthening the path of the airflow causes better airflow mixing, allowing higher heat transfer rates. The higher the wave amplitude, the higher is the heat transfer rate. In the VCHPs absorption or release of the heat tends to be radial. However, the heat transported across it through vapour transport is longitudinal, the fluid evaporates at one end of the pipes, crosses the length of the evaporating region, and condenses further downstream, at the cooler regions of the pipe. The region further downstream of the vapour region is nearly adiabatic and is occupied by the non non-condensable gas which was pushed out of the active region of the VCHPs by the vapour. Vapour Chambers (VCs) are also capillary driven heat carriers with the same fundamental operating mechanism as VCHPs, including the possibility of operating with variable conductance, but with two or three-dimensional thermal flow. The main difference between VCHPs and the variable conductance vapour chambers (VCVCs) is geometrical, as they tend to be flat instead of round. VCs are also called flat HPs, and they can be directly machined into the medium (in this case, the aluminium block). They also have the capillary improving structure that can be porous metal or micro-texturized surfaces, as the LaMoTA researchers are researching in new project CoolSpot, with IST and micro-manufacture researchers from CMEMS. Their geometry affects the distance the liquid and the vapour can travel, how liquid is transported back to the evaporating region and the area in contact with the heat source. In VCs the bottom of the

chamber, the evaporator, is in contact with the heat source. In comparison with the cylindrical shape of the VCHPs, due to the rectangular shape VCs have a larger area of contact. This heat will be dissipated along the porous support column and absorbed by the working fluid, which evaporates. The generated vapour is immediately diffused in the vapour core, condenses on the top plate of the VC, condenser, and returns to the base through the capillary wicks. This will enhance the heat flux cooling because of its low resistance and temperature uniformity. LaMoTa has been developing a laser texturized 6061 aluminium alloy VCs prototype. This technique, besides being more cost-effective and allowing customized dimensions, boosts the nucleation sites allowing faster phase changing [12–14].

Outlining the project, the corrugated tube will be replaced by WFs, as they will be explored in the present study, as a better and effective way of absorbing the thermal energy flux from the exhaust gas to the rest of the system. The VCs will be implemented as an alternative to the VCHPs, reducing the production costs, as they are directly machined onto the aluminium block instead of adding complementary components. Additionally, there is the possibility of using working fluids with a phase change at lower pressures. These VC are being developed by CoolSpot with advanced procedures of texturization. Hence, the VC act as exhaust thermal energy controllers, ensuring that the temperature reaching the TEGs, does not exceed their maximum working temperature. Since the VCs are only active when the working fluid boiling temperature is reached, the system will only retrieve heat from the regions where it is excessive. It will then spread and deliver this heat to regions where there was a lack of heat, raising the temperature to the optimal level. This way, the available heat will not be wasted but it will be delivered to a proportional number of module rows. which will all display an optimized temperature level. Avoiding the dissipation of heat will culminate in more efficient energy generation from TEGs as their hot side will work at a temperature close to the optimal/maximum temperature. These VC Cooling plates with a high surface to volume ratio will also be attached to the cold face of the modules to maximize the temperature gradient across the modules, thus maximizing the Seebeck effect. There is a huge potential for applying this system to HD vehicles since these vehicles will rely upon combustion engines for a long time and have cycle runs with very high loads.

1.3 Goals

The purpose of the present dissertation is to simulate an HD vehicle along with two cycle runs and reformulate a compact HE with the possibility of temperature control, previously used in light-duty vehicles, into HD applications. Relatively to previous work, it assesses a novel geometry of high-performance exhaust channels from BorgWarner, WFs, and a novel geometry of heat spreaders, VCs machined in the HE body developed by CoolSpot. With AVL software, an HD truck with an internal combustion engine will be simulated under two cycle runs with different cargo loads. The main outputs from this simulation are the exhaust gas temperature and the exhaust gas mass flow along each point of the cycle runs. Following a CAD modelling of the system with the new components, a thermal analysis of the HE model with a new stacked geometry and a recent TEGs model is done via two-dimensional quasi-steady-state simulation on COMSOL software. Two designs are evaluated. This enables the visualization of the thermal resistances in the system. Basic heat transfer theory, empirical correlations of the elements to obtain heat transfer coefficients and thermoelectricity knowledge, are applied to analyse the electrical outputs of the system. Aiming for the validation of the HE model, the optimization of a Matlab algorithm projects the best geometry build-up for the most efficient electricity generation. This algorithm combines the cycle points data from the HD truck simulations, with the thermal constraints and thermoelectric properties of the HE system, resulting in an analysis for each cycle point. Regarding the outputs from the algorithm, the HE system is dimensioned.

1.4 Structure

The development demonstration of the present case study is divided into seven chapters:

- Chapter 1 provides the study contextualization, motivation and objectives to be achieved and the dissertation outline;
- Chapter 2 confers the necessary theoretical information to assimilate the subjects of the dissertation. Cycle runs and heavy-duty vehicles are the main topics in this research as well as thermodynamic concepts involving waste recovery systems by applying thermoelectricity and heat exchangers;
- Chapter 3 describes the process to be followed in order to meet the specified objectives while reflecting in the project constraints;
- Chapter 4 explains the simulation and definition of an HD vehicle and presents the results regarding the exhaust gas, further implemented in the simulation model of the TEGs;
- Chapter 5 presents the heat exchanger model design and its components. The thermal analysis is done by empirical correlations and by a simulation in COMSOL. The algorithm which provides the thermoelectric outputs of the system is also explained. Here is displayed the design of the system;
- Chapter 6 presents and discusses the results in terms of exhaust power through the system, electrical production, pressure drop, efficiencies and savings in fuel and CO_2 emissions;
- Chapter 7 presents the conclusions of the project and future work for its improvement.

Chapter 2

Fundamental Concepts and Literature Survey

To better assimilate the case study and on behalf of its optimization and improvement, along with straightforward problem-solving, it is important to know the scientific background of the subject. In the present chapter, topics about driving cycles, HD vehicles (HDV) and waste energy recovery systems are presented followed by a literature survey about thermoelectricity, basic heat transfer concepts, and HE components.

2.1 Driving Cyles

Environmental pollution and human health are not recent concerns, since these have been suffering a long term degradation from early years, thus the implementation of emissions legislation has improved the air quality. Nowadays, particulate matter, nitrogen dioxide, and ground-level ozone are the most harmful, not only for our respiratory system but also affecting the cardiovascular one. As referred above, on-road transportation is accountable for the main of these emissions, however, emissions legislation has encouraged constant automobile development resulting in even more clean vehicles. Addressing this objective techniques on which the vehicles and engines are tested have been set. Cycle runs, act not only as a standardized analysis of the pollutant emissions but also aid the maintenance and evolution of vehicles [15].

2.1.1 History Background

The very beginning on which air pollution was associated with engine vehicles, occurred in the 40s, where the smog started to float in Los Angles result of the increase of gasoline-engined vehicles. This led to the first emissions standards for all motor vehicles, focusing on carbon monoxide (CO), and hydrocarbon (HC)

emissions. Establishing for the first time the terms "emission level"and "emission control". These first limits led to an exciting engine and vehicle advancement. However, one of the manufacturer's solutions was to make the air-gasoline mixture poorer leading to a higher amount of nitrogen oxides (NO_x) emissions. As result, NO_x became one of the three controlled pollutants by legislation in the early 70s. Result of the abundant emission of black smoke from diesel-engined trucks, emission regulations started to also include vehicles with these types of engines. Sooner, to meet the legislation after-treatment systems and cleaner fuels started to become mandatory in several countries. Hence, since the 60s, vehicles have been tested to meet the emission standards adopting standardized tests, known as driving cycles [15].

2.1.2 Cycles Run Fundamentals

Towards the achievement of the legal emission targets, there's the need to formulate precise test methods for the examination of the vehicle's emitted pollutants, where their approvement depends on whether the pollutants are within the established emission limit or not. The tests must comply not only with the typical vehicle or engine daily operation but also with its application, so a wide range of speed and load conditions in a transient operation should be considered, enabling the approximation to real-world driving. Test cycles are established by setting test points along with time steps with predefined vehicle velocity or rotational engine speed/torque.The test points can also follow a road grade, with defined distance and inclination. To best simulate the real-world driving conditions, the test cycles require cold and hot starting points, different accelerating and decelerating phases, as well as load changes and representative stages of rural, suburban, urban, and highways. Besides, these tests must be practical, repeatable, and entirely controlled [15].

Cycle runs in heavy duty vehicles are primarily categorized into two classifications, chassis dynamometer, which are usually transient, and engine dynamometer, working as steady-state or transient, cycles. During a chassis dynamometer cycle vehicles undergo the test points on a chassis dynamometer. The vehicle remains stationary and only two wheels are spinning. The dynamometer simulates the different speeds, the driving rolling resistances, and the aerodynamic and inertia forces while the vehicle is driven by an expert who follows the defined cycle schedule. Because the dynamometer can't simulate the road grade component these forces are simulated in a previous coast-down test and then adjusted to the dynamometer. As for the engine dynamometer cycles, they are defined by normalized engine speed and torque operation points along with time steps. The engine dynamometer considers the drive-train and vehicle properties, mainly resistance factors from the frontal area, weight, and aerodynamics. Due to the complexity of heavy-duty (HD) drive-train, these vehicles are commonly tested in engine dynamometer cycles [15].

2.1.2.1 WLTP

The Worldwide Harmonized LD Vehicles Test Procedures (WLTP) sets several test methods for testing mostly LD vehicles emissions and fuel consumption, one being the Worldwide Harmonized Light Vehicles Test Cycles (WLTC). WLTCs are chassis dynamometer tests divided into four categories presented in Table 1.

Table 1: WLTC categories [15]

Category	**Duration (s)**	**Distance (km)**	**Maximum Velocity (km/h)**	**Maximum Acceleration (m/s^2)**	**Average Velocity (km/h)**
Class 3b	1800	23.27	131.3	1.67	46.5
Class 3a	1800	23.19	131.3	1.67	46.4
Class 2	1800	22.65	123.1	0.97	45.3
Class 1	1022	8.1	64.4	0.81	28.5

2.1.2.2 WHTC and WHVC

The World Harmonized Transient Cycle (WHTC) is a transient engine dynamometer test cycle for HD vehicle certification. This transient cycle covers hot and cold startings. The World Harmonized Vehicle Cycle (WHVC) is a chassis dynamometer version of the WHTC. In the WHVC, with a duration of 1800 s, the vehicle goes through three driving conditions: an urban driving along 5.3 km with an average speed of 21.3 km/h and a maximum speed of 66.2 km/h, a rural driving with an average speed of 43.6 km/h and a maximum speed of 75.9 km/h, and to conclude, a highway driving with average speed of 76.7 km/h and a maximum speed of 87.8 km/h. Figure 4 represents both engine and chassis dynamometer cycles [16].

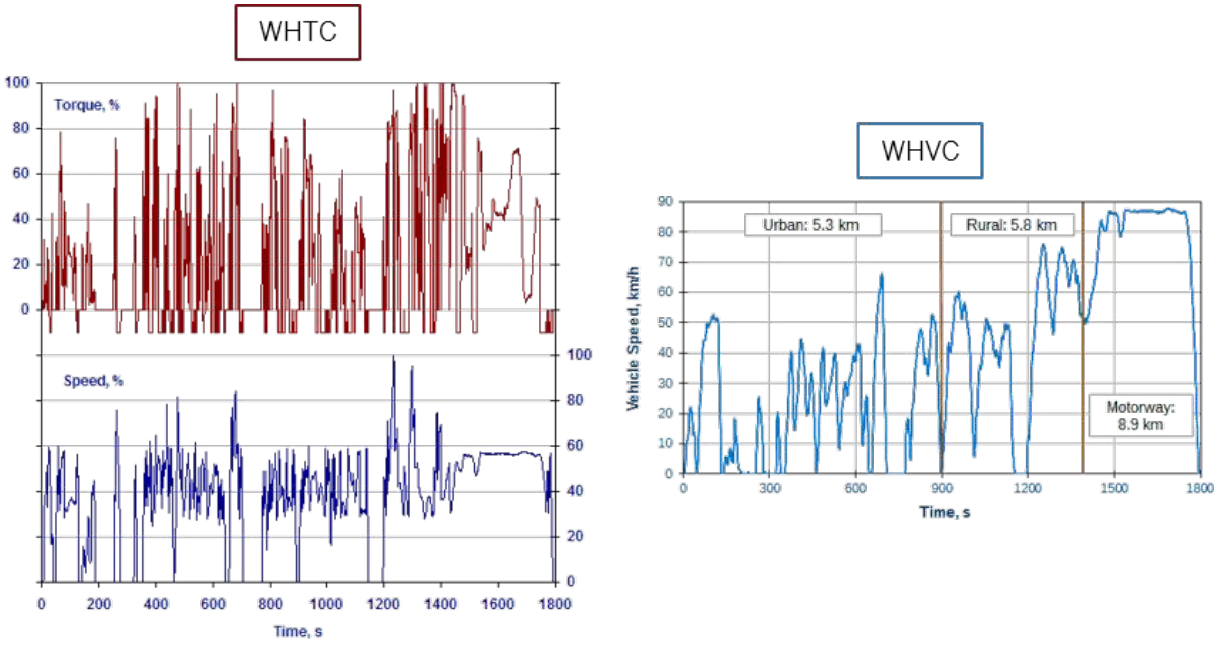

Figure 4: WHTC engine dynamometer cycle and WHVC chassis dynamometer cycle [16](adapted)

2.2 Heavy-Duty Vehicles

In a world where the concern of vehicle emission reduction is progressively increasing, emerges the interest of establishing more efficient vehicles. Is believed that the development of electric trucks may be one way. Since the foundation of the transport industry economy depends on transporting the maximum payload along a specific itinerary at a designated cost, is important to analyse the constraints that the present Li-ion battery technology cause on this industry. Viswanathan [17] attempted to create a model to analyse these limitations concluding that the current batteries, for now, are not convenient due to their small specific energy values, lower than Petrol and Hydrogen. This means that for the required energy to overcome the aerodynamic drag, frictional and inertial forces and road gradient is necessary a great amount of battery pack which means more truck weight. Considering the maximum legal gross vehicle weight, by including more batteries the truck will have a greater range but will be able to carry less payload. Or, by creating a smaller battery pack, which compromises the range, more payload will be available. Taking as an example a Diesel engine truck with a payload of 20 tons and 1448 km range, an electric truck would only have four tons of payload for the same range. This is the main reason why, for now, medium and HD on-road vehicles are primarily powered by diesel engines [17].

2.2.1 Heavy-Duty Classification

Mainly due to safety aspects regarding not only the HDV drivers but also the drivers and passengers they share the roadways with, HDV manufacturers and workers must comply with to the Gross Vehicle Weight

Rating (GVWR) and the vehicle dimensions. The GVWR includes the weight of the tractor and trailer, plus the driver and passengers, full fuel tank, and the payload. In Europe, GVWR and the vehicle dimensions are set by the EU directive 2015/719 which reformulates de directive 96/53. These directives establish not only maximum lengths, but also maximum GVWRs. For trailers, a maximum length of 13.6 m is designated, for articulated vehicles, with semitrailers, 16.5 m, and for rigid trucks with a trailer a maximum of 18.75 m. As for the GVWR, a maximum of 42 tons for tractors of two axles with semitrailers of three axles is defined. And for HVD with three axles and semitrailers of two or three axles, a maximum GVWR of 44 tons is set. These types of modules can be combined with up to two coupling units, the European Modular System is a solution for increasing the payload by allowing the combination of existing loading units into longer and heavier vehicle combinations. Figure 5 presents the most common combinations, these combinations can have a maximum length of 25.25 m with a maximum weight of 60 tons. EMS assigns swap bodies with a maximum length of 7.28 m to fully complete these dimensions [16–18].

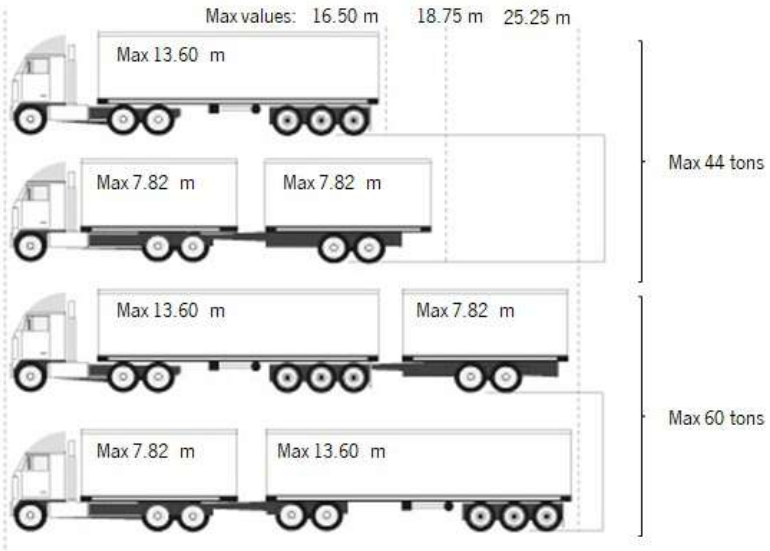

Figure 5: Load carriers and European Modular System most commonly used vehicle carrier combinations [19](adapted)

2.2.2 Compression-Ignition Engine

Diesel engines are compression ignition engines. They are the core of the commercial transportation industry, commonly used in long-haul, LD to HD vehicles, trucks, or buses, and even in the nautical industry due to their great fuel economy, higher engine torque output, and greater durability and longevity. The Diesel combustion resides in a heterogeneous chemical process where the liquid fuel composed

by hydrocarbon species meets an air in-cylinder charge leading to heat release and therefore emission formation. This cycle, divided into four stages, begins with the admission of clean air. The piston goes from the Top Dead Center (TDC) to the Bottom Dead Center (BDC) this under-pressure results in the entrance of air through the admission valve. When both of the valves are closed, the piston rises to the TDC, compressing the air inside, leading to temperature rising. The fuel is injected into the hot air, burning quickly, raising temperature and pressure and thus pushing down the piston, performing mechanical work along with the lowering of the piston. Once the piston is in the BDC, the exhaust valve is opened and the burned mixture flows through it until the piston reaches the TDC again. Since the fuel is injected directly into the cylinder at the end of the compression stroke, the air-fuel mixture is not pre-heated and compressed, thus, there is no danger of pre-ignition of the mixture due to excessive compression. This allows higher compression ratios than in traditional gasoline-fueled Spark Ignition, SI, engines. In gasoline engines, the air-fuel mixture is admitted into the cylinder during the intake stroke and is compressed up to the TDC, this can lead to premature combustion if the mixture is overly heated and compressed during the compression stage, or to the appearance of destructive detonating combustion (knock) in the latter phases of combustion, therefore SI engines have lower cylinder compression pressures. Also, Diesel Engines can work with very lean burn combustion where the excess of air to burn the fuel can reduce heat transfer losses and thus enhance the engine efficiency, unlike most gasoline engines where neither unburned oxygen nor fuel is left after the combustion stoichiometric mixture process, a measure that is necessary for the suitable elimination of most pollutants with the Three Way Catalyst. Thus, with higher compression ratios, more power is produced, and lower fuel consumption is achieved [20].

2.2.2.1 Brief Comparison Between a Light-Duty and Heavy-Duty Engines

HD engines have thermal efficiencies of about 46%, whereas LD engines are around 30% in SI and 40% in CI engines. HD engine's higher efficiencies are mainly influenced by the lower heat transfer and friction losses, impulsed by lower surface/volume ratio typical of larger machines, the burnt mass fraction shape, which describes the process of the chemical energy release, and higher air-fuel ratio, AFR, because lean combustion leads to explosions far from the cylinder walls, thus lower heat losses through the cylinder walls. Also, HD engines usually have lower rotating speeds of the rotating components, causing lower friction losses compared to LD vehicles [21].

Within Diesel engines, there are obvious differences between HD and LD. For instance, HD engines have higher displacements between 5 to 16 L and can have up to 12 cylinders, also they have lower engine speeds and higher torque and power ranges. Table 2 presents a comparison of LD engine incorporated in the Ford Focus 3 and an HD Detroit DD13 engine available in Cascadia trucks.

Table 2: Light-duty vehicle engine and heavy-duty truck engine [22, 23]

Data	**Ford Focus 3 1.6 TDCi 95HP**	**Detroit DD13**
Number of Cylinders	Inline: 4	Inline: 6
Engine Displacment (L)	1.56	12.8
Bore x Stroke (mm)	75 x 88.33	18.4
Compression Ratio	16	18.4
Maximum Power (kW)	70 at 3600 rpm	505 at 1625 rpm
Maximum Torque (N.m)	230 between 1500 - 2000 rpm	2508 between 975 - 1450 rpm

2.2.3 Emission Reduction strategies

Although Diesel engines emit less CO2 per km, due to the higher efficiency than petrol, they still emit nocive particles, and NOx is hardly totally erased in the catalytic systems. One of the challenges in the heavy-duty engine industry is to improve its viability with good drivability, low fuel consumption, and high reliability, along with its weight in the global economy, and ensure the strict emission requirements of NOx, CO, unburned hydrocarbons (UHC) and soot. Thus, manufacturers have beem optimizing several technologies to enhance the fuel economy such as electronically controlled fuel injection, exhaust gas recirculation (ERG), turbocharging, exhaust gas aftertreatment systems, and waste heat recovery methods.

2.2.3.1 Injection Systems

IC engines require a high-pressure precise injection of fuel at a precise timing into the combustion chamber. The Diesel injection pressures range from about 200 bar, when the vehicle in operation in idle conditions, to around 2500 bar, or over 4000 bar for newly injection systems, at high speed with full loads. Electronically controlled fuel injection systems can grant precise injection fuel quantities, pressure, and number of injections and allows flexible durations and startings. These systems have higher injection pressures enabling more homogeneous air-fuel mixtures, avoiding locally over-rich mixtures. The most common system in HD engines is the common rail injection system that can generate multiple injection events during the combustion cycle. The injections discharges are continuously calculated by the injection rate shaping which defines different injection moments, starting from the pilot injections to main injections, till post-combustion injections depending on the crank rotation, each injection per cycle can be as fast as ten-thousandths of a second [24, 25].

2.2.3.2 Exhaust Aftertreatment Systems

Visible changes in reinforcing the emissions reduction are enabled by cleaning the noxious emissions, such as NO_x and particulate matter, produced in the cylinders after the combustion process. Exhaust Aftertreatment Systems (EATS) like Diesel particulate filters (DPF), Diesel oxidation catalyst (DOC), and selective catalytic reduction (SCR) can help the achievement of the tailpipe emission regulations [26].

- **Diesel Oxidation Catalyst**

  DOCs have been mandatory since emission regulations were applied. The CO, unburned HC, and organic particulates present in the exhaust gas, when passing through the DOC, are oxidized into harmless products. First, the oxygen is bonded to a catalytic site, then the pollutant reactants diffused in the DOC surface react with the oxygen molecules resulting in reaction products like CO2 and water vapor. However, these reactions can sometimes result in harmful products like sulfuric acid. Today's DOCs oxidize nitric oxide into nitrogen dioxide, a gas that is further used in the DFP filters and SCR catalysts [27].

- **Diesel Particulate Filters**

  DFP technology traps soot particles from the exhaust gas stream in a ceramic filter. However, these filters can easily be clogged therefore can't be applied as a single EATS technology since they require an oxidation catalyst upstream of the DFP. This catalyst will heat the cool exhaust to burn the clogged soot in a passive regeneration, if the driving conditions can't produce enough heat to naturally regenerate the filter, the catalyst is dosed with diesel fuel resulting in a chemical reaction heating the exhaust gas and the DFP filter - active regeneration [26].

- **Selective Catalytic Reduction**

  Within the several NOx reduction techniques like lean NOx traps, NOx adsorbing catalysts, and liquid SCR systems, the last one is the most efficient in HDV. SRC is a technology exclusive to diesel engines in which ammonia is injected and selectively reacts with NOx oxidizing it into harmless nitrogen and water. Since is unsafe to carry ammonia on board it is necessary to apply urea as a precursor. AdBlue, a eutectic solution composed of urea and water, is injected into the exhaust system upstream of the SRC catalyst. Due to the thermal energy, urea is decomposed into two equivalents of ammonia and one equivalent of CO2, finally, the produced ammonia is stored on the surface of the catalyst. Three major reactions occur in SCR depending on the NO2/NOx ratio, the fast SRC which takes place with a 50% ratio, being the most favorable reaction since maintains higher conversions in low temperatures. The standard SRC and the NO2-SCR reaction, where the NO2 is higher than 50% and the required amount of ammonia is bigger resulting in an increased AdBlue consumption. The main difference between LD and HD vehicles EATS stands on the SRC setup. Most LD vehicles have the SCR catalyst combined with the particulate filter, unlike HDVs which have the DFP followed by a separate SCR [26].

2.2.3.3 Exhaust Gas Recirculation

Another important method for pollutant reduction in both SI and CI engines is EGR. The exhaust gas is taken directly from the cylinders to the EGR valve, which will regulate the mixing of the exhaust gas

with the intake air, meaning more air with less oxygen will reach the cylinders for the new combustion process. Excess air with less oxygen implies lowers combustion temperatures resulting in lower production of NOx, as the production of this pollutant directly depends on temperature increasing and on the amount of oxygen. Notwithstanding, EGR is not limited to NOx reduction since it can also enable closed-cycle diesel engines or improve the SCR catalyst performance. In conformity with the Euro VI legislation, HD engines manufacturers choose from a combination of an uncooled EGR and SCR, or SRC without ERG. However, both these setups have disadvantages. In EGR combined with SCR, the EGR is rarely used in higher load operating conditions like long haul routes, being restricted to low load conditions. On the other hand, in systems of SRC without ERG the complexity, cost, and weight may be reduced but the urea consumption is increased, therefore a larger tank is necessary [28].

2.2.3.4 Turbocharging

The turbocharger main function is to compress more air into the cylinders. Because the oxygen molecules are more closed together more fuel can be introduced in the same aspirated amount. This leads to higher mechanical power for a given engine displacement, lower pumping losses, greater combustion efficiency, enables engine downsizing, thus improving fuel economy. Usually, the turbocharger is divided into the turbine section and the compressor section. The turbine housing leads the exhaust gas to the turbine wheel, which spins the turbine and then exits through the exhaust outlet area. Because the compressor wheel is attached to the turbine they turn at the same time resulting in high-speed air spinning twirls, compressing the air. The compressed air goes to the compressor housing which turns the high-velocity, low-pressure air flux into a high-pressure, low-velocity by diffusion. *BorgWarner* is aiming for HDV turbochargers with efficiencies of 65% (major competitors have around 56%) by optimizing the matching between the turbine and the compressor's ideal blade speed and offering not only monoscroll turbines but also twin-scroll and dual volume that make use of the exhaust gas pulses more efficiently. Also, the turbine's outlet has a coned design where the exhaust gas is separated, goes downstream the turbine, and allows the heating of the EATSs [29, 30].

2.2.3.5 Waste Heat Recovery Systems

As mentioned above, heat losses are still a problematic issue during the conversion of fuel into work, undermining fuel consumption and therefore increasing pollutant emissions. Thus the development of systems for recovering the substantial thermal energy that is currently wasted through the exhaust of HDVs has been of interest by HDV manufacturers. Systems like mechanical or electrical turbo-compounding, ORC, and TEGs have been assessed in the automobile industry to enhance the engine efficiency [31].

- **Mechanical and electrical turbo-compounding**

  The turbo-compounding systems work similarly to the turbochargers but the turbine produces mechanical work for compounding the mechanical work done by the engine (or produce electricity) and not only for moving the compressor. The turbo-compounding turbine is capable of translating the leftover heat energy into torque, being driven by exhaust airflow coming from the primary turbine. The electric turbo-compounding system converts the turbine rotational shaft power into electrical power with an alternator. In the mechanical system, the power is transmitted with a shaft through the gearbox to the power unit crankshaft.However, this arrangement takes a lot of maintenance and causes the increment of the engine backpressure [31].

- **Organic Rankine Cycle**

  The ORC is a WHRS composed of a pump, evaporator, a power expansion turbine, and a condenser. The cycle begins with the pumping of a working fluid through the system which, on the evaporator region, will have its temperature and pressure raised by the recovered heat. The fluid is expanded till the turbine generating power through a shaft. The fluid will then be condensed and back to its initial form. This system although with higher heat recovery potential than TEGs, tends to increase the pumping loss and has a complex system construction which has the need for frequent maintenance [31].

- **Thermoeletric Generators**

  TEG technology has been seen as a valuable low-maintenance, "install-and-forget"alternative to complex ORC systems due to its low complexity without any moving parts and low maintenance, simplicity, modularity and reliability, if well designed. TEGs are capable of converting heat into electrical power only due to their semiconducting materials and a temperature gradient from the exhaust gas by the Seebeck effect. These modules have limited working temperature and for a more efficient thermal to electrical energy conversion must operate close to the limit [32].

2.3 Thermoelectricity Fundamental Concepts

By applying a temperature gradient across the junctions of a pair of p and n semiconductors, an electromotive force will appear. If the circuit is closed, a current will be generated, providing useful power. This is called the Seebeck effect. Conversely, the flow of current across these p-n pairs also causes the flow of heat in the direction of the flow of charge. This is called the Peltier effect. Both these phenomena are the core of Thermoelectricity. However, in the present study, only the Seebeck effect is described in detail, as it is the one involved in TE generation. Important thermoelectricity concepts for this project will be demonstrated in this section.

2.3.1 Seebeck Effect

The development of an electromotive force (EFM) across two semiconductors in response to the imposition of a temperature gradient is known as the thermoelectric effect or Seebeck effect. The Seebeck coefficient (α) defines the EMF and the temperature difference ratio and measures the entropy transported with a charge carrier. These charges swap from the hot junction to the cold junction of the semiconductor, implementing a variation in the number of charge carriers in the thermoelements fabricated from n-type and p-type semiconductors, generating the EFM, explained in Figure 6. Please note that the direction of current shown in Figure 6 is according to convention (direction of the positive charge flow). In reality, there is a flow of electrons (negative charge) in the n-type and of holes (positive charge) in the p-type, both from the hot to the cold junctions. Equation (1) defines defines the Seebeck coefficient (α), where ΔT is the temperature difference between the hot (Th) and the cold (Tc) junction, and ΔV the generated EFM. α varies as a function of the temperature and depends on the composition of the semiconductor[33, 34].

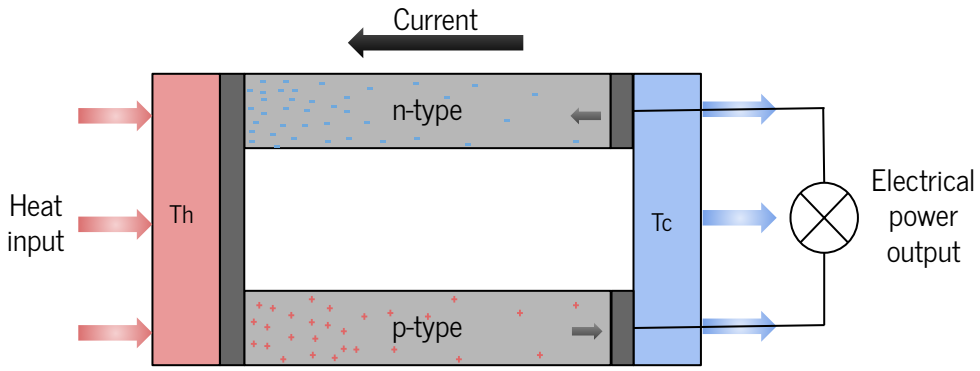

Figure 6: Seebeck effect operating scheme [33](adapted)

$$\alpha = \frac{\Delta V}{\Delta T} \tag{1}$$

The voltages produced through the Seebeck effect are usually small, about 10 microvolts per Kelvin of temperature difference at the junction, and for large temperatures a few millivolts. Therefore, a series of devices working by this principle should be connected electrically in series to increase the output voltage or in parallel to increase the maximum deliverable current.

2.3.2 Thermoelectric Figure of Merit

The figure of merit (ZT) is essentially a non-dimensional temperature dependent material property derived from temperature dependent material properties. This dimensionless figure combines the Seebeck coefficient with the electrical conductivity (k), the thermal conductivity (λ_m) and the absolute temperature (T) of the materials by equation (2). Efficient materials will be characterized with high α and high k along with low λ_m [35].

$$ZT = \frac{\alpha^2 k T}{\lambda_m} \tag{2}$$

The thermoelectric power generation efficiency (η_{TG}) depends on the ZT of the semiconductor materials of which the thermoelectric device is composed. The maximum efficiency of the generator device is limited by the Carnot factor ($\Delta T/Th$) and is affected mainly by the temperature gradient and the ZT. Equation (3) provides the determination of η_{TG}, assuming that the properties of the thermoelectric material are constant according to temperature and for one dimensional heat flow with no other losses. This efficiency is essentially the ratio of the energy supplied to the load and the heat energy absorbed at the hot junction.

$$\eta_{TG} = \frac{\Delta T}{T_h} \frac{\sqrt{1+ZT}-1}{\sqrt{1+ZT}+T_c/T_h} \tag{3}$$

For a given heat source, the design of a thermoelectric device starts with the selection of the thermoelectric material. This thermoelectric material usually is a poor thermal conductor but a good electrical conductor in order to obtain a high ZT. Higher ZT means higher electric generation of the thermoelectric device. Figure presents the thermoelectric ZT figure of merit as a function of temperature for several common thermoelectric materials, enhancing the high dependence of ZT as function of the temperature. The most conventional thermoelectric materials from 20 °C to 300 °C are heavy metal alloys such as Bismuth (Bi), Tellurium (Te), Antimony (Sb) or Lead (Pb). Recent promising affordable materials for automotive generator applications include Magnesium silicide and tetrahedrite, as developed by LaMoTA, IST and University of Cyprus researchers in recent Project THERMOSS ([36]), Skutterudites, and Half Heusler alloys [37].

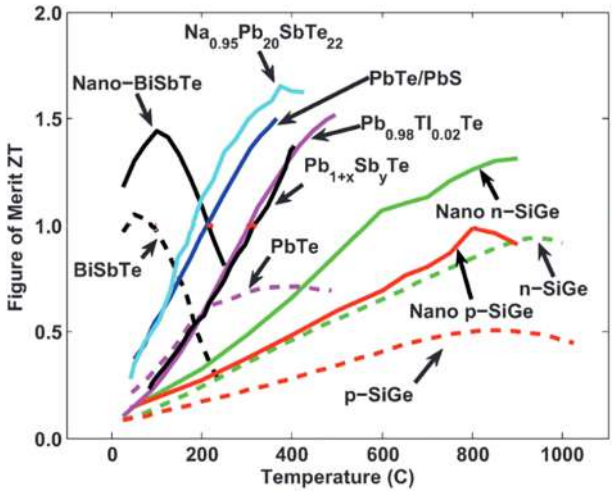

Figure 7: Thermoelectric figure of merit (ZT) as a function of temperature for thermoelectric materials. Solid lines - bulk materials. Dotted lines - nanostructured materials [37]

2.3.3 Thermoeletric Generators

TEGs convert thermal energy directly into electrical energy through the Seebeck effect - by placing the TEG between a hot heat source and a cold heat sink, the temperature difference will be converted into an electric current across the module terminals. These electric power generators assembly two thermoelectric junctions and deliver electric current through an external electric load. TEGs principle can be described in Figure 6, one device compound contains positive type charge carriers and the other compound contains negative type charge carriers. These two semiconductor compounds are connected in series forming the p-n junction. When heat is applied to the hot junction an electrical potential difference is created, which is proportional to the applied temperature difference.

Commercially available TEGs have a ZT≈ 1, resulting in a thermal to electrical conversion efficiency of about 5% . Most commercially available TEGs are made of Bismuth Telluride ($Bi2Te3$), which works in low temperature settings (<250°C). Lead Telluride ($PbTe$) and Silicon Germanium ($SiGe$) alloys are also used but for higher temperature applications, 630°C and 1020°C, respectively, however, both have limitations, with lead being mostly banned from automotive applications and with germanium being a rare and expensive material, used mostly on the Radioisotope Thermoelectric Generators (RTGs) that supply the electricity needed by deep-space missions and other applications with no cost constraints. Most of the modules are manufactured using multiple TE materials. On operation, p-n legs will suffer a large temperature gradient. Therefore, using different thermoelectric materials in the direction of the heat flow is also an option: each TEG leg will be of segmented material. Thus each material along the TEG leg is chosen for optimum performance at the temperature gradient [6, 37].

A significant temperature difference across the TEGs is a key to achieve higher power outputs. Thus the cold face should ideally be closest to the ambient temperature as possible. Cooling systems manage to dissipate most of the heat produced on the hot side, though, since the water running through fins is

cooled in that same environment, the temperature of the cold face can never reach the ambient because the heat dissipated by the cooling system decreases with the temperature difference, thus, temperatures equal or lower than the ambient can't be achieved:

$$\dot{Q} = h \cdot A \cdot \Delta T \tag{4}$$

Another aspect to take into consideration is the maximum operating temperature of the TEG. There is a limit in the maximum heat that the hot face can bear without damaging the module. For instance, although some $Bi2Te3$ TEGs are designed to intermittently operate at 380 °C their ideal operating temperature for a steady state is about 250 °C.

2.4 Waste Recovery Systems via Thermoelectricity

This section presents the history and state of the art regarding systems using thermoelectricity in vehicles, several novel concepts aiming at the generation of thermoelectricity done by Universidade do Minho, and the application of TEGs in HDV application.

2.4.1 History Background and Thermoeletric Developments in Vehicles

Since the decisive discovery of thermoelectricity by Thomas Johann Seebeck in 1821, many investigations have been done trying to control and improve this phenomenon. For instance, right in 1834, Peltier managed to evoke the opposite effect - the electrical current between the junctions emits or absorbs heat. However, ZT had been near a value of 1 for a long time, until the end of the early 1990s were several nanoscales approaches developed thermoelectric materials with ZT higher than 2. Figure 8 presents the breakthrough of ZT through the years:

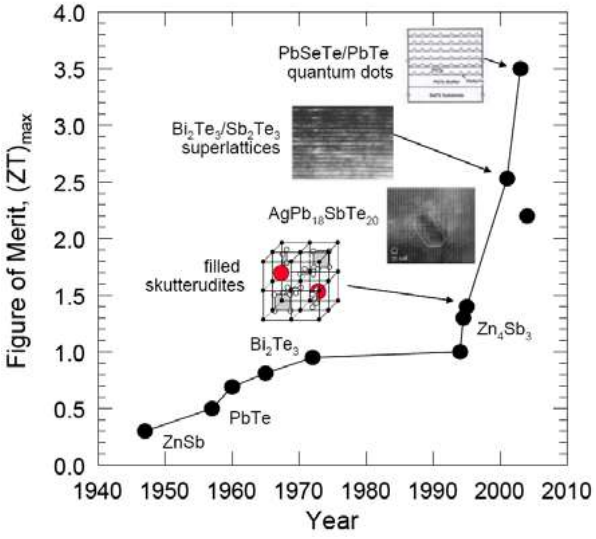

Figure 8: Progress in thermoelectric materials ZT [38]

These advancements contributed to incentive of thermoelectric applications in vehicles, for fuel economy and reducing greenhouse gas emissions. In 1995, the U.S. Department of Energy together with Hi-Z Technologies (one of the precursors in the enhancement of ZT) developed a TEG able to convert waste heat from the exhaust gas of a HDV diesel engine into electricity. The cooling was done by extracting the heat from the cold face with the HD radiator cooling water. The modules with Bismuth Telluride cells had provided an output power of 1 kW. This accomplishment prompted the use of TEGs in transportation vehicles to decrease the alternator dependency. [38]. Since 2004, projects have been conducted to design TEGs systems that can accommodate the thermal and mechanical stress due to the wide temperature difference of the exhaust gas, from ambient to 800°C, while preserving good thermal conductivity. For

instance, Delphi Corporation managed a study for testing a TEG system installed in the exhaust pipe of the 1999 GMC Sierra pick-up, Figure 9. The automobile TEG setup was assembled with 16 HZ-20, with 71 series-connected thermothermocouples, TEGs from Hi-Z technology. These modules, connected in series, were arranged by eight on each side of a carbon steel heat exchanger with offset strip fins, by which, the exhaust gas flowed. The engine coolant was chosen to cool the generator instead of air cooling, so the heat from the cold face was rejected by two aluminum heat exchangers with cooling liquid. Although this prototype accomplished a power output of 255 W at a constant velocity of 112.6 km/h, temperatures higher than the maximum supported by the modules (250°C) were shortly obtained [39].

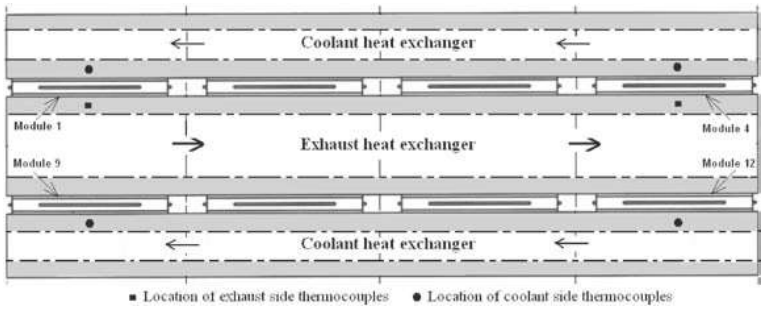

Figure 9: Arrangement of HZ-20 modules and heat exchangers in the GMC Sierra pick-up [39]

BMW Group assembled a thermoeletric generator system consisting of three hot gas heat exchangers, 24 Bi_2Te_3 thermoelectric modules and four coolant heat exchangers with an alternately layered construction, Figure 10a. The gas goes trough a diffuser at the TEG inlet, enhancing the thermal transfer and homogenization. This prototype, integrated in the exhaust system of the BMW 535i was assembled with a bypass parallel to the TEG, preventing excessive pressures and overheating. The exhaust mass flow is divided between the two flows by means of an automated control depending on the load. This mechanism, presented in Figure 10b achieved an output of 200 W at constant speed of 130 km/h, where temperatures of 250°C were reach in the TEG system [40].

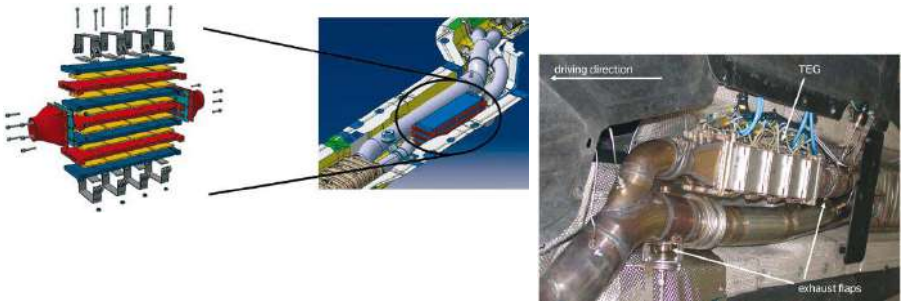

(a) Thermoelectric generator concept (b) Integration

Figure 10: Waste heat recovery system of a BMW 535i US [40]

Since then, a significant number of studies, in cooperation with several automotive manufacturers, have been performed studies to introducing new thermoeletric generator prototypes, whether in real engines or exhaust simulators. The most common TE material is still Bismuth Telluride, in spite of its low optimal working temperature it offers great thermoeletric efficiencies. To figure out the temperature limit, investigators have been selecting several methods to better harvest or expel the heat to/from the hot/cold faces of the TEGs. These hot heat exchangers are usually flat plane fin while the cooling are cold planes with finned structures. Table 3 gathers experimental systems regarding TEGs in automobiles [6].

Table 3: Summary of physical properties of TEG systems applied to automobile industry [6]

Year	Engine	TEG Max Power (W)	Driving Conditions	Hot HE	Cold HE	TEG Material	Location
1988	Porsche 944 2.7L	58	max engine load	square channel	coolant block	FeSi2	exhaust manifold
1995	Cummins 14L	1068	1700 rpm constant speed	octagonal fins	coolant block	HZ-13	turbo-charger exit
2007	1999 Sierra 5.3L V8	255	112.6 km/h constant speed	offset strip fin	coolant block	HZ-20	after CC
2012	BMW 530i 3L 6cyl	450	110 km/h constant speed	fins in cylinder	coolant tubes	Bi2Te3	after CC
2013	Chevrollet Sub. 5.3L	235	US06 drive cycle	-	coolant block	Skutte-rudites BiTe	after CC
2017	Golf 1.4 TSI	111	NEDC drive cycle	square channel	cold plate	TEG1-12611	after CC
2018	2L 4 cyl SI for hybrid	98.8	3000 rpm constant speed	hexagonal fins	hexagonal fins	1261G-7L31	exhaust manifold

2.4.2 Recent Innovative Systems

The German Aerospace Center (DLR) , Institute of Vehicle Concepts, conducted a state of the art project improving the efficiency of modern HD commercial vehicles using a new type of heat recovery system. This was the first survey where the integrated development and potential of the technology in use was demonstrated in an HDV with a natural gas engine (Iveco Stralis NP with 300 kW power). The engine and exhaust gas aftertreatment were simulated through empirical values, and not by measuring the necessary data on the test bench. The model follows a counterflow stacked design concept, where stacks of several

flat plane compact HE channels, TEMs, and coolant HEs are positioned on top of each other fixed by a pre-tensioning device, described in Figure 11. A thermal interface material is placed between each layer and all layers are pressed together by bolts to minimizing the thermal contact resistance. The TEM modules were specifically manufactured for the HDV application by the Korean company LG, made of Bismuth Telluride on the cold side and Skutterudite (SKD) on the hot side, these modules bear a maximum temperature of 500 °C [34, 41].

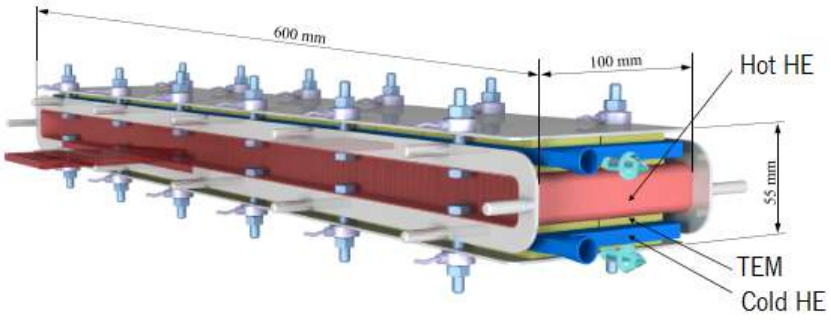

Figure 11: TEG model with one hot HE layer [34]

The system with 144 TEMs and three hot gas HE staked between the TEGs results in an area of 530 x 355 x 180 [mm], including maintenance flaps and diffuser/confuser. The project concluded great potential for thermoelectric technology to increase efficiency in the natural gas engine, resulting in fuel reduction of 2.5% with a maximum electrical power output of around 2.7 kW. Figure 12 presents the described model with the stacked layers. Although the TEMs models used in this project have a maximum temperature of 500 °C most commercial available modules have breaking temperatures of 250 °C, meaning that the described model would not be appropriate for common TEMs because it has not a temperature control mechanism to prevent modules overheating. Nevertheless, these high temperature modules are useful for natural gas engines, that have much higher exhaust temperatures than conventional HDV with Diesel engines. Since Natural Gas exhaust temperatures can exceed 800°C, so a temperature control similar to the one assessed in the present study adapted to 500°C would also be useful for these modules [41].

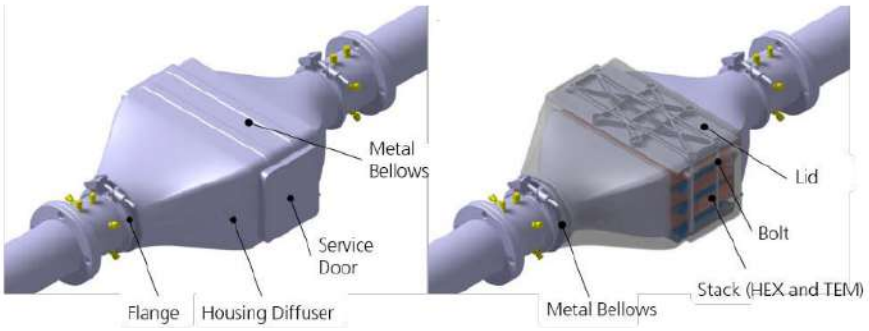

Figure 12: Staked TEG design [41]

2.4.3 Developments Made by Universidade do Minho Research Group

Uminho research group has been developing systems aiming the generation of electricity from the exhaust gas heat. In the study exposed in [42], the research group developed a system for the recovery of engine exhaust energy by converting it into electricity with commercially available TEMs and HPs for controlling the temperature gradients. The model is presented in Figure 13.

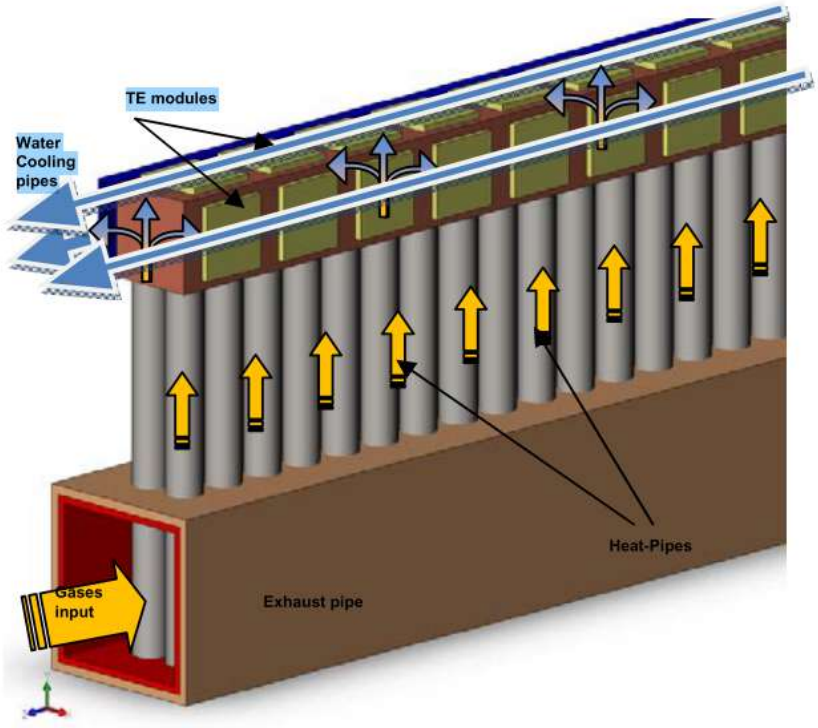

Figure 13: Artwork of a thermoelectric generator for waste heat recovery in exhaust gases of combustion engines, using heat pipes [42]

Prototypes and experimental results culminated in [43], where various types of HPs were designed, manufactured, tested and improved with the aim of enhancing the overall heat transfer process, enabling an optimal level of electric energy recovery from the referred TEG modules by the testing of different

fluids inside the HPs. The model is presented in Figure 14. From this concept a improved prototype was developed and tested, again with positive results regarding the capability of temperature control in [44].

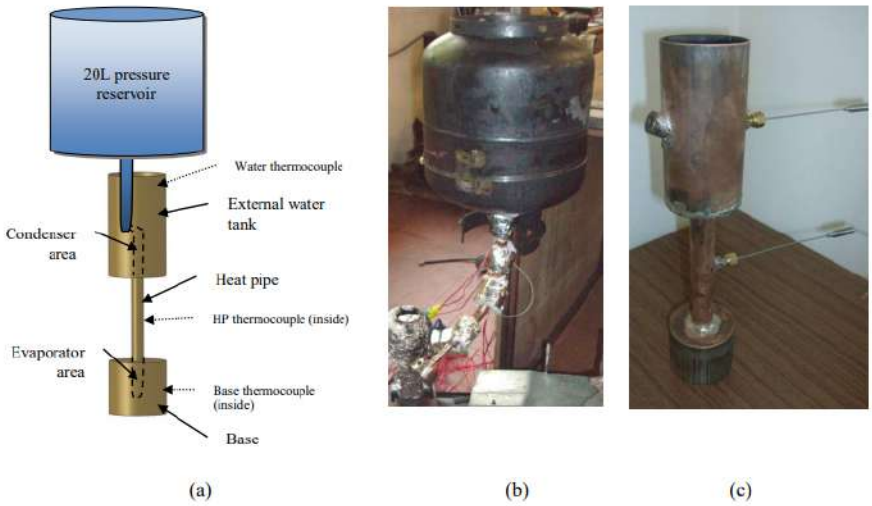

Figure 14: (a) Outline and (b) photograph of the improved Heat Pipe setup, with optional 20 L cylinder tank for VCHP operation.(c) Detail of the bare HP without the tank attached [43]

Concerning the electrical power accurate determination, in [45], the influence of the HP temperature in the electric output of a thermoelectric generator with the exhaust gas of a small diesel engine and a generator was analysed, Figure 15. Due to the low available thermal load from the engine and inefficient HE, the optimal working temperature of the HPs was low (130°C), by increasing this temperature the electrical load of the active TEGs would be higher but less modules would absorb the necessary heat and there forte less active TEGs.

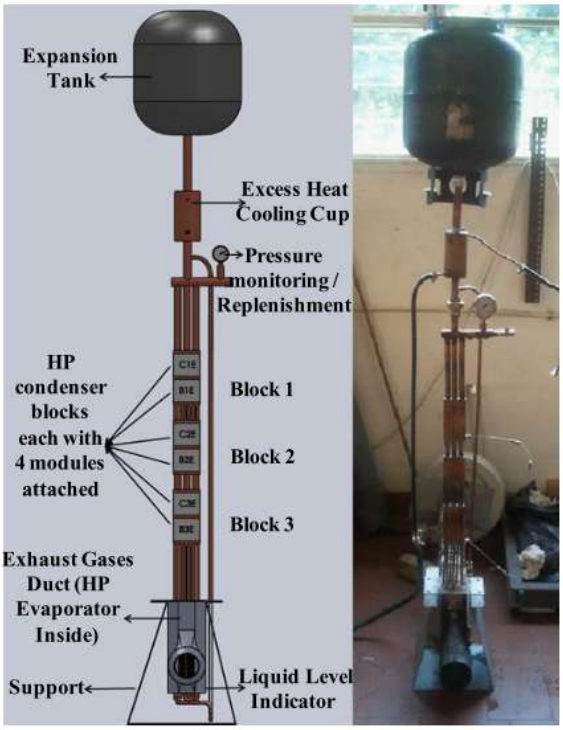

Figure 15: Design and photograph of the prototype [45]

After these experimental approaches, new models have been developed using VCHPs as thermal controllers and corrugated tubes or offset fins through where the exhaust gas flows through. In [11] the performance of temperature-controlled thermoelectric generator (TCTG) concept in a light duty vehicle and its impact on fuel economy and greenhouse-gas emissions under realistic driving conditions was analysed. The HE system, displayed in Figure 3 is composed of corrugated pipes in a cast aluminium block along VCHP (that act as excess heat spreaders) where only the excess heat, instead of all the heat load (as in the primary models), is transmitted through phase change. Figure 16 displays the heat flow inside the mentioned HE system, where the VCHPs absorb the excess heat in high temperature regions and release it through condensation in colder regions of the system. One major achievement in these recent models was the ability to prevent the heat from diffusing along all TEGs in medium to low power events and focusing the heat on fewer modules, enabling these to work at their maximum working temperature. Additionally, by enabling a horizontal layout, the concept is more suitable for vehicle industry applications. Also, a Matlab algorithm was built to predict the prototype behaviour under the designated cycle runs. This algorithm has been adapted for the present work.

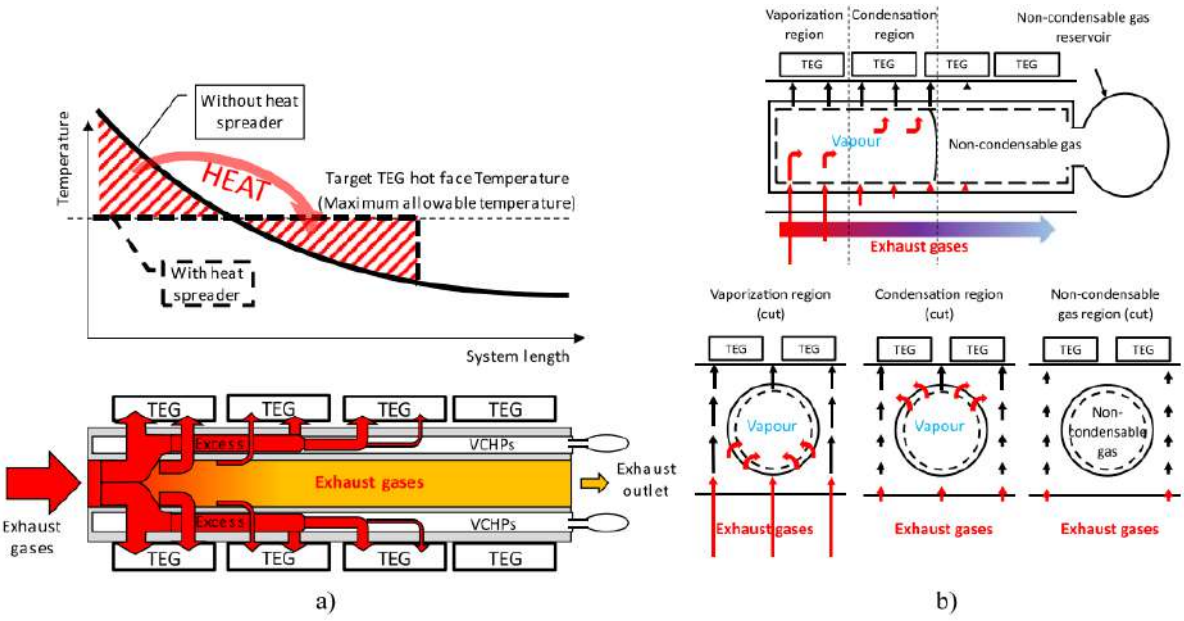

Figure 16: Representation of the excess heat (a) spreading enabled by the use of VCHPs and (b) being absorbed by the VCHP at the hotter regions and released to the cooler regions through phase change [11]

2.4.3.1 Offset Fins and Corrugated Tubes

Offset fins have substantial heat transfer enhancement due to the periodic interruption on the boundary layers. Primarily used in air-side compact heat exchangers, these fins can reduce the space, weight, and support structures. Usually made in aluminium or stainless steel, depending on the working conditions. However, these types of fins are prone to fouling, hence the Uminho group adopted copper corrugated tubes embedded in an aluminium matrix instead of offset fins in the recent projects. Corrugated tubes, commonly used in EGR coolers, are adapted to the exhaust environment conditions, not being vulnerable to fouling. Besides, the heat transfer enhancement ratios are larger than the increment of pressure drop penalties. However, corrugated tubes are limited to the conceivable minimum thickness on casting procedures which jeopardizes the compactness factor and the heat transfer performance. In the present work, WFs will be used as an alternative to the offset fins or the corrugated tubes [11, 46].

2.5 Heat Transfer and Fluids Basic Concepts

Heat and fluids behavior can be predicted through the use of suitable correlations. Important temperature dependent properties are presented in the present section and in Annex I.

2.5.1 Pressure Drop

When aiming at energy recovery in fluid flow, pressure drop (Δp) is an important parameter to keep within a minimum, because this loss is associated with exhaust pumping losses at the engine and pumping power needs in the cooling circuit. These deprecate the electric power produced by the system, so they need to be minimized as much as possible. This value reflects the difference between the pressure on the inlet and outlet of a given system like a CHE and can be measured by equation (5) where f is the Friction factor to be further detailed.

$$\Delta p = \frac{1}{2}\rho u^2 \frac{4L}{De} f \tag{5}$$

The power necessary to overcome the channel resistance and move the fluid across it at a given flow rate is called pumping power ($\dot{W}p$), which is proportional to Δp and a parameter to consider when analyzing the system efficiency. Δp is obtained through equation (6), where $\dot{m}$ and ρ are the mass flow rate and the density of the fluid [47].

$$\dot{W}p = \frac{\dot{m}\Delta p}{\rho} \tag{6}$$

2.5.2 Colburn Factor

The Colburn factor (j) is a dimensionless quantity that relates to the convection coefficient, the fluid properties, the flow conditions, and the system geometry. The j factor, like f, are strong functions of fin geometries and the ratio j/f is used for the measure of the performance of the fin surfaces.Thus, j can be defined by equation (7) [48].

$$j = \frac{h}{\rho u C_p} Pr^{2/3} \tag{7}$$

2.5.2.1 Thermal Power

The thermal power ($\dot{Q}$) transported by a given fluid can be obtained by equation (8). For the calculation of the enthalpy power presented in the exhaust gases, $\dot{m}$ is the sum of both fuel and intake air mass flows, T the exhaust gas temperature and T_∞ the ambient temperature [49].

$$\dot{Q} = (\dot{m})(C_p T - c_{p_\infty} T_\infty) \tag{8}$$

2.6 Compact Heat Exchangers

HE are devices that perform the heat exchange between two fluids at different temperatures preventing them from mixing. HE mechanisms usually involve convection in each fluid and conduction through the wall separating the two fluids. Is important to understand that the heat transfer rates depend on the temperature gradient and that they differ along the HE. The HE can be classified based on the flow path configuration, Figure 17, by the following categories:

- Parallel flow - the two fluids enter together in one end, flow trough the HE in same direction, and leave it together at the other end;
- Countercurrent - the fluids flow in oposite directions;
- Single-pass crossflow - the fluids flow in perpendicular directions inside the HE;
- Multipass crossflow - One of the fluids goes from side to side crossing the other fluid stream.

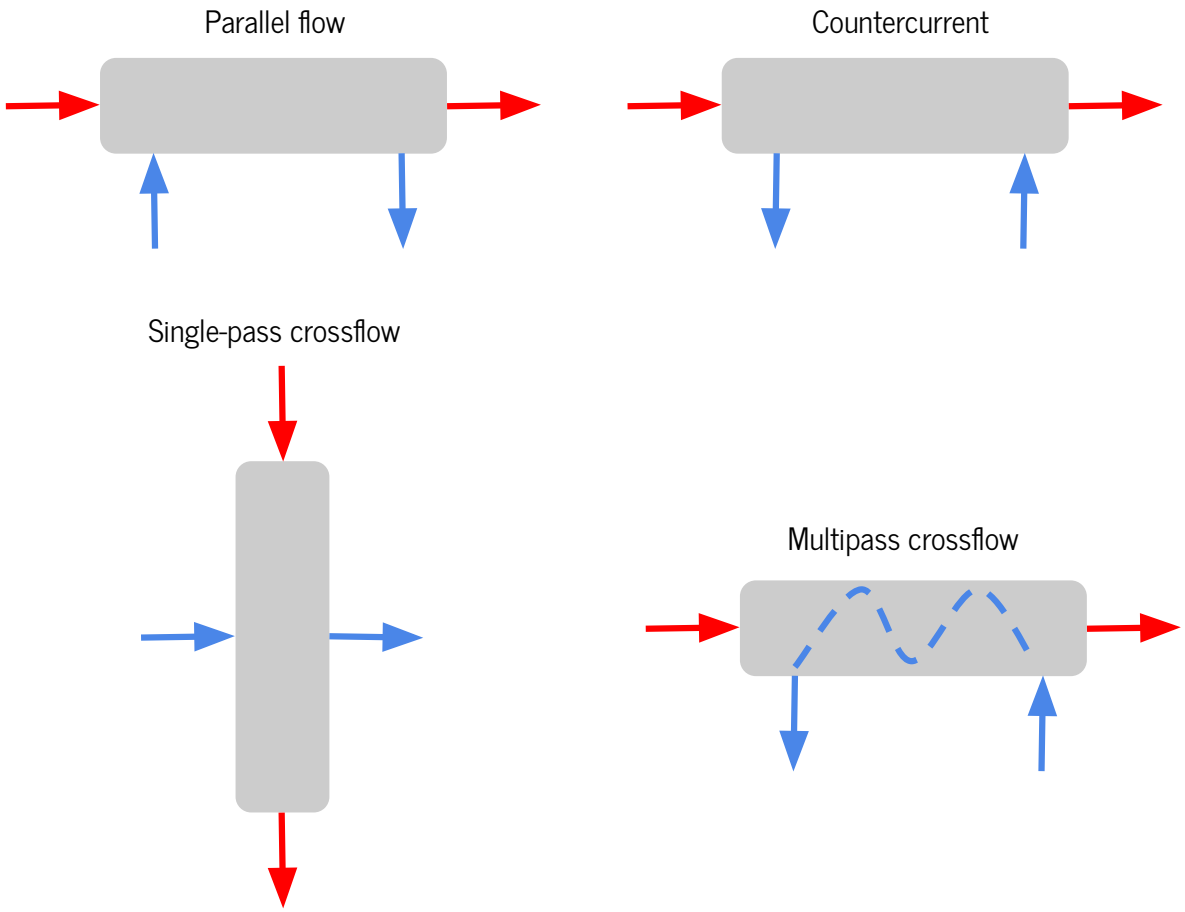

Figure 17: Flow path configuration through heat exchanger

Compact heat exchangers (CHE) are characterized by their high area density, meaning a high ratio of heat transfer surface to the heat exchanger volume. CHE are classified as "compact"when the area density is higher than 700 m^2/m^3. Since in the vehicle industry, space and weight are strict limitations, the compactness feature is decisive in the selection of this type of HE. For gas-to-gas heat transfer applications, the CHE will rectify the low heat transfer coefficient associated with gas flows [47, 48].

2.6.1 Available Types of CHE

Different CHE technologies and principal applications will be presented in order to understand the possible geometries and setups to further apply them in other operations.

2.6.1.1 Plate and Frame Exchangers

Plate and Frame Exchangers usually cover heat transfer surfaces with several pressed, corrugated metal plates compressed together into a frame usually in stainless steel. The hot and cold fluids flow in alternate channels so that each cold fluid stream is surrounded by two hot fluid streams, Figure 18, resulting in very effective heat transfer. These CHE have a flexible response to the application needs since in the case of higher heat transfer demands it is just necessary to add more plates to the setup. In terms of operating limits, the operating temperatures commonly range from -35°C to 200°C while the maximum bearing pressure is 25 bar, depending on the material and manufacturer. Flow rates up to 5000 m^3/hour can be tolerated when with a double port entry. Plate exchangers applications are mostly classified by the streams to be treated like liquid-liquid and condensing or evaporating purposes. [47, 50].

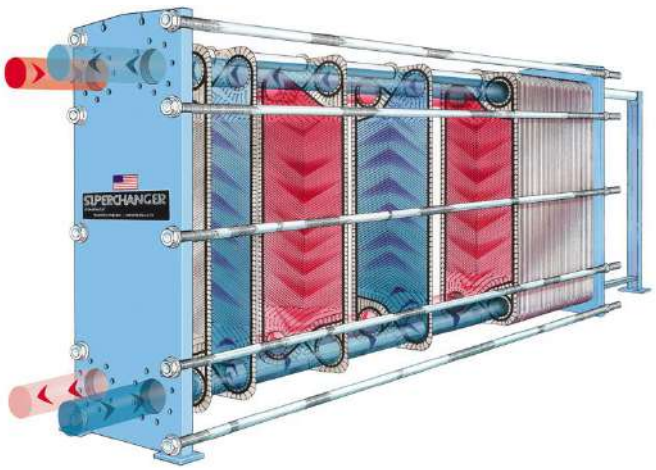

Figure 18: Exploded view of a Plate CHE [51]

2.6.1.2 Brazed Plate Exchangers

These CHE are assembled by a pack of pressed plates brazed together and don ´t require the use of gaskets as well as the frame, unlike the plate exchangers. The corrugated plates, Figure 19, are capable to induce high turbulent flows, this can act as a cleaning method, reducing the surface deposits. Copper brazed parts are possible to temperatures ranging from -195°C to 225°C, with a maximum operating pressure of 30 bar. Nickel units can support 400°C, but lower pressures - 16 bar. Brazed plate exchangers are mainly used in heat pumps for evaporators and condensers or water heating and heat recovery [50].

Figure 19: Brazed plate exchanger [52]

2.6.1.3 Plate Fin and Tube Fin Exchangers

Commonly used in gas-to-gas applications, plate fin exchangers are distinguished due to their compactness factor, while plate exchangers have an area density of about 230 m2/m^3, plate fins go up to 6000 m^2/m^3. This surface area is composed of flat plates separating corrugated or louvered, Figure 20a fins where cross-flow, counterflow, or parallel flow types of flow paths can be established. Depending on the material these CHE can operate at temperatures up to 650°C (for stainless steel). Tube fin exchangers, Figure 20b are used for applications where high pressures or extended surfaces are needed. Typical configurations stand on round tubes or flat tubes. These exchangers are used for a range of tube fluid operating pressures up to 30 bar and operating temperatures to about 870°C, yet, these have a lower area density than the plate fins [48, 53].

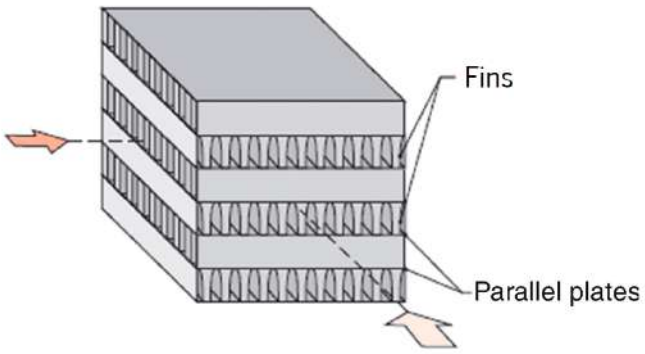

(a) Plate fin

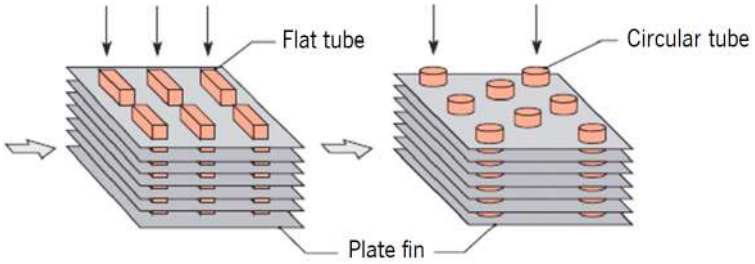

(b) Fin tube (flat tubes, and circular tubes)

Figure 20: Finned compact heat exchanger cores [53]

2.6.1.4 Printed Circuit Heat Exchanger

The printed circuit heat exchangers have great compactness, with an area density of roughly 2500 m^2/m^3, are corrosion resistant, capable of working at high pressures of 200 bar in steady operations and from -200°C up to 800°C. The plates are done by chemical milling and then stacked and diffusion bonded, converting them into a solid metal piece containing precisely engineered fluid flow channels, Figure 21. This CHE can operate gases, liquids, and two-phase flows. More than two fluids can exchange heat in a single core, maximizing the HE effectiveness [50].

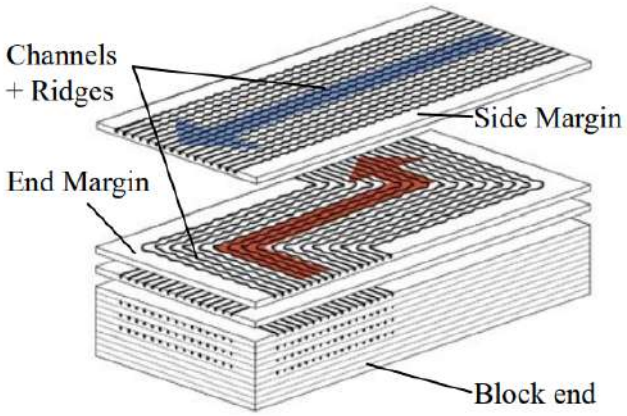

Figure 21: Printed Circuit Heat Exchanger block [54]

2.6.2 Wavy Fins

Compact heat exchangers are usually composed of extended or finned surfaces with the purpose to increase the heat transfer area and the convection coefficients. In response, the heat transfer rates are magnified. Among the common fin geometries, like offset, perforated or plain fins, wavy fins are distinguished due to their basic manufacture process, ability to enhance the thermal-hydraulic performance, and versatility. These type of fins are used HE in exhaust systems, mainly in the EGR cooler. The wavy pattern surface expands not only the length of the airflow path, causing better airflow mixing, which improves the heat transfers, but also the surface area, increasing the area density. Several studies concluded that the flow stream inside the WF is both steady and unsteady, where the beginning of the mixing depends on the Reynolds number and geometry. The WF wall corrugations lead to a swirl flow in their base with a low Reynolds number, inducing the airflow mixing. The WF can either contain triangular, sinusoidal, or trapezoidal patterns. The WF performance depends on the WF complex geometry, presented in Figure 22. Geometrical elements like the corrugation aspect ratio (Ld/L), fin spacing ratio ($F_p/2A$), flow length ratio (Ld/L) and the flow cross-section aspect ratio (F_p/F_h) are used for the analysis of the heat transfer events [12, 55].

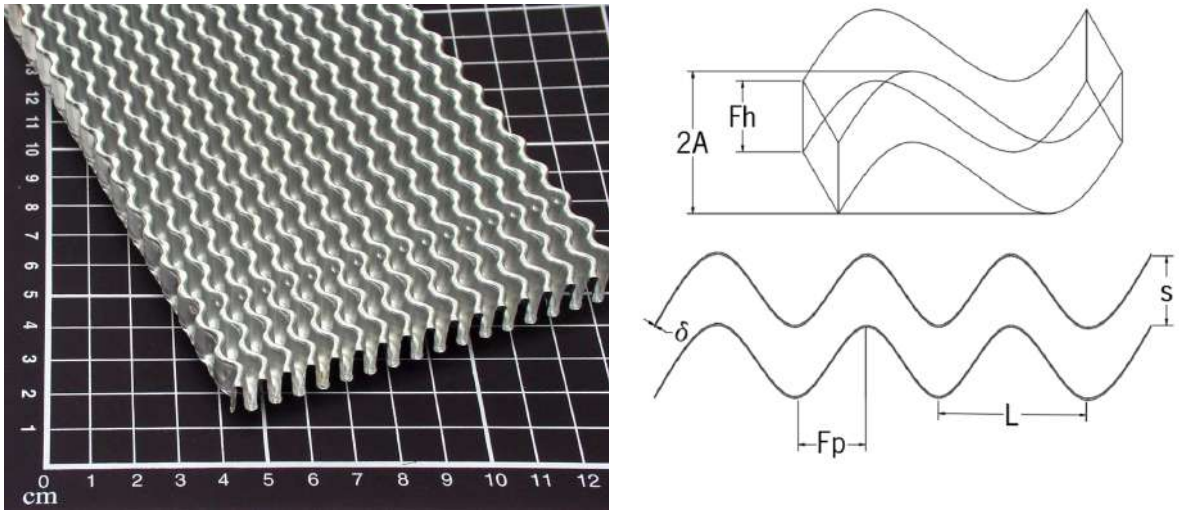

(a) WFs image [56]

(b) WFs geometry

Figure 22: Wavy fin geometry parameters: Fin pitch (Fp); fin high (Fh); fin spacing (s); fin thickness (δ); fin wavelength (L); twice the amplitude (2A)

2.6.2.1 WF Empirical Correlations for Thermal Analysis

WF require empirical correlations to calculate the heat transfer coefficient (h) as a function of the properties of the fluid flowing through them. The maximum air velocity in the fin (ui) is obtain by equation (9), where $\dot{v}$ is the gas volume flow and Ac the section area of the fin channels. The hydraulic diameter of the the fin entrance ($De = 4sF_h/2(s + F_h)$) and the air viscosity v are used for equation (10).

$$u_i = \frac{\dot{v}}{A_c} \tag{9}$$

$$Re = \frac{u_i \times De}{\mu} \tag{10}$$

The characteristics of heat transfer and pressure drop for different geometry parameters, like WF, can be reported in terms of the j factor and f, as a function of Re. Where L_d is the wavy fin length:

$$j = 0.0836Re^{-0.2309}\left(\frac{F_p}{F_h}\right)^{0.1284}\left(\frac{F_p}{2A}\right)^{-0.153}\left(\frac{L_d}{L}\right)^{-0.326} \tag{11}$$

$$f = 1.16Re^{-0.309}\left(\frac{F_p}{F_h}\right)^{0.3703}\left(\frac{F_p}{2A}\right)^{-0.25}\left(\frac{L_d}{L}\right)^{-0.1152} \tag{12}$$

Although the friction factor (f) can be determined by equation (5), Dong Junqi [55] performed its analysis on WF by using a general CHE equations for f, where the constants kc and ke were graphically obtained according to the geometry parameters, hence the kc and ke are 0.4 and 0.2 in equation (13), where Ao is the total air side heat transfer surface area.

$$f = \left(\frac{A_c}{A_o}\right)\left(\frac{2\Delta p}{\rho u^2} - kc - ke\right) \tag{13}$$

The surface effectiveness (η_a) and fin efficiency (η_{WF}) for the of wavy fins are determined by:

$$\eta_a = 1 - \frac{A_f}{A_o}(1 - \eta_f) \tag{14}$$

$$\eta_{WF} = \frac{tanh(m'l')}{m'l'}; m' = \sqrt{\frac{2h}{k_f \delta}}; l' = \frac{Fh}{2} \tag{15}$$

Where A_f is the total finned area of the WF, k_f the thermal conductivity of the fin material.

2.7 Thermosiphons and Heat Pipes

Thermosiphons and Heat Pipes are devices that perform heat transfer between a heat source and a heat sink through phase change of a fluid that is contained within a chamber. In thermosyphons, a two-phase working fluid is placed in a vacuum tube. The lower end of the tube is heated leading to the vaporation of the fluid. The vaporized fluid rises to the top (cold) end where it is condensed returning to the vaporizing area by gravity. This heat transfer mechanism allows very high heat transfer rates. HPs differ from the thermosyphons due to the application of a wick at the inner surface of the HPs enabling the return of the condensate to the evaporating region through capillary forces without the need of gravity forces. With this technology, the HP is no longer restricted to a vertical position [57].

As explained in Chapter 1, VCHPs, besides the condensable fluid, also comprise a reservoir and a non-condensable gas attached to the condenser, operating in wider ranges of heat fluxes and temperature gradients this way, it is possible to regulate the temperature at which the phase change will start to occur, enabling a temperature controlled heat transfer process. Also, VCHP active condensation area will range according to the thermal load, where the generated amount of vapour is proportional to the available thermal power. The vapour mass generated pushes the non-condensable gas out of the active condenser region, expanding the active condenser area. Significant pressure increases are prevented due to an expansion tank that accommodates the extra vapour mass present in the VCHP during high thermal power events [45].

2.7.1 Variable Conductance Heat Pipes Operation

The VCHPs operation is fairly the same as HPs but filled with two fluids: a non-condensable fluid and phase change fluid. This enables different thermal conditions to occur inside the pipes, according to the pre-charge pressure with which the non-condensable gas was inserted, instead of a constant state of saturation like in the HPs. The VCHPs will only begin the heat transmission when the saturation condition is achieved, under specific temperatures. This temperature can be adapted to each application by regulating the preload pressure of the non-condensable gas, establishing the boiling temperature of the phase change fluid. As mentioned above, the VCHPs feature two different regions under two operations: the active region, where heat is absorbed and vapour generated and the inactive region occupied by the non-condensable fluid, where the thermal transfer rates are practically null. These regions will have different sizes depending on the available power. When in the presence of high thermal loads, the vapour region will increase, shrinking the non-condensable gas area [11].

The possibility of a variable active heat transfer area makes these devices useful for waste recovery applications when the thermal loads are not constant and the temperature grades have limits. Thus, when in the presence of excess heat the VCHPs absorb this thermal excess until their saturated state generating vapour and filling a portion of the pipes downstream to the cooler regions, where it condensates and releases heat. Figure 23 displays the simulation results of the application of VCHPs in a waste recovery system, designed by Uminho research group, [11], which conceptually is similar to the system assessed in the present dissertation. The VCHPs are absorbing the excess heat, absorbed by the HE (red line), accumulating it (light orange line) until the first 7 cm, while the VCHPs working fluid is in a state of saturated vapour. Beyond the 7cm, since no excess heat is present, the vapour starts to condensate releasing heat (dotted black line) to the colder sections until no vapour is left beyond the 20 cm. At this stage all excess heat has been absorbed and released, thus this region is inactive (or adiabatic), filled with the non-condensable gas [11].

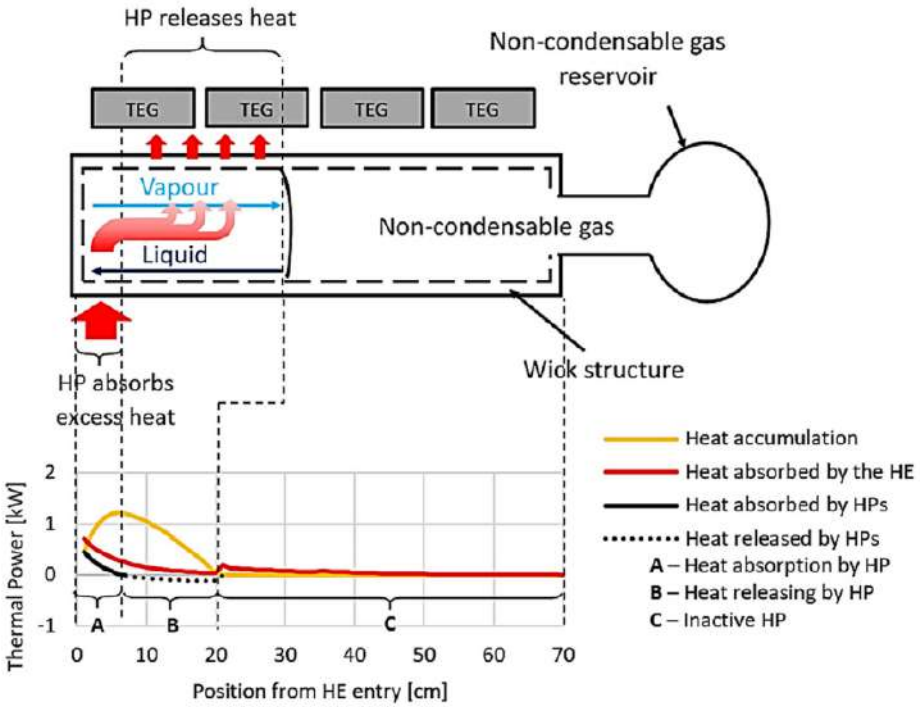

Figure 23: Schematic representation of the excess heat spreading by VCHPs [11]

2.7.2 Vapour Chambers

Also referred to as flat plane HPs, VCs are recent devices for effective heat transfers within high heat flux sources. These devices are commonly used in the electronics industry as heat spreaders from high flux integrated circuits. Like HPs, the heat is absorbed in the evaporator area causing the two-phase fluid to evaporate and cross the VC until the condenser zone, where the heat is absorbed by the heat sink condensing the fluid, which goes back to the bottom by the wick structure allowing the cycle to repeat. The dynamic is similar to the HPs but, instead of the heat being transferred axially, in VCs the heat is mostly transferred across the thickness of the VC due to its rectangular design. These devices can also be filled with a non-condensable gas providing a variable conductance characteristic. One of the ways in which VCs may be implemented is by direct machining of a surface and then tighting the VC cavity adding a cover. This can be done in the body of the HE. For instance, the HPs of the concept shown in Figure 3 (used in [11]) could be substituted by such VCs machined in the aluminium body [58].

2.7.2.1 Wick Structures

VCs can either have a traditional wick system, where the wick structure is the same along with the VC, or can follow a hybrid arrangement where different types of wicks are used. Traditional wick structures include screen mesh, grooved or sintered powder. A screen mesh, Figure 24a, is composed of a multi-layered metal usually of copper. These wicks tend to have larger permeability. A grooved wick, Figure 24b, is made of channels machined on the internal walls of the VC either from copper or stainless steel. Sintered metal powders, Figure 24c, are designed to provide specific capillary and liquid transport properties, usually of copper and tend to have the highest effective thermal conductivity. Some hybrid VCs have the combination of the wick types, for example, is possible to have an evaporator area with a mesh wick and a grooved condenser, which increases the heat transfer rates [58, 59].

(a) Screen mesh wick [60]

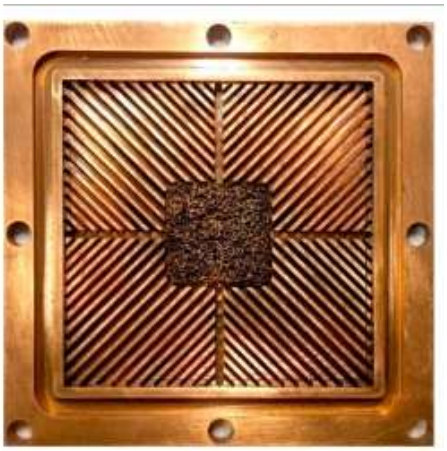

(b) Grooved wick [61]

(c) Sintered metal powder [62]

Figure 24: Wick structures in copper

2.7.3 Working Fluids

The working fluid selection must be done considering the operating temperature gradients, the operating pressure range and the limits to be imposed on the heat flux. Besides, compatibility with the VC materials, either avoiding its corrosion and enabling the wettability, thermal and chemical stability, and suitable vapor pressures are factors to be taking into consideration. The working fluids should have:

1. High latent heat - enables greater heat transfer per unit mass of fluid vaporized;
2. High thermal conductivity;
3. Low liquid and vapour viscosities;
4. High surface tension

Common working fluids used on VCs are presented in Table 4, DowTherm-A is being taken into consideration for the present study, as it has the same boiling point temperature as the maximum operating temperature of the commercial available TEGs hot face .

Table 4: Working fluids and temperature ranges of vapor chambers [58]

Working Fluid	**Melting Point (°C)**	**Boiling Point at atm. pressure (°C)**	**Range (°C)**
Refrigerant 141b	−103.5	32.1	-
N-Pentane	−129	36	-
Acetone	−95	57	0 to 120
HFE7100	−135	61	-
Methanol	−98	64	10 to 130
Ethanol	−112	78	0 to 130
Water	0	100	30 to 200
Propylene glycol	−59	188.2	-
DowTherm-A	-12	250	12 to 400

2.7.4 Wick Dynamic Structure

The evaporation, condensation and fluid transport rates depend on the VC, mainly the wick part, geometric, and structural properties: porosity, pore size, permeability, surface area, thermal conductivity and wettability by the working fluid. The major operating limit is the capillary limit. In order to the VC work , the capillary pressure generated in the wick, P_c must be greater than the total Δp:

$$P_c \geq \Delta p_l + \Delta p_v + \Delta p_g \tag{16}$$

Where Δp_l is the required pressure to return the liquid from the condenser to the evaporator, Δp_v the pressure necessary to make the vapour flow from the evaporator to the condenser and Δp_g the gravitational head. The maximum mass flow rate promoted by the wick can be expressed by the equation (17) [57].

$$m = \frac{\rho_f K A_{c_f}}{\mu_f L}(P_c - \rho_f g_f L_f) \tag{17}$$

Where K and $L_w$is the permeability and length of the wick and $\rho, A_{c_f}$and g_l are the working fluid properties, density, section area, viscosity, acceleration due to gravity respectively [58].

Chapter 3

System Analysis

The development approach of the system under study is supported by real driving data from a conventional HDV, that is simulated with standard driving cycles. The HDV simulation is performed using these these cycles after providing the software (AVL Cruise) with the vehicle data, namely the vehicle mass and aerodynamic and rolling resistance coefficients, as well as engine maps. The software the provides as an output the instantaneous exhaust temperature and mass flow rate. This data is then integrated in the heat recovery system model to calculate the system electrical output over the time. The validation of the model has been partially done through computational models and has also been done experimentally recently in the scope of a parallel ongoing dissertation work. For a more functional development, the main objectives requirements and obstacles to be completed should dissected and solved, the system interactions exposed and the simulation environments associated.

3.1 Systematic Design

Figure 25 shows the methodology for the development of the TEG system. There are four major sequential steps for the achievement of the final design, as well as the limitations the system has to be able to overcome.

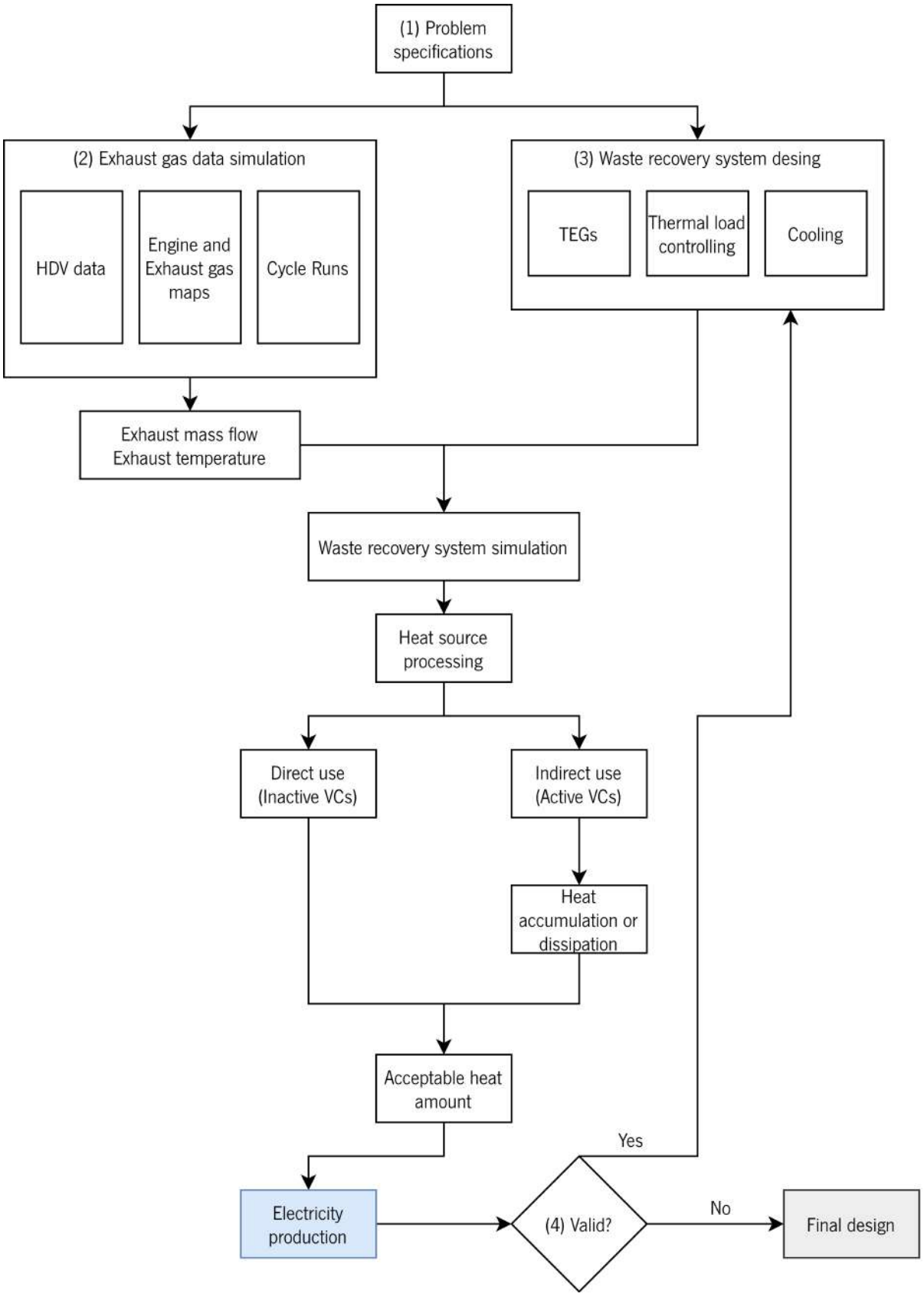

Figure 25: Flow chart for developing the waste heat recovery system

1. **Problem specifications:** The main goals, limitations, and system features are discussed. The settled main goal is the production of electricity from waste heat. However, the technology used for this conversion does not simply take the heat directly from the exhaust gases and convert it into electricity. Thus the thermal control is mandatory. For an attractive design, the model has to be compact (low volume, and low wight), with simple integration in other HDVs, hence easy maintenance and no moving parts, and finally effective and simple to control.

2. **Exhaust gas data simulation:** Since the purpose of the system in development is to use the thermal load from the exhaust gas, the simulation of an HDV with real driving cycles and different loads endorses the viability of the TEG system modelation. Specification maps from a real HDV should be used. From this simulation, two major values are crucial: exhaust gas mass flow rate and exhaust gas temperature values along the driving cycle.

3. **Waste heat recovery system:** This system has to be capable of controlling the thermal load from the exhaust gas (simulated data) as the hot face of the modules is attached to the surface of the exhaust HE. If the temperature is higher than the working temperature of the TEGs, the system will dissipate the heat along with the VCs, if it is too low the heat will be absorbed by the HE will be transmitted by conduction to the modules without any phase change, activating only a few modules. Besides, since the modules require a wide temperature difference a cooling system should be placed on top of the cold face of the modules.

4. **Valid system:** The final design is ready when the system is able to produce a greater amount of electricity than the pumping power due to the generated pressure drop.

3.2 System Interactions

The stimulation method of this approach relies on the dependency of the two major components, the heat source and the electricity generator. The system interactions are presented in Figure 26, where the lines represent energy fluxes. Part of the fuel goes to the engine radiator, to the exhaust system and to produce mechanical power. This mechanical power goes both to move the vehicle or goes to the alternator which produces electricity. Part of energy flowing from the exhaust system through heat is converted by the TEG system into electricity, which depends on a HE to control the thermal load and to keep the needed temperature gradients, the rest is lost to the environment through heat. The TEG system will produce electricity aiding the alternator response to the electrical needs of the HDV, thus reducing the fuel consumption.

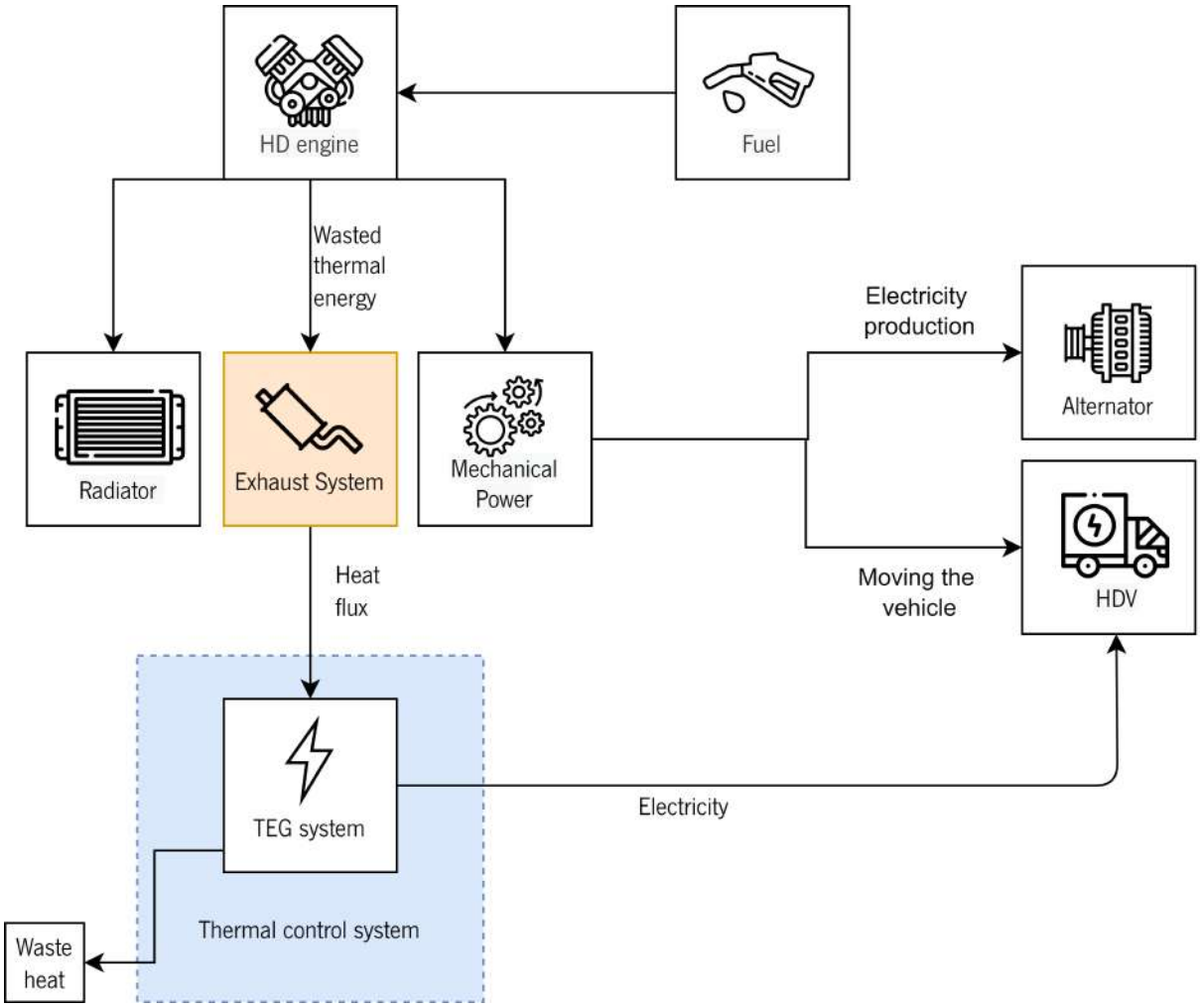

Figure 26: System interactions

3.3 Simulation Environments

Three major simulation/modeling environments have been used in this project. The project can be characterized by two simulation milestones, the HDV simulation and the TEG system simulation. For the HDV simulation the CRUISE and BOOST applications from AVL allow the fully exploitation of a real HDV. AVL CRUISE is a flexible vehicle driveline simulation solution that can output the needed data due to its numeric solver and the ability to run real time applications. Here all the components (such as the engine, trailer and wheels) and simulation barriers (cycle runs and weight loads) are defined. CRUISE interpolates the components data with the simulation barriers, providing, after the simulation, results, for instance, of the engine power, fuel consumption, exhaust gas mass flow rate and temperature for each cycle point. CRUISE simulation has to run simultaneously with a BOOST model to provide information regarding the exhaust gas. In BOOST is possible for the user to simulate (and not only define like in CRUISE) vehicle components, here an exhaust gas after treatment system was simulated.A Matlab algorithm is used to

facilitate the data gathering from the AVL simulations. For the design of the TEG system concept, CAD tools are the most indicated, mainly AutoCad and Inventor, both from Autodesk Inc.. The thermal analysis can rely on COMSOL Multiphysics software with a "Heat transfer in Solids"approach, where is possible to attribute the materials, heat transfer coefficients, and temperatures to the components and analyze the final conductive heat fluxes or temperatures. Due to the complex geometry a 2D thermal simulation was done to enable the calculation of the thermal resistances of the system. Subsequently, a Matlab algorithm simulates the system with all its variables, including the thermal resistances obtained through the COMSOL simulation, and delivers not only the amount of electricity produced but also the pressure drop and an analysis of the modules activated during the cycle. Depending on the results, primarily, electrical load, pressure drop, thermal resistance, and weight, the system is optimized until suitable results are achieved. Figure 27 represents the connection of the described software tools.

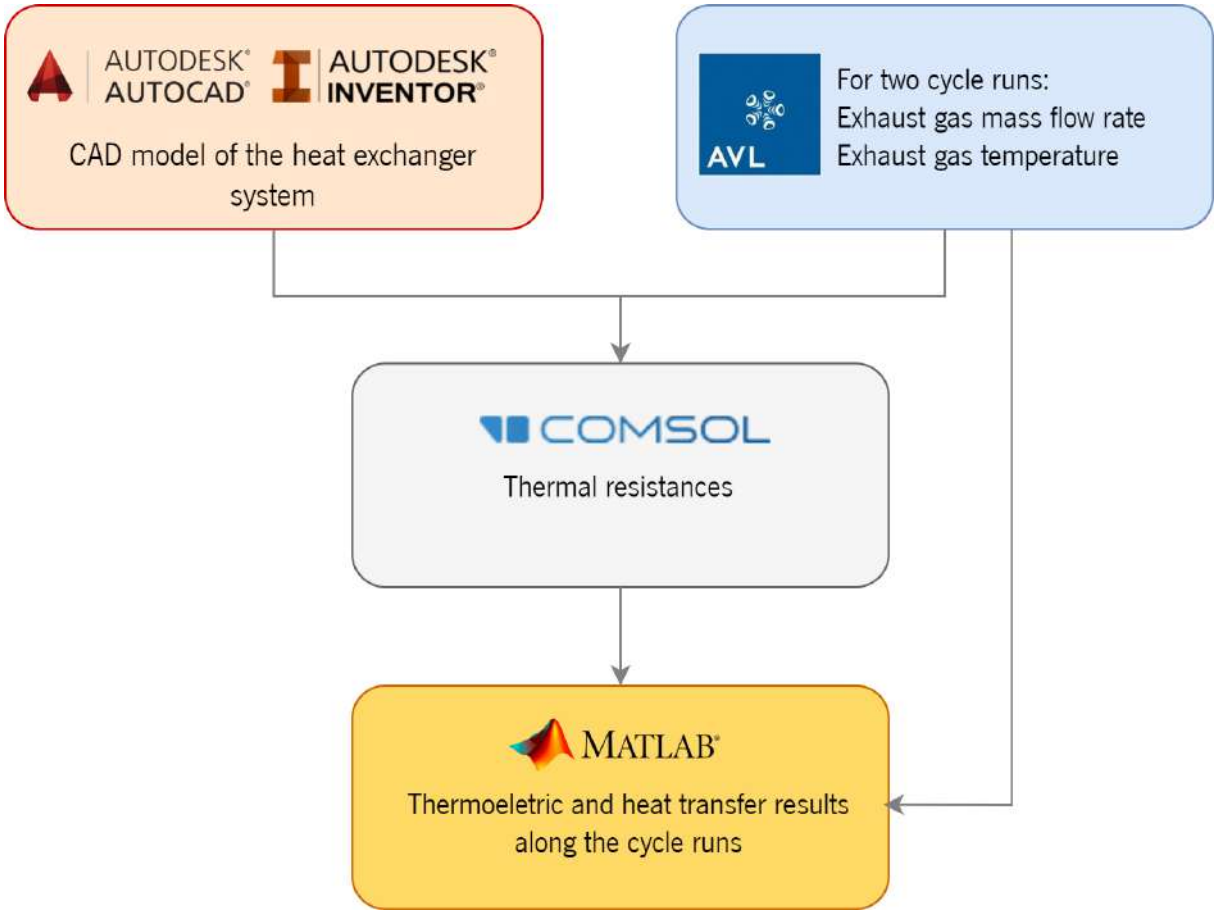

Figure 27: Simulation environments connection

Chapter 4

Heavy-Duty Truck Simulation

The realistic simulation of the performance of a generator applied to an HDV during a driving cycle requires the prediction of the HDV operation during that cycle. Namely, it is necessary to predict the engine load and speed required to perform the driving cycle and the resulting exhaust temperature and flow rate along the duration of the driving cycle. The present chapter approaches the transient simulation of an HDV, focusing on the simulation software, the vehicle setup, engine specifications, load, and cycle runs. For a complete specification of the vehicle simulation refer to Annex II.

4.1 Software Analysis

The integration of the AVL CRUISE software made possible the simulation of an HDV. AVL is a company that focuses on the development, simulation, and testing in the automotive industry featuring several programs like AVL CRUISE and BOOST. AVL CRUISE software is qualified for simulating the driving performance, fuel consumption and emissions, transmission ratios, braking performance, and drive train vibrations, and so on. Is important to have in mind that CRUISE main function is to simulate fuel consumption and emissions within designated conditions, and not to simulate, for example, an engine. The engine has to be defined not only with its generic characteristics, like cylinder number and displacement, but also with specific maps like the performance maps, exhaust gas temperature, and motoring curves. Then the final results are obtained by iterations according to the chosen calculation method. If the simulation is dependent on the cycle run, the driving velocity profile, and the course conditions are defined. If the cruising task is applied, driving on a real road is simulated and the distance-based velocity profile is defined as top speed, which may not be exceeded. And if the user selects constant drive, the fuel consumption and emissions are calculated for running with constant speeds. For a precise simulation of the engine, another software

is used, AVL BOOST. AVL BOOST simulates a wide variety of engines, 4-stroke or 2-stroke, spark or auto-ignited, and can also simulate the chemical and physical processes occurring in the EATS. It is possible to run a CRUISE-BOOST co-simulation by applying interface modules. The AVL CRUISE simulations has followed the presented workflow:

1. **New project or version**

   AVL CRUISE offers the option of starting a new project from blank or adapting pre-created templates into different versions. For instance, several HDV models, LDV, with SIE or ICE or hybrid and electric, off-road vehicles and motorcycles are granted. Here a commercial truck template was adapted.

2. **Components Input Data**

   In this stage, all the vehicle components are defined. These components are arranged into groups, Vehicles, Clutches, Gear Box, Engines, Electrical Modules, Controls, Brakes, Auxiliaries, Special Modules, Interfaces, Wheel, and Macro Modules. The engine specifications (displacement, number of cylinders, number of strokes, fuel, among others) and engines maps were defined.

3. **Connections**

   Two types of connections are possible to join the system, energetic and informal connections. Energetic connections transfer energy and are divided by the type of energy being transferred: mechanical, exhaust system, and electrical. Informal connections transfer information to the data bus between the components. For this example, the cockpit delivers the information about the actual load signal to the engine, where it is used to determine the output torque.

4. **Project Data**

   In the Project Data it is possible to create several task folders, different simulations run with the same model. Is possible to run the model with several cycle runs, load states and friction coefficients. Also, the calculation settings (number of iterations, type of numerical analysis, accuracy) and outputs format (is possible to create results files for Matlab) is defined .

5. **Run Calculation and Result Analysis**

   After running the simulation in the Calculation Center the results are graphically presented in the Result Manager and saved in the designated file in the form chosen in the Project Data.

4.2 Heavy-Duty Vehicle Model Simulation

The HDV in this study was obtained by reformulating a layout of a commercial HD truck in CRUISE. For this purpose, the engine characteristics were defined and an interface model, AVL Exhaust System, was

added and coupled with an AVL BOOST aftertreatment, to allow the inclusion of exhaust data into the analysis. The calculations were done to three weight load states, empty, half and full, and two cycle runs were performed and analyzed.

4.2.1 Operational Parameters

The HDV design used for the study is represented in Figure 28. The several components must be defined in order to correctly run the simulation. For instance, in the tractor and trailer geometrical parameters like dimensions and weights are defined and the road and air resistances and dynamic wheel loads are calculated for road and dynamometer runs based on the dimensions and the load state of these components. Based on the wheel load the rolling drag is also computed. The HDV consists of a tractor with a 4x2 drive-train and 7050 kg of curb weight with an attached 3 axle trailer with a gross weight of 25500 kg and a 15.9 litre in-line six-cylinder diesel ICE and 384 kW rated power. This represents a typical long haul HDV. The most important layer for this project is the drive-line, highlighted in Figure 28, which covers the main components, to be discussed further on, as well as the energetic connection lines, blue for mechanical connections and grey for the exhaust ones.

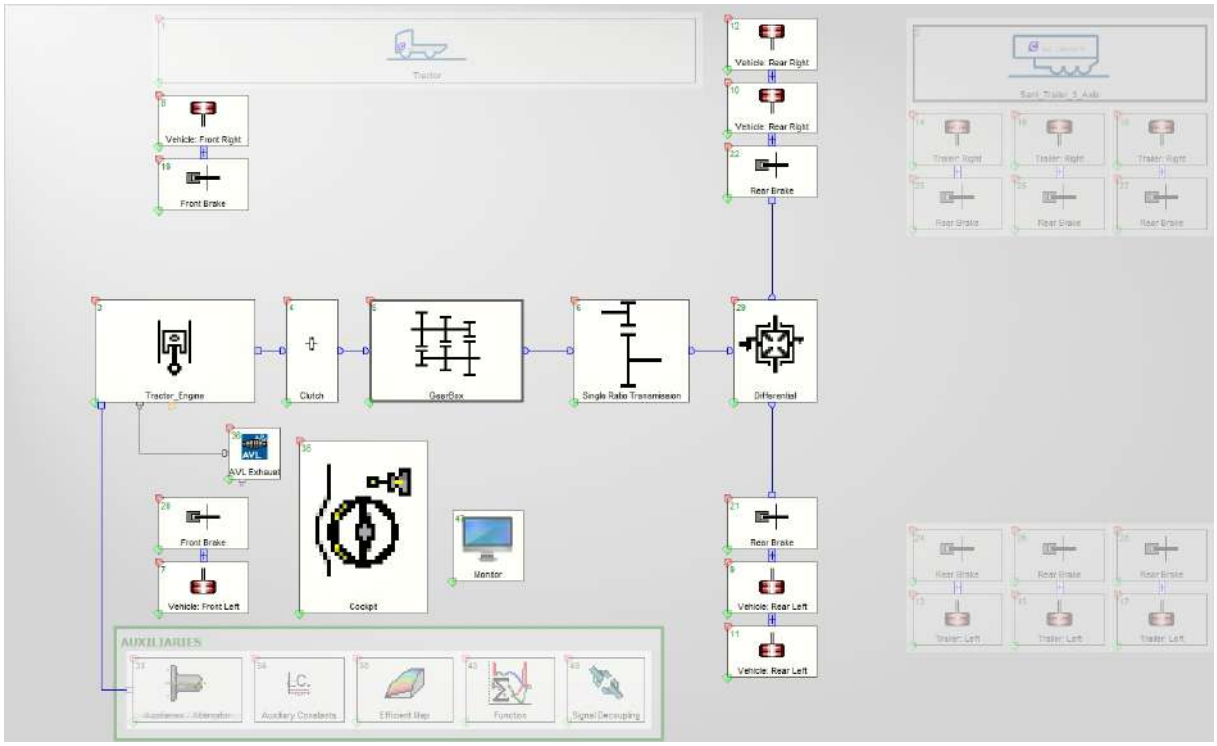

Figure 28: HDV CRUISE setup

4.2.1.1 Tractor and Trailer

The tractor and trailer components contain general data of the vehicle like geometrical parameters (dimensions and nominal weights) and road and air resistances. The parameters used are presented in Table 5. This data is part of the commercial HDV template from AVL. Within these inputs, the dynamic wheel loads and resistance forces are calculated by AVL. The dynamic wheel loads are calculated for road and dynamometer runs based on the dimensions, the load state, inclination, acceleration, height of the gravity center. The driving resistance was analyzed by physical values, drag coefficient, and rolling resistance. Therefore, the force of resistance is the addition of the air drag force and the longitudinal force that is caused by the road inclination.

Table 5: Tractor and trailer input settings (AVL CRUISE commercial HDV template)

TRACTOR				
Gas Tank Volume			275 L	
Vehicle Body dimensions				
Distance from Hitch to Front Axle			7120 mm	
Wheel Base			6070 mm	
Height of Support Point at Bench Test			200 mm	
Load Dependent Characteristics				
Load State	**Gravity Center Distance**	**Gravity Hitch Height**	**Height Hitch**	**Tire Inflaction Pressure Front/Rear Axle**
empty (7050 kg)	2250 mm	952 mm	400 mm	9 bar
half (7275 kg)	2855 mm	935 mm	390 mm	9 bar
full (75000 kg)	3363 mm	900 mm	368 mm	9 bar
Nominal Weight				
Curb/Gross Weight			7050 / 7500 kg	
Aerodynamic drag data				
Frontal Area			10.28 m2	
Drag Coefficient			0.7	
TRAILER				
Trailer Body dimensions				
Distance from Hitch to Axle				7700 mm
Distance from Axle to Rear Hitch				4500 mm
Load Dependent Characteristics				
Load State	**Distance Gravity Center**		**Height of Gravity Center**	**Tire Inflaction Pressure**
empty (7500 kg)	-650 mm		1150 mm	9 bar
half (12750 kg)	-1000 mm		1450 mm	9 bar
full (25500 kg)	-1700 mm		1850 mm	9 bar
Nominal Weight				
Curb/Gross Weight			7500 / 25500 kg	

4.2.1.2 Tractor Engine

The tractor engine component contains the model for a combustion engine incorporating a turbocharger with an intercooler. The geometric parameters, the characteristics for full load, motoring curve, fuel consumption maps, and the exhaust mass flow and temperature curves were defined based on a literature engine where the engines maps were obtained ([63]). As mentioned above, AVL CRUISE is not intended for the simulation of the engine as a single unit but it integrates the engine maps data to estimate engine load and speed over time, integrating it within the whole vehicle. So, the engine parameters (full load, motoring curve, fuel consumption, exhaust gas mass flow and temperature) must be pre-defined and the outputs are the result of the iterations between the simulation boundaries (cycle runs and weight loads) and the HDV demands with the HDV definition. Table 6 presents the primary parameters of the engine and Figure 29 the maps regarding the full load, brake-specific fuel consumption (BSFC), exhaust mass, and temperatures used in the simulation introduced in CRUISE. The fuel consumption map was calculated by selecting several points from the BSFC map and applying equation (18) and (19).

Table 6: Truck engine primary parameters [63]

Type	**Parameter**	**Unit**
Cycle	4 strokes	-
Displacement	15999	cm^3
Number of cylinders	6	-
Valves per cylinder	4	-
Fuel	Diesel	-
Fuel Heating Value	44000	kJ/kg
Fuel injection system	Common-rail	-
Engine speed range	[800 - 2000]	rpm
Maximum power	384 (515)	kW (hp)
Maximum torque	2292 at 1200	N.m at rpm
Emission Standards	EURO VI	-

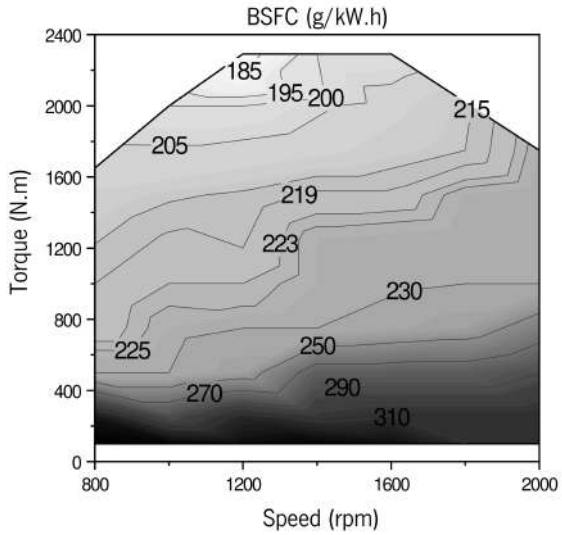

(a) BSFC map

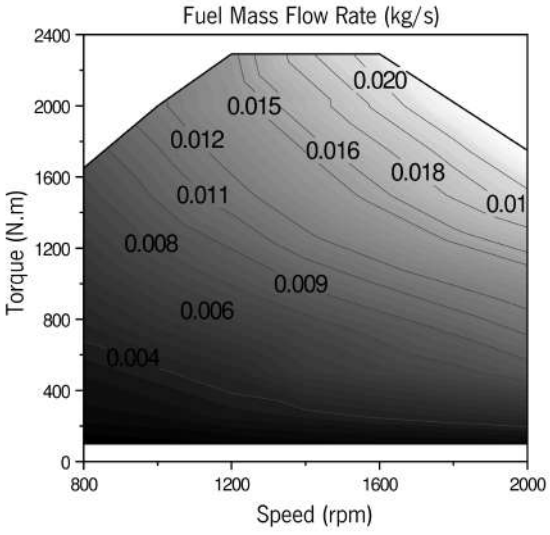

(b) Fuel consumption map

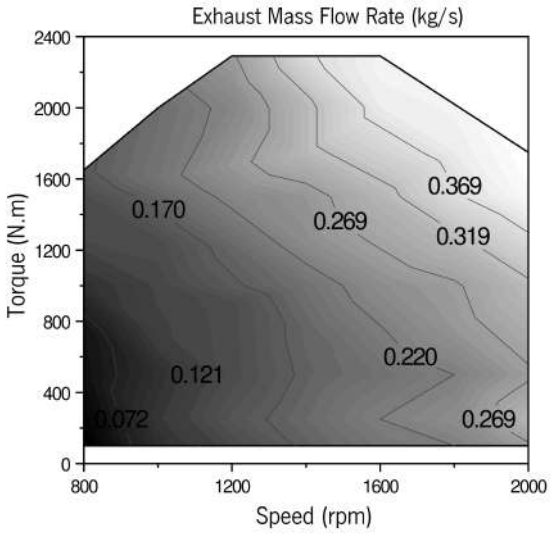

(c) Exhaust mass flow rate map

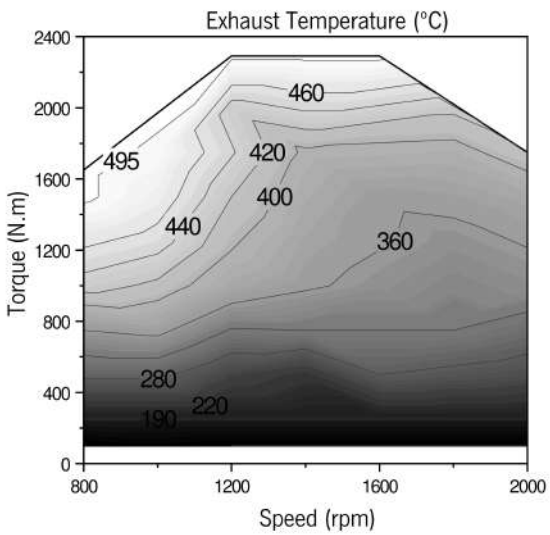

(d) Exhaust gas temperature map

Figure 29: Engine specification maps used for interpolation [63]

$$BSFC = \frac{\dot{m}_f \times 3600}{\dot{W}_e} \tag{18}$$

$$\dot{W}_e = 2\pi NB \tag{19}$$

4.2.1.3 AVL Exhaust System

A special component is necessary to add to the setup for the evaluation of the exhaust gas after the EATS, where the HE system is to be placed. Thus, a simulation of and EATS was obtained from the available layouts in BOOST, present in Figure 30.The AVL Exhaust System is a component that supplies a connection to the aftertreatment system of BOOST and enables the coupling with the BOOST aftertreatment model, .atm file, in the CRUISE vehicle simulation. This is a crucial component because it enables the calculation of the exhaust gas temperature and mass flow, the main outputs for this study. The system has one DOC and one SCR which are sized for a HDV. Since the purpose of this simulation was only to analyze the exhaust mass flow and temperature, the pollutant emissions were not calculated. Therefore, for means of simulation simplification, and because CRUISE requires another AVL Exhaust System component per catalyst, the DPF was not included. Without the AVL Exhaust System component, CRUISE couldn't provide any information about the exhaust gases.

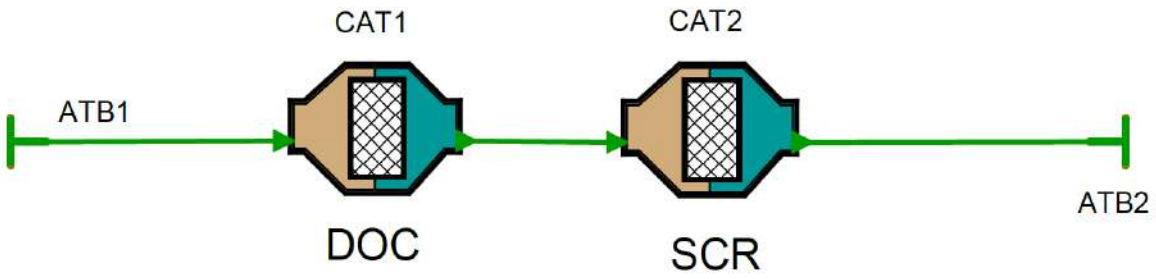

Figure 30: Exhaust aftertreatment system setup in AVL BOOST

4.2.2 Project Parameters - Cycle Runs

Two cycle runs were used, WHVC, Figure 31, and a Long Haul cycle, Figure 32. The WHVC, usually used for HDV certification, was obtained from literature ([16]) and introduced in CRUISE. In the Long Haul cycle run, available in the CRUISE libraries, the HDV reaches a maximum velocity of 85 km/h along 100 km with different inclinations. This cycle was also simulated because, besides the fact that HDVs travel very long distances, it can represent a regional delivery with a longer distance than WHVC, aiding the visualization of the HE performance.

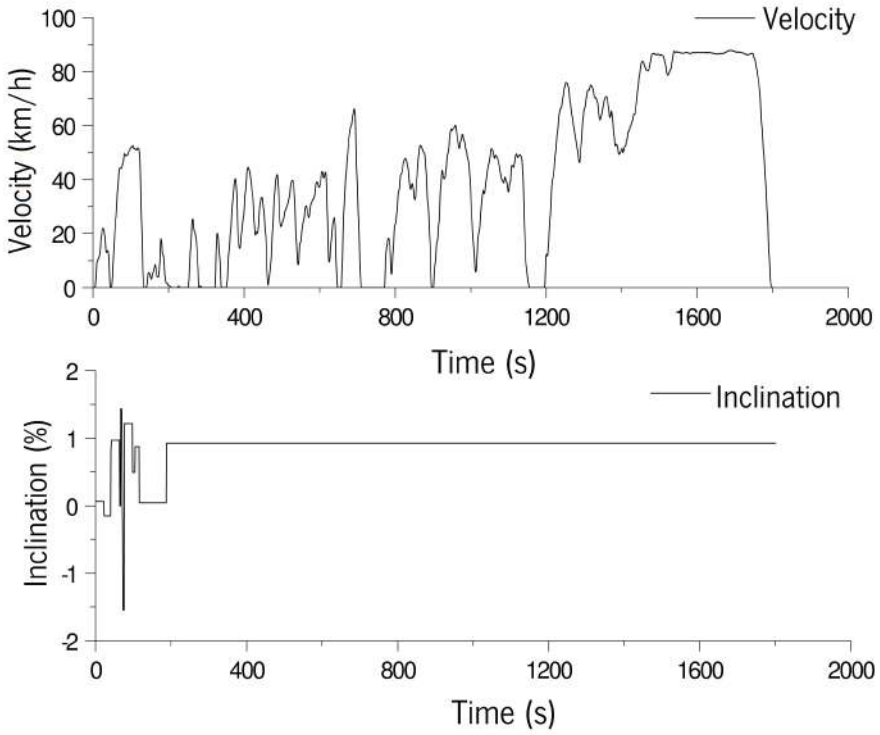

Figure 31: WHVC parameters [16]

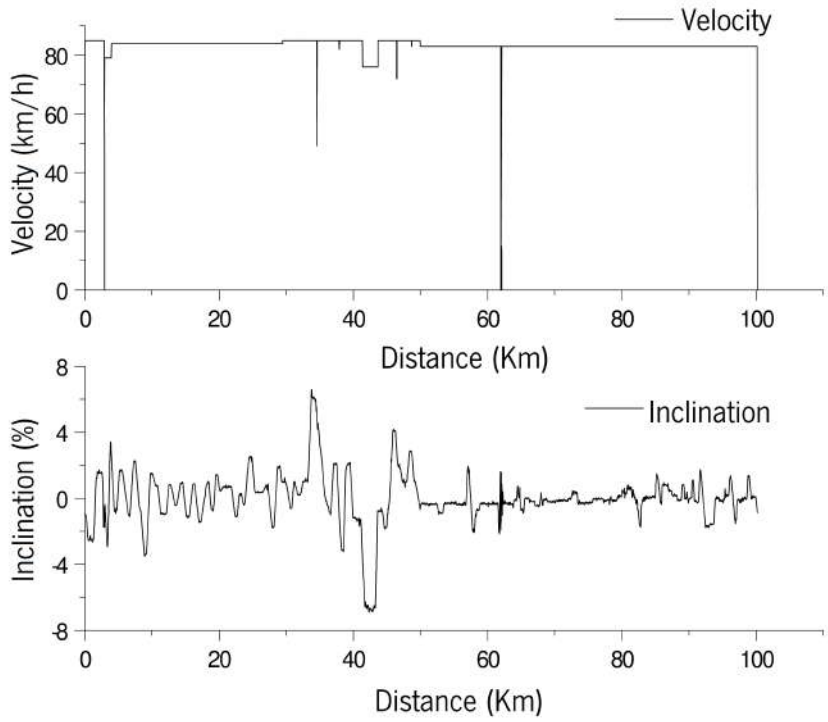

Figure 32: Long Haul cycle run parameters from AVL software

4.3 Simulation Results

The maximum and average values of the engine power, exhaust temperature, exhaust mass flow rate and exhaust power, can be visualized in Figure 33, here is possible to compare the difference between the weight loads in the WHVC cycle and the Long Haul. Figure 34 illustrates the exhaust power outputs from the engine simulation along with two driving cycles with different weight loads, where is clear the heterogeneous contour surfaces in both maps. The dynamic behaviour of both exhaust and mass flow values after the EATS is one of the main motivations for the implementation of HE capable of controlling these gradients. Detailed data about both the full cycle simulations, WHVC, and Long Haul, is presented in Annex III where the several engine maps obtained by the simulation of the driving cycle can be found. The exhaust temperature and mass flow rate are, as expected, higher at higher weight loads (as the the weigh load increases the the point cloud moves to higher powers levels). Figure34 to Figure 38 reflects the exhaust power dependence on the two driving cycles by the different weight load settings and consequently by the engine power needs. Since the exhaust heat flow depends on the necessary engine power and because the Long Haul driving cycle has higher inclination gradients, more power to overcome the inclination is needed, this justifies the higher values of exhaust thermal power in the Long Haul driving cycle. For more profitable reasons, commercial HDV travel most of the time with the maximum curb weight on long distances, and on average, HDVs spend at least a quarter of the route on maximum engine power due mostly to different inclination gradients, this leads to higher exhaust energies and higher wasted energy to be recovered.

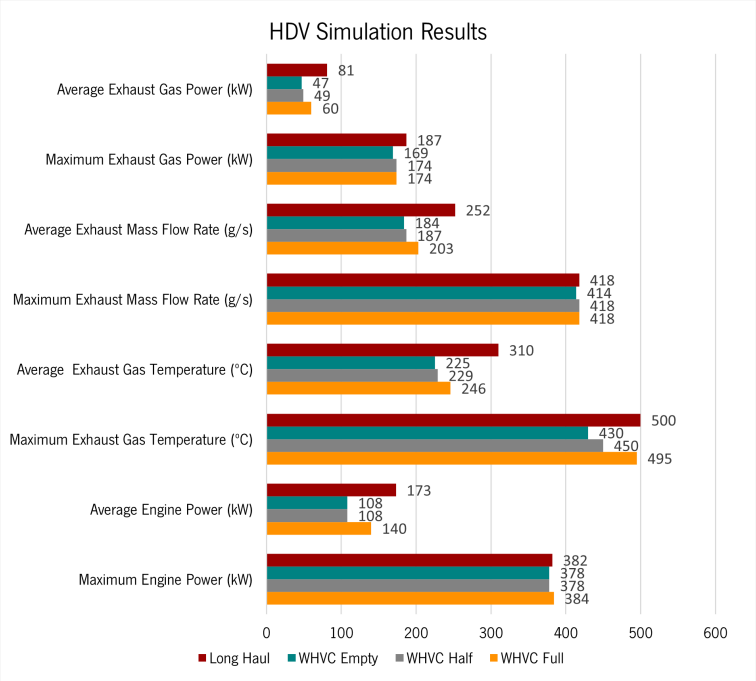

Figure 33: AVL simulation results for each driving cycle

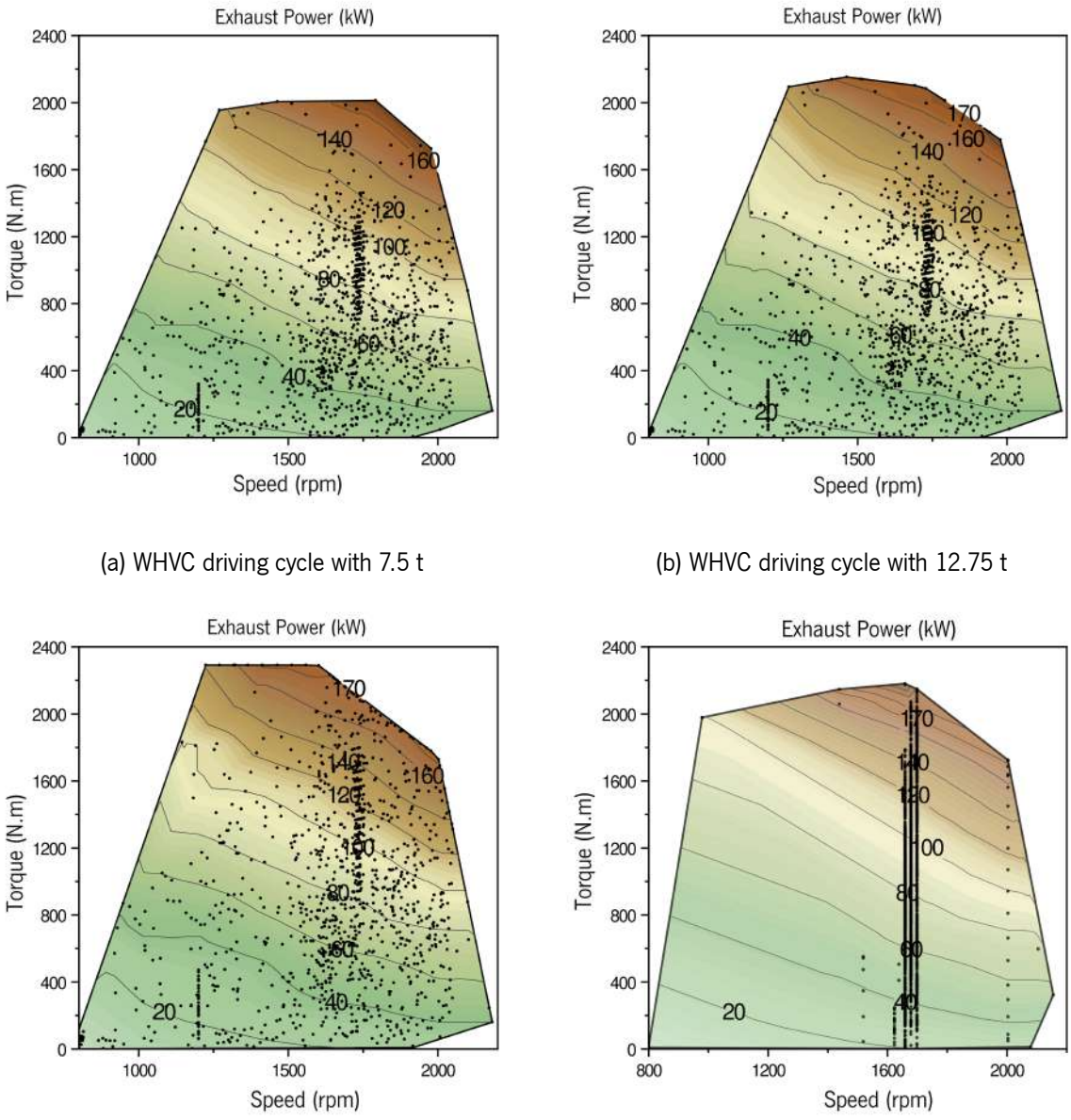

(a) WHVC driving cycle with 7.5 t

(b) WHVC driving cycle with 12.75 t

(c) WHVC driving cycle with 25.5 t

(d) Long Haul driving cycle with 25.5 t

Figure 34: Engine load points along the engine map, for the WHVC and the Long Haul driving cycles

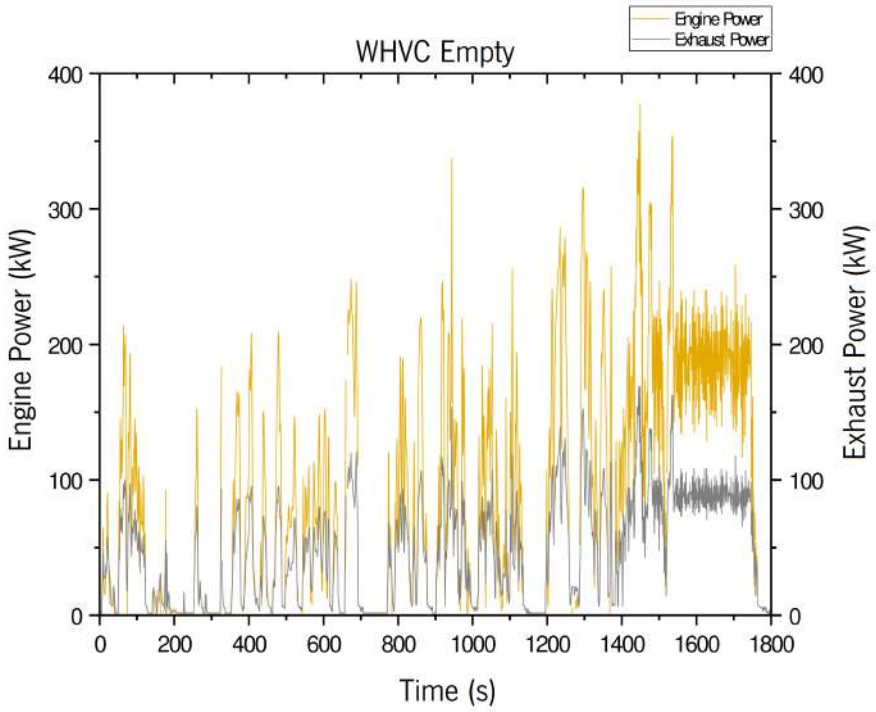

Figure 35: Engine power and exhaust power along the WHVC cycle run with 7.5 t

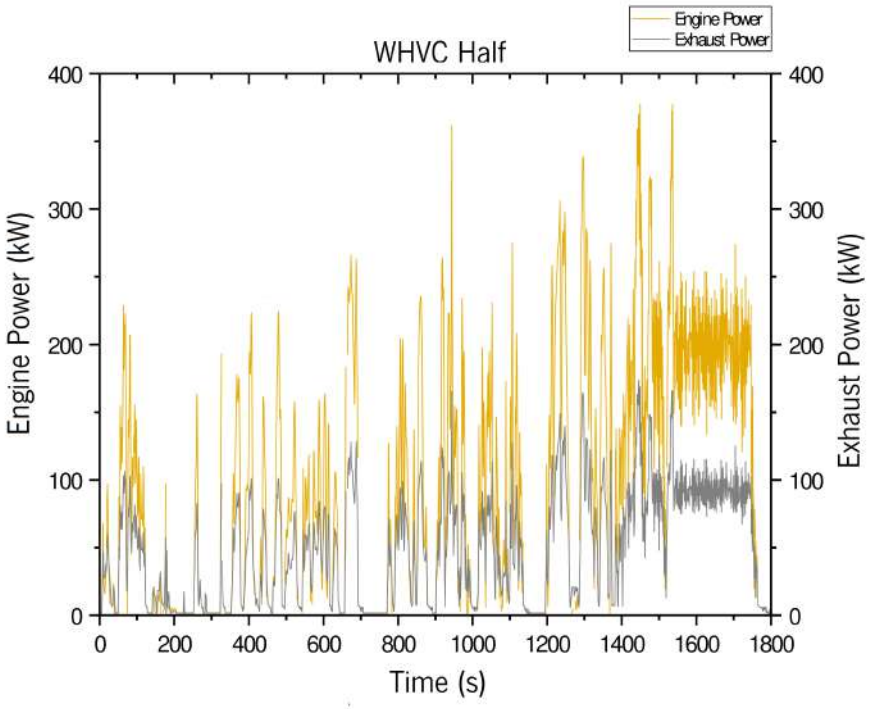

Figure 36: Engine power and exhaust power along the WHVC cycle run with 12.75 t

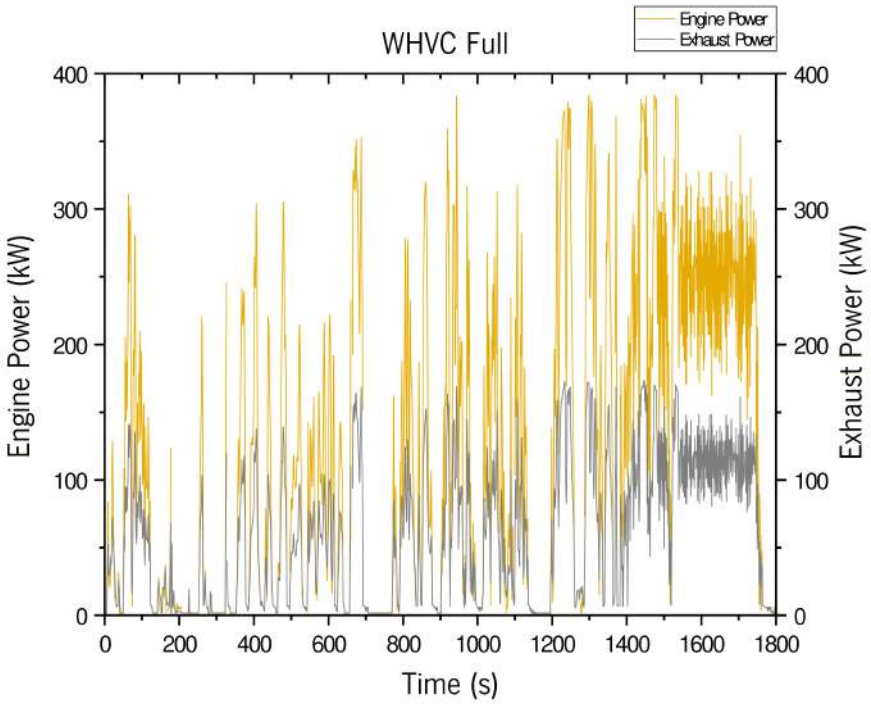

Figure 37: Engine power and exhaust power along the WHVC cycle run with 25.5 t

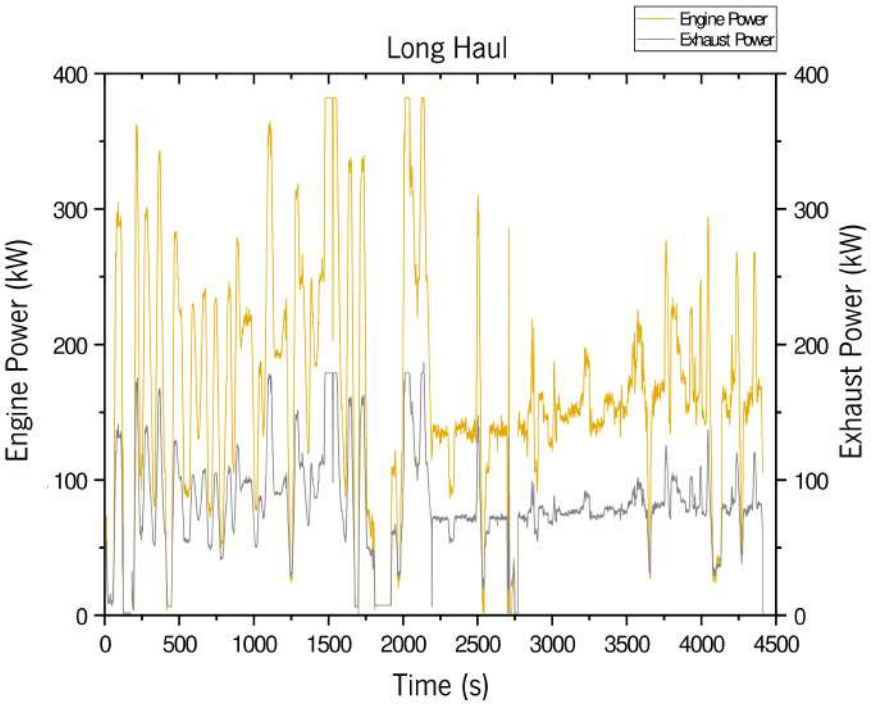

Figure 38: Engine power and exhaust power along the long Haul cycle run with 25.5 t

Chapter 5

Model Design

5.1 System components and working principle

For a comprehensive analysis of how the system works and how its thermal simulation is performed, the first step should be the exploitation of each of the components. The system proposed consists of a HE that absorbs the exhaust heat through WFs embedded in cast aluminium represented in Figure 39. Then, it transfers this heat by conduction across the aluminium to the TEG modules that are attached to the surface of the aluminium block. A part of the heat absorbed by the modules is converted into electricity, while the rest of the heat crosses the TEG modules by conduction and is dissipated to the heat sinks attached to the cold faces of the TEG modules, here called CP, where a water flow exists. Now, this system has a specificity, which is the ability to spread the heat from overheated regions of the HE to underheated regions avoiding excess temperature and providing heat flux uniformity. To implement this thermal management, vapour chambers have been embedded in the heat exchanger, between the exhaust flow and the hot face of the thermoelectric modules. As long as the temperature is below the maximum, these VCs are inactive. Once the maximum allowable operating temperature is overcome at the upstream regions of the HE, the working fluid that is contained within the VCs starts boiling and absorbing the heat at the overheated regions and then releases this heat by condensation at the cooler downstream regions of the HE. The WFs are embedded in cast aluminium at the center of the HE. Above and below the WFs the VCs have been machined, including laser textured surfaces to improve phase change heat transfer (as is being currently explored in Project COOLSPOT). Aluminium plates act as covers to the VCs at the inner side. The TEG modules are attached at the outer side. It is important to note that the geometry of these components has still not been optimized. An industrial prototype will have much lower thicknesses and aluminium masses.

Once the exhaust gas starts flowing through the WFs, the heat is absorbed by the HE and is spread

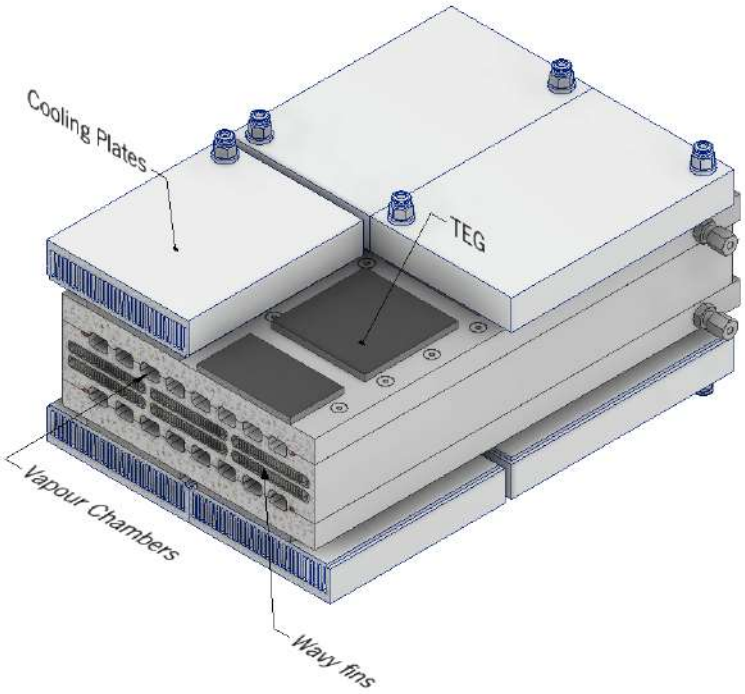

Figure 39: Heat exchanger system scheme

towards the modules. When the temperature that reaches the VCs from the WFs is higher than the VCs's boiling temperature, 250°C, they will turn into "active"devices by absorbing the excess heat, and consequently evaporating the working fluid, this vapor will expand along the VCs until it condensates in regions below 250°C were the heat is released. When the temperatures are lower than the boiling point, the VCs will be inactive and the only type of thermal flux is by conduction through the walls of the VCs. Essentially, when temperatures reaching the VCs are higher than 250°C they become isothermal, otherwise, they will be adiabatic, this enables the thermal control in the HE, both by spreading the excess heat and equalizing the temperature.

5.1.1 Heat Exchanger - Wavy Fins

As mentioned in Chapter 2, the WFs are CHE components of interest due to their great area density which enhances the heat transfer effectiveness. In the system, WFs produced by BorgWarner Vigo were introduced, similar to the presented in Figure 40. All important geometric parameter were measured and culminated in the values presented in Table 7. The WF length is dependent on the HE size so that it can be suitable for the exhaust gas load, thus the length of the wavy fin will be the same as the CPs total length.

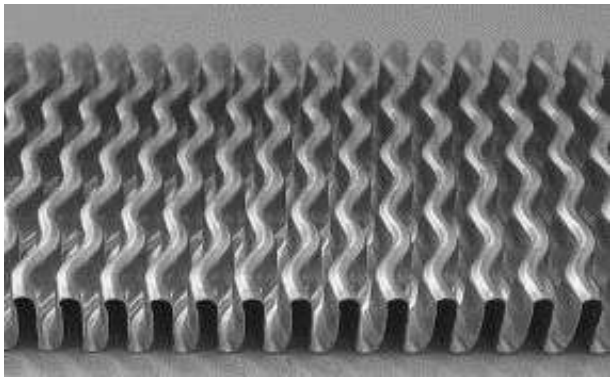

Figure 40: WFs similar to those used in the HE [55]

Table 7: Geometric parameter of WFs (See Figure22)

Geometric parameters (mm)	
Fp	0.0018
Fh	0.0051
s	0.0017
δ	0.0001
2A	0.0008
L	0.02

5.1.2 Vapour Chambers (VCs)

The VCs in the system are part of the CoolSpot project: Interfacial Cooling Strategies for high Power dissipation conversion Technologies. These VCs act as thermal controllers as they transport the heat excess to areas where the limit temperature is not reached. Since the purpose is to prevent the TEGs from overheating, the boiling temperature of the working fluid must be as closest as possible to the maximum temperature of the TEGs' hot face, 250°C. To achieve the main thermal control purpose, keep the TEGs hot face closest to its maximum tolerated temperature, and to address the volatile thermal gradients present in the exhaust gases, these VCs are pressurized with a non-condensable gas, with an adjusted preload pressure for a boiling temperature of the working fluid of 250°C, enabling the variable conductance characteristic. With water as a working fluid, this pressure would be around 40 bar, however, the materials used here, recommend a fluid with saturation pressures at 250 °C which may be closer to ambient. Such fluid could be the Dowtherm-A, which has a saturation pressure around ambient for 250°C. Regarding to the exhaust thermal power, the active and inactive regions of the VCs will occupy different portions of the VCs following the same operation as a VCHP, explained in Chapter 2. Figure 41 represents the VCs channels, without the lid, through where the fluids will flow. Their geometry differs from HPs in the rectangular shape and the manufacturing procedure. These are to be designed and machined by LaMoTA and CoolSpoot researchers in the aluminium block, that follows the WFs. By machining through laser ablation the VCs textures, these can have customized measures, enabling a more suitable design for each situation, and better texturizing

in the wick walls, which improves the nucleation and therefore promotes phase change. These customized VCs are in fact, more similar to VCHPs than commercially available VCs given the heat transfer path. This is not necessarily from the bottom to the top, but longitudinal through the vapour flow path.

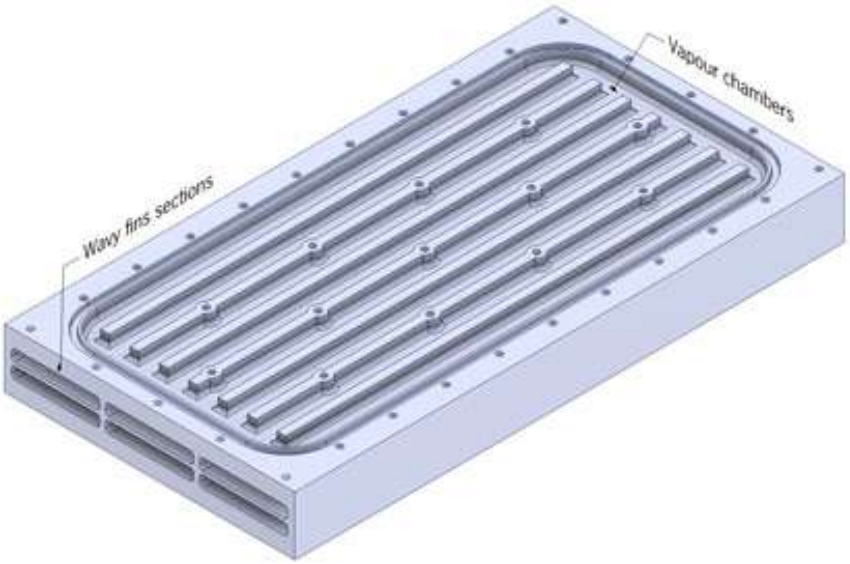

Figure 41: CAD section view of the VCs

5.1.2.1 Texturization of the surface of VCs through Laser ablation for better thermal performance

Along the convection heat transfer process, the heat transfer rate is proportional both to the convective heat transfer and the surface area. The maximization of the surface area is being investigated by the CoolSpot project. In cases where the surface area cannot extend beyond a certain plane's dimension, textures can be created at the milli/micro-scale. One of the most recent ways to produce these textures is by removing material through the incidence of a laser beam. When a solid surface is under laser beam radiation, the solid material absorbs the laser energy and heats up. This produces particle acceleration which, when at the sublimation temperature, sublimate and become vaporized particles. The generation of textures using laser is possible with numerous approaches ranging from geometry, slot depth, slot topology to the creation of dimples. Through the realization of SEM (Scanning Electron Microscopy) and Profilometry analyses, Figure 42, CoolSpot has already observed a significant increase in the heat transfer surface area, creating milli/micro-scale fins in the surface. Experiments showed that the textures allowed the substantial improvement of the convective heat transfer. Their use with phase change is likely to further improve heat transfer, as textures may be used to promote the nucleation of vapour bubbles in vaporization.

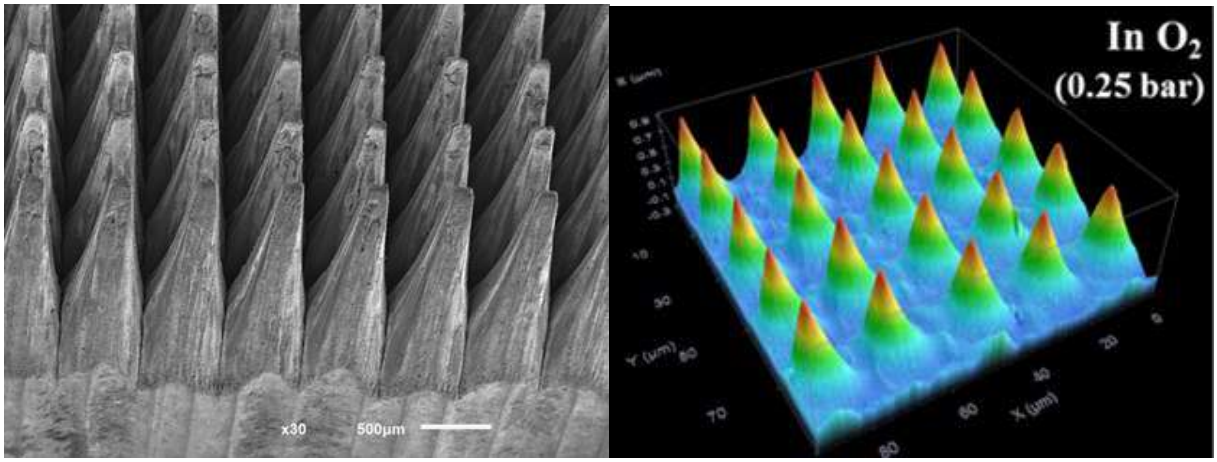

(a) SEM (b) Profilometry

Figure 42: Solid surface analyses: Visualization of the creation of milli/micro-scale fins in the aluminium surface

5.1.3 Thermoeletric Generators (TEG)

The thermoelectric generators in use for the simulations are the GM250-127-28-10 from Adaptive Power Management ([5]). The geometrical features are presented in Figure 43, used for the CAD model construction and simulation. The power curves were provided by the TEG data sheets ([5]) This TEG has a maximum operating temperature of 250°C and 175°C at the hot and cold face, respectively, it is not an especially good performing module. For example, the modules used by Heber and Swab ([10]) have a better performance. However, these modules have been used because of their availability in the market. It is expected that further improvement in electrical output if better modules are used. The important assessment in the present work is the capacity for utilizing the maximum amount of the available exhaust heat without incurring overheating.

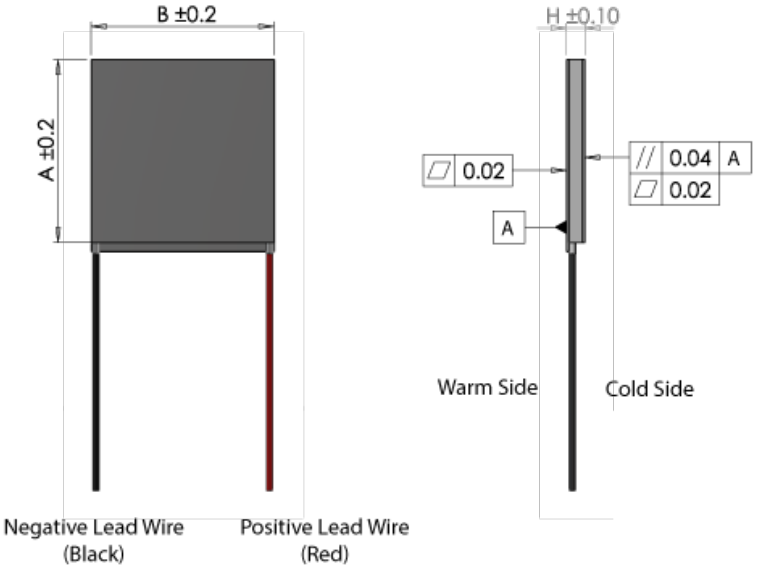

Figure 43: Geometrical features of the TEG: A- 62 mm; B- 62 mm; H- 4 mm [5]

5.1.4 Cooling Plates (CP)

The CP design used is based on the CPs manufactured at LaMoTA from a commercially available heat sink obtained from an extrusion process, to which a cover has been welded. These CPs have a high fin density, which minimizes their thermal resistance, and a large flow cross-section to minimize pressure drop. Another lighter, more compact design could have been chosen for the simulation and indeed it is expected that the industrial prototype will be much lighter and compact. However, this geometry was used to allow future experimental validation of the simulations. The CPs have a typical working operation, water flows through the channels ensuring the cold face of the TEGs stays coldest as possible. Figure 44 shows half of the CPs with the channels in a Fischer Elektronik SK624 ([64]) profile inside an aluminium case, which due to its thickness allows the uniform temperature of the TEGs cold face.

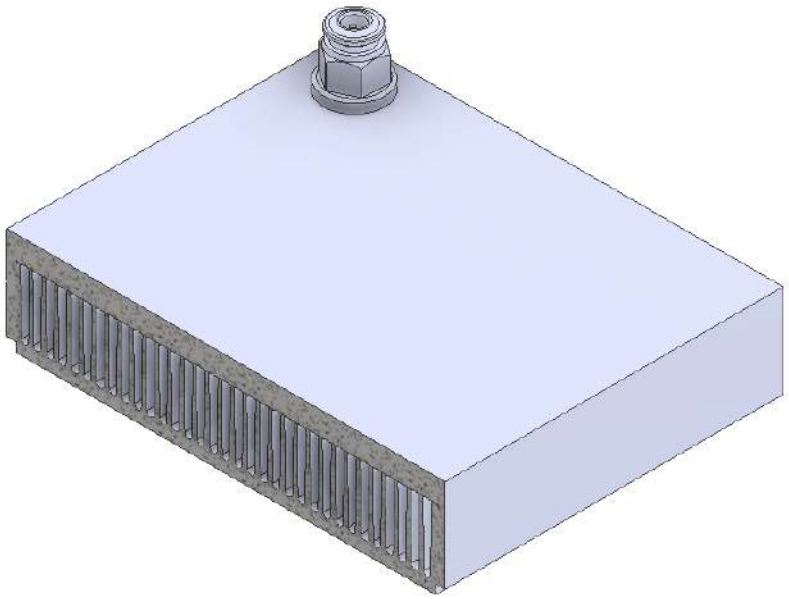

Figure 44: CAD representation of half section of the CP

The fundamental geometric parameters are presented in Table 8.

Table 8: CPs geometric parameters

Variable	**Value**	**Unit**
Fin with, w	1.98	mm
Fin height, a	14.5	mm
Number of channels	66	-
Channel length, l_{CP}	144	mmm
Metal thickness, ε_{CP}	2	mm
Inlet water temperature, $T_{waterin}$	30	°C

5.2 Thermal evaluation and computational simulation

The heat transfer process is usually three-dimensional, however, when the significant conduction of heat occurs mainly in one direction, the system calculation can be performed as one-dimensional, which will be the case in the present study. To be more precise, the model relies on a series of one-dimensional analyses performed to consecutive discretized slices of the system in the direction of the flow. This one-dimensional steady heat transfer approach can predict the system interactions with the aid of empirical correlations for convection at the exhaust and cooling water flows, and through the calculation of equivalent thermal resistances of complex geometries using finite element calculations. This was the case when

calculating the equivalent thermal resistance of the conductive heat transfer between the wavy fins and the VCs, and between the VCs and TEGs. Although the geometry is complex, an equivalent 1D resistance can be extracted from the 2D geometry of the system components. The HE purpose is to transfer the heat absorbed from the exhaust gases, through the VCs until the TEGs, which will be finally absorbed by the CPs. To understand the thermal behaviour of each of these components, the CP, TEGs and WF thermal resistances calculation procedure is presented, followed by COMSOL one-dimensional simulation to analyse the entire system interaction, where the convective thermal resistance of the VCs was calculated.

5.2.1 Cooling Plates

The thermal resistances of the CP can be described by Figure 45. These resistances are a function of the the water flow and the CP material properties and the thermal loads, the approach followed to calculate the total thermal resistance of the cooling system is now presented.

Figure 45: Thermal resistance network for heat transfer through the CP

First, the fluid dynamics inside the channels should be analysed. The Reynolds number is calculated through the CPs channels hydraulic diameter. These were consider as rectangular, with the hydraulic diameter being defined by equation (20) and the water velocity inside the channels, equation (21)).

$$De_{CP} = \frac{2aw}{a+w} \tag{20}$$

$$u_{water=\frac{\dot{V}_{water}}{A_{sec_{CP}}}}; A_{sec_{CP}} = aw \tag{21}$$

Where $\dot{V}_{water}$ is the cooling water volume flow rate per channel at the inlet, which depends on the number of channels and the cooling water mass flow rate per CP. In the case of these CP the cooling mass is divided by 66 channels. Using the Prandtl number (Pr), by combining the equations from j, and the Nusselt number it is possible to calculate the CP heat transfer coefficient (h_{CP}) as it follows:

$$Pr = \frac{0.564}{(1+(1.664 \cdot Pr_{water}^{\frac{1}{9}})^{\frac{9}{2}})^{\frac{2}{9}}} \tag{22}$$

$$Nu = \frac{h_{CP} D_e}{k_{water}}; j = \frac{Nu}{RePr^{1/3}} \tag{23}$$

The heat transfer performance of finned surfaces can be formulated in terms of their thermal resistances. The fin efficiency (η_{fin}) represents the ratio between the actual heat transfer rate in the fin and

the ideal heat transfer rate if the entire fin were at base temperature. For CPs, the η_{fin} can be determined by equation (24), where k_{Al} is the aluminum conductivity.

$$\eta_{fin} = \frac{tanh(mh_{water})}{mh_{water}}; m = \sqrt{\frac{hP_{fin}}{k_{Al}A_{fin}}} \tag{24}$$

Nonetheless, equation (24) only is accountable for one fin because P_{fin} and A_{fin} refer to the perimeter and area of the top of the fin, respectively. Thus, is necessary to calculate the group efficiency which is given by equation (25). Where A_f and A_t are the finned area and the total heat transfer area.

$$\eta_{CP} = 1 - \frac{A_f}{A_t} \tag{25}$$

Now, is possible to calculate the thermal convective resistance by the following relation:

$$\dot{Q}_{cp} = \frac{\Delta T}{R_{CP}} = h_{water}A_{t_{CP}}\eta_{CP}(\Delta T) \Longrightarrow R_{cv_{CP}} = \frac{1}{h_{water}A_{t_{CP}}\eta_{CP}} \tag{26}$$

The CPs have a 2 mm thick aluminum layer between them and the TEGs hot face. This results in thermal conductive resistance by equation (27), where A_l is the base area of the layer.

$$R_{cd_{CP}} = \frac{\varepsilon}{k_{al}A_l} \tag{27}$$

When two surfaces are in contact, in this case CP and TEGs, an interface between the two is created that will contain numerous air gaps of varying sizes that act as insulation due to the low thermal conductivity of air, this creates a thermal contact resistance dependent on the variable thermal contact conductance (h_c) between these couple:

$$R_{contact_{CP}} = \frac{1}{h_c} \tag{28}$$

5.2.2 Thermoelectric Generator Modules

Due to the device complex variety of materials the TEGs are composed, is not correct to select the thermal conductivity of one material. Thus, from the TEG parameters presented in Table 9, the equivalent thermal conductivity of the device (k_{TEG}) is calculated by equation (29), where A is the base area of the module.

Table 9: Parameters for hot side temperature 250°C and cold side temperature 30°C

Designation	Value
Model	GM250-127-28-10
Matched load output power	28.3 W
Heat flow through module, Q	566 W
Maximum operation temperature	Hot side - 250°C Cold side - 175°C
Temperature gradient,ΔT)	220 °C

$$k_{TEG} = \frac{Q}{\Delta T \times \frac{A}{H}} \tag{29}$$

Hence, is possible to obtain the thermal conductive resistance, present in Figure 46, through equation (30), where, H is the TEG thickness.

Figure 46: Thermal resistance network for heat transfer through TEG

$$R_{cd_{TEG}} = \frac{H}{k_{TEG} A_l} \tag{30}$$

5.2.3 Wavy Fins

Inside the WFs there is a convective heat flux. The convective heat transfer coefficient is obtained by the empirical correlations given in chapter 2. This is used to calculate the thermal convective resistance, Figure 47.

Figure 47: Thermal resistance network for heat transfer through the WFs

Likewise in CPs thermal resistance, the fin efficiency of the WFs, equation (15), is used to calculate its thermal resistance. Again, is necessary to calculate the group efficiency. The convective thermal resistance results them in the following equation:

$$R_{cv_{CP}} = \frac{1}{h_{air} A_o \eta_{WF}} \tag{31}$$

5.2.4 One-dimensional Steady Heat Simulation

The heat flux simulation to obtain the 1D equivalent thermal resistances of the 2D shapes, was executed through a two-dimensional steady-state thermal analysis in COMSOL Multiphysics. The software allows the user to upload the CAD model in the study, select the respective component materials and their thermal properties, and add convective properties, such as the calculated heat transfer coefficient of the fins. Two different simulations were conducted: VCs as adiabatic bodies and as isothermal bodies, this corresponds to the situations where the VCs are either inactive (no phase change) or active (phase change present). Also, two models were analysed to conclude which one had the lowest thermal resistance and, therefore the best heat transfer efficiency: One model with six WFs plates and another one with nine WFs plates. The simulation in COMSOL should follow a workflow to get valid results. The first step is to choose the simulation type. Although an equivalent one-dimensional thermal resistance is to be obtained from this analysis, in reality, a 2D analysis is performed to extract the 1D thermal resistance, thus, for a representation of the model, a "Space Dimension 2D"is selected. Then, from the type of "Physics", the "Heat Transfer in Solids" simulation is selected, as well as "Stationary"mode. For this analysis were not considered the TEGs thermoelectric characteristic since only the thermal resistances are to be studied. After setting the simulation environment, the next steps are followed:

1. Geometry import;
2. Material selection;
3. Definition of the heat transfer parameters;
4. Mesh settings;
5. Compute and data gathering;
6. Results processing: calculation of the thermal resistances.

5.2.4.1 Geometry import

Two different HE configurations were constructed in AutoCAD and converted into a ".dfx"extension to be imported to COMSOL. Figure 48 shows one model with six plates of WFs, (48a), and nine plates of WFs (48b), already in the COMSOL environment. No modifications were done in the sizing of the system because the box were the casting is done has limited dimentions.

5.2.4.2 Material selection

COMSOL software has a wide library of materials with their respective mechanical and thermodynamic properties, enabling the right attribution of the the respective material of each component. Although each

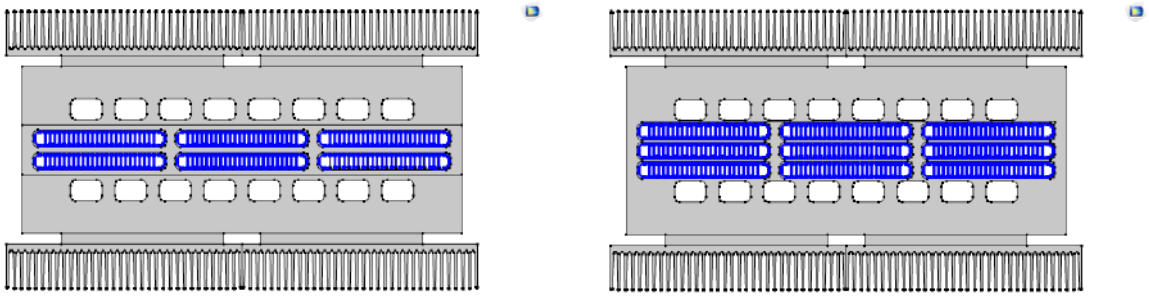

(a) Six WFs plates model (b) Nine WFs plates model

Figure 48: Two different HE designs simulated in COMSOL

material has their default properties is possible for the user do change them. This is the case of the TEGs, since they are not formed by one material, for structural purposes tellurium was defined as the main material which, on the material properties, the thermal conductivity was changed to the calculated general k of the TEGs, as presented in Figure 49. For the rest of the components their respective materials were defined:

- CPs and VCs support: aluminum 6061;
- WFs: stainless steel.

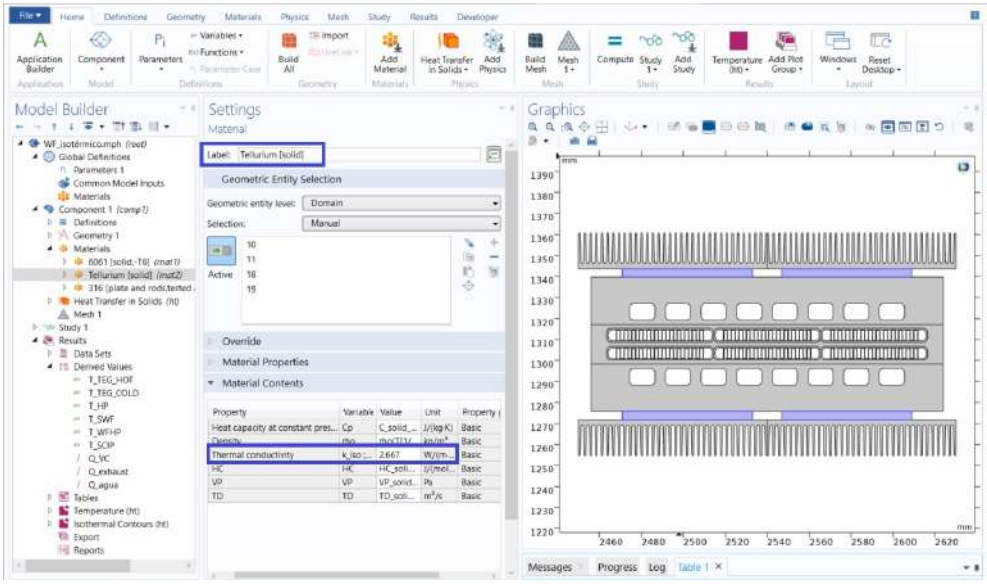

Figure 49: Material attribution: Change of the thermal conductivity of tellurium for k_{TEG}

5.2.4.3 Definition of the Heat Transfer Parameters

In the "Heat Transfer in Solids"section, the thermal conditions and barriers are defined. Here is where the different stages of the VCs are distinguished as adiabatic or isothermal. The simulations were conducted

with data from two cycle points of the WHVC driving cycle with the full exhaust gas mass flowing through the HE.

- Adiabatic VCs: The WFs have a convective heat flux boundary with the temperature of the exhaust gases, in a cycle point were the resulting temperature is not higher than 250°C, and the respective h. A thermal insulation barrier is added to the VCs interior, ensuring no heat exchanges occurs. The CPs are also designated with a convective heat flux boundary with their respective h at the temperature of 30°C. Table 10 displays the WHVC driving cycle point and the respective thermal properties used for the inactive VCs simulation.

Table 10: Parameters for inactive VCs simulation

Propertie	Value	Unit
Time	72	s
Exhaust Gas Mass Flow	236	g/s
Exhaust Gas Temperature	177	°C
CP Water Temperature	30	°C
h_{WF}	356	W/m^2.K
h_{CP}	1337	W/m^2.K

- Isothermal VCs: Similar to the adiabatic condition, the WFs also have a convective heat flux boundary, but with a driving cycle point were the exhaust gases are higher than 250°C. The CPs maintain the same convective properties as their temperature does not change. The VCs are no longer thermal insulated but are attributed the boiling temperature of the working fluid, 250°C. In Table 11 is presented the cycle point where the exhaust gas exceeds 250°C used for the simulation.

Table 11: Parameters for active VCs simulation

Propertie	Value	Unit
Time	63	s
Exhaust Gas Mass Flow	348	g/s
Exhaust Gas Temperature	358	°C
CP Water Temperature	30	°C
h_{WF}	474	W/m^2.K
h_{CP}	1337	W/m^2.K

5.2.4.4 Mesh Settings

Since the purpose of the study is not to do a structural analysis, the mesh settings were left "normal"by default, Figure 50.

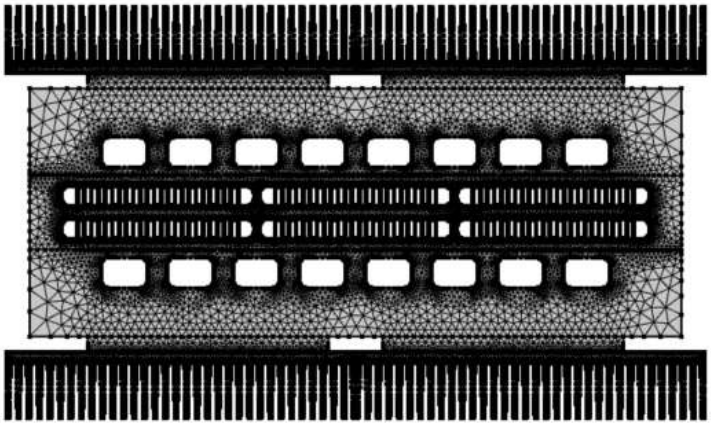

Figure 50: Mesh of the HE model

5.2.4.5 Compute and data gathering

Once all the thermal parameters are defined, is possible do run the simulation. The outputs to take into consideration include the medium temperatures of the components, as well as heat fluxes in the system. Therefore, temperatures from the cold and hot faces of the TEGs, (T_{TEC_c} and T_{TEC_h}), the WFs surface (T_{WFs}), the dividing line between the WFs and the VCs (T_{WFVC}), the internal surface of the CPs (T_{CPs}) and the interior of the VCs (T_{VCs}) were gathered in Table 12. In Annex IV are illustrated the mentioned surfaces in Figure 83.

Table 12: Components medium temperatures after the simulations

	6 WFs model			**9 WFs model**	
	Inacitve VCs	**Active VCs**		**Inacitve VCs**	**Active VCs**
T_{TEG_h} (K)	414	516		419	515
T_{TEG_c} (K)	312	327		319	327
T_{WF_s} (K)	443	601		445	610
T_{WFVC} (K)	431	531		434	529
T_{CP_s} (K)	306	317		314	317
T_{VC_i} (K)	425	523		428	523

Through the integration of the heat flux, the thermal power of the system is obtained, this is enabled by the "line integration: normal convective heat fluxes"COMSOL tool. Because it is a 2D simulation, the software outputs the results per unit of length (W/m), thus the multiplication by the system length is

necessary. Hence, for the scenario where the VCs are adiabatic the heat flux present in the TEGs hot surface was integrated (selecting the TEGs hot face) to provide the total thermal power absorbed by the system, Q_{TEG}:

Table 13: Thermal power for the two models with inactive VCs

	Inactive VCs	
	Six WFs model	**Nine WFs model**
Q_{TEG} (kW/m)	16.98	16.33

When the VCs are active, more heat fluxes need to be considered, therefore, the power absorbed from the exhaust gases ($Q_{exhaust}$) was obtained by the integration of areas were there is no heat absorption by the VCs, the exterior and interior of the WFs. For the VCs (Q_{VCs}) the heat flux flowing through their interior was integrated by selecting . Finally, for the thermal power absorbed by the water (Q_{water}), the integration was done in the cold face of the TEGs plus the surface of the CPs. Here, is already possible the visualization of the VCs effectiveness, as the power absorbed by the VCs is higher than the HE:

Table 14: Thermal power for the two models with active VCs

	Active VCs	
	Six WFs model	**Nine WFs model**
$Q_{exhaust}$ (kW/m)	81.21	79.47
Q_{VCs} (kW/m)	96.39	104.9
Q_{water} (kW/m)	62.57	62.13

5.2.4.6 Results processing

The main reason for the simulation in COMSOL is to examine which model design is the most appropriated and to evaluate the thermal resistances in the system. When the VCs do not exchange heat, the thermal power is considered constant along the system. The following relations were used to calculate the thermal resistances of the WFs (R_{WF}), VCs (R_{VCs}), TEGs (R_{TEG}) and CP (R_{CP}):

$$R_{WF} = \frac{T_{WF_s} - T_{WFVC}}{Q_{TEG}} \tag{32}$$

$$R_{VCs} = \frac{T_{WFVC} - T_{TEG_h}}{Q_{TEG}} \tag{33}$$

$$R_{TEG} = \frac{T_{TEG_h} - T_{TEG_c}}{Q_{TEG}} \tag{34}$$

$$R_{CP} = \frac{T_{TEG_c} - T_{CP_s}}{Q_{TEG}} \tag{35}$$

When the VCs are active, as they are absorbing heat, the heat flux does not go directly from the wavy fins to the modules, hence the above mentioned thermal power were gathered. For the thermal resistance between the exhaust gases and the WF ($R_{WF_{cv}}$), the VCs, TEGs and CPs, the following statements were used:

$$R_{WF_{cv}} = \frac{T_{exhaust} - T_{WF_s}}{Q_{exhaust}} \tag{36}$$

$$R_{VC_1} = \frac{T_{WFVC} - T_{VCs}}{Q_{exhaust}}; R_{VC_2} = \frac{T_{VCs} - T_{TEG_c}}{Q_{water}}; R_{VCs} = R_{VC_1} + R_{VC_2} \tag{37}$$

$$R_{TEG} = \frac{T_{TEG_h} - T_{TEG_c}}{Q_{water}} \tag{38}$$

$$R_{CP} = \frac{T_{TEG_c} - T_{CP_s}}{Q_{water}} \tag{39}$$

The results are discriminated in Table 15. Since the analysis is for evaluation purposes, the results were obtained for the length of one CP, 0.144 m. The model with nine WF plates offers a little bit more resistance than the six model. Thus the six WFs plate model was selected.

Table 15: Thermal resistances of the two different models

	Inactive VCs			**Active VCs**	
	6 WFs model	**9 WFs model**		**6 WFs model**	**9 WFs model**
R_{WF}	0.005	0.005		0.006	0.007
R_{VCs}	0.006	0.007		0.002	0.001
R_{TEG}	0.042	0.042		0.021	0.021
R_{CP}	0.002	0.0023		0.001	0.002
Total	0.053	0.056		0.029	0.031

5.2.5 System Thermoeletric Analysis

By considering all thermal resistances and thermal loads in the system it is now possible to evaluate the TEGs thermoeletric behavior. The thermoeletric conditions and equations for the evaluation of the energy conversion are now presented. Three efficiencies can define the system. The thermoeletric conversion efficiency of the system (η), defined by the output power (P_{out}), generated by the TEGs, and the available thermal load from the exhaust gases (Q_{in}), equation (40).The HE thermal efficiency, η_{HE},representing the ratio of the available exhaust power that is absorbed by the HE (Q_{hot}), equation (41). And the thermoeletric efficiency (conversion efficiency) of the TEGs, η_{TEGs}, ratio of the thermal power reaching the TEGs (Q_{TEG}) that is effectively converted into electricity, equation (42).

$$\eta = \frac{P_{out}}{Q_{in}} \tag{40}$$

$$\eta_{HE} = \frac{Q_{hot}}{Q_{in}} \tag{41}$$

$$\eta_{TEG} = \frac{P_{out}}{Q_{TEG}} \tag{42}$$

Thus, the system thermal efficiency is dependent to the interaction between the generated electric power and the input exhaust heat flow ($\dot{Q}_{exh}$):

$$\eta = \frac{P_{TEG_{el}}}{\dot{Q}_{TEG}} \tag{43}$$

However, one can not just simply apply the the total thermal load from the exhaust gases without considering the energy lost to the HE. The total thermal resistance of the system (R_{HE}), whether for active or inactive VCs must be considered to evaluate the right amount of energy reaching the hot and cold face of the TEGs. Therefore, by gathering the thermal resistances above mentioned, R_{HE} is calculated:

$$R_{HE} = R_{WF} + R_{VP} + R_{TEG} + R_{CP} \tag{44}$$

TEGs generate electricity due to the thermal gradient across their faces. The hot face is heated by the energy absorbed from the exhaust gases, while the cold face is cooled down by the water flowing through the coolers (Q_{CP}). For the HE analysis either the T_{TEG_h} and the T_{TEG_c} must be calculated for each cycle point. The HE is divided into several longitudinal slices in which the heat transfer calculations are performed in 1D. Energy balances are performed to each slice and a calculation of vaporization or condensation power is also performed if the VCs happen to be active. In the first iteration of a slice it is considered that there is no excess heat and that the VCs are not operating (no phase change). Under these conditions, the thermal resistances with adiabatic VCs are applied. Then, on that slice, there is the need to discover which one of the following situations are occurring, according to what is shown in Figure 16:

- The heat transfer calculations confirm that indeed there is no excess temperature (T_{TEG_h} < 250°C). This means that the VCs are indeed not operating, and the thermal resistances with adiabatic VCs have been correctly applied;

- The calculations confirm that there is an excess temperature (T_{TEG_h} > 250°C). This means that the VCs are in reality operating and absorbing heat so that T_{TEG_h} does not exceed 250°C. Therefore, the calculation must be repeated, now using the thermal resistances considering an isothermal VCs. Under these conditions, three different heat fluxes will be obtained from the calculations: the heat absorbed by the HE from the exhaust, the heat reaching the TEGs and the heat absorbed by the

VCs, which will be the difference between the two. thus, only a fraction of the heat absorbed by the HE reaches the TEGs;

- There is a third possibility, in which the calculations confirm that the temperature is below 250°C but the excess power that has been calculated from the previous slices (which represents vapour produced) has still not been absorbed by the subsequent slices. Under these conditions, it means that the slice is located in a condensation region of the VCs. The calculations are redone, but now using the isothermal VCs condition. Three different heat fluxes will also be obtained from the calculations: the heat absorbed by the HE from the exhaust, the heat reaching the TEGs and the heat released by the VCs to the TEGs, which will be the difference between the two. Thus, in a slice like this, the heat absorbed by the TEGs will be higher than the heat absorbed by the HE because part of this heat is being supplied by the VCs through condensation.

Once no more accumulated excess heat is available, all slices will operate with inactive VCs and a T_{TEG_h} which will be lower than 250°C.

- **Inactive VCs** (T_{exh}<250°C): Because any component is absorbing heat, all thermal load from the exhaust gases flows along the HE. Thus, Q_{hot} is obtained by equation (45), where R_{HE} is the system total thermal resistance when the VCs are inactive. Here T_{TEG_c}=T_{water}:

$$Q_{hot} = \frac{T_{exh} - T_{water}}{R_{HE}} \tag{45}$$

$$T_{TEG_h} = T_{exh} - Q_{hot} \times (R_{VC_{inactive}} + R_{WF}) \tag{46}$$

- **Active VCs**(T_{exh}>250°C): The Vcs are absorbing heat so that the thermal load reaching the TEGs does not exceed their maximum temperature $T_{TEG_{max}}$.Therefore, the Q_{hot} absorbed by the system and the Q_{CP} should be distinguished. The difference between these two heat fluxes is the excess heat (Q_{excess}) that is absorbed by the VCs by vapour production, to be released in cooler areas:

$$Q_{hot} = \frac{T_{exh} - T_{TEG_{max}}}{R_{WF} + R_{VC_{active}}} \tag{47}$$

$$Q_{CP} = \frac{T_{TEG_{max}} - T_{water}}{R_{TEG} + R_{CP}} \tag{48}$$

$$Q_{excess} = Q_{hot} - Q_{CP} \tag{49}$$

While T_{TEG_h} is the same as $T_{TEG_{max}}$ (250°C) , T_{TEG_c} is no longer the same as T_c since was absorbed Q_{CP} :

$$T_{TEG_c} = T_{water} + Q_{CP} \times R_{CP} \tag{50}$$

- **VCs releasing heat excess** ($T_{TEG_h} = T_{TEG_{max}}$): The excess heat is accumulated (Q_{acc}) until the VCs stop being active. When the excess heat is no longer generated but there is still Q_{acc}:

$$Q_{accumulated} = \sum Q_{excess} \tag{51}$$

5.3 Model Analyses

The present model is an adaptation of a system designed to convert heat from the exhaust gas of a LDV with a SI engine into electricity. In the original model, Figure 3 the exhaust gas flowed through corrugated fins, instead of WFs, and the thermal control was done by VCHPs, rather than VCs. To comply with the HDV attributes the concept model must be dimensioned to be suitable for the HD application. Figure presents the adapted model, with the WFs and CP but only suitable for LD applications. An algorithm will aid in the selection of the ideal model setup.

5.3.1 System Algorithm Simulation

To predict the outcomes of the model, a Matlab algorithm gathers the component's thermal and electrical properties, taking in consideration the stages of the VCs, providing the fundamental results for the optimization of the study. For instance, important outputs are the electrical load produced by the modules and how many TEG lines were active during the cycle run, which enables the visualization of the heat diffusion. Figure 51 presents the important outputs of the algorithm. The electric power produced may seem the decisive aspect for determining the best dimension for the model, however, the pressure drop plays an important role because if the pumping loss is higher or near the generated electrical power, then the system purpose stops being valid.

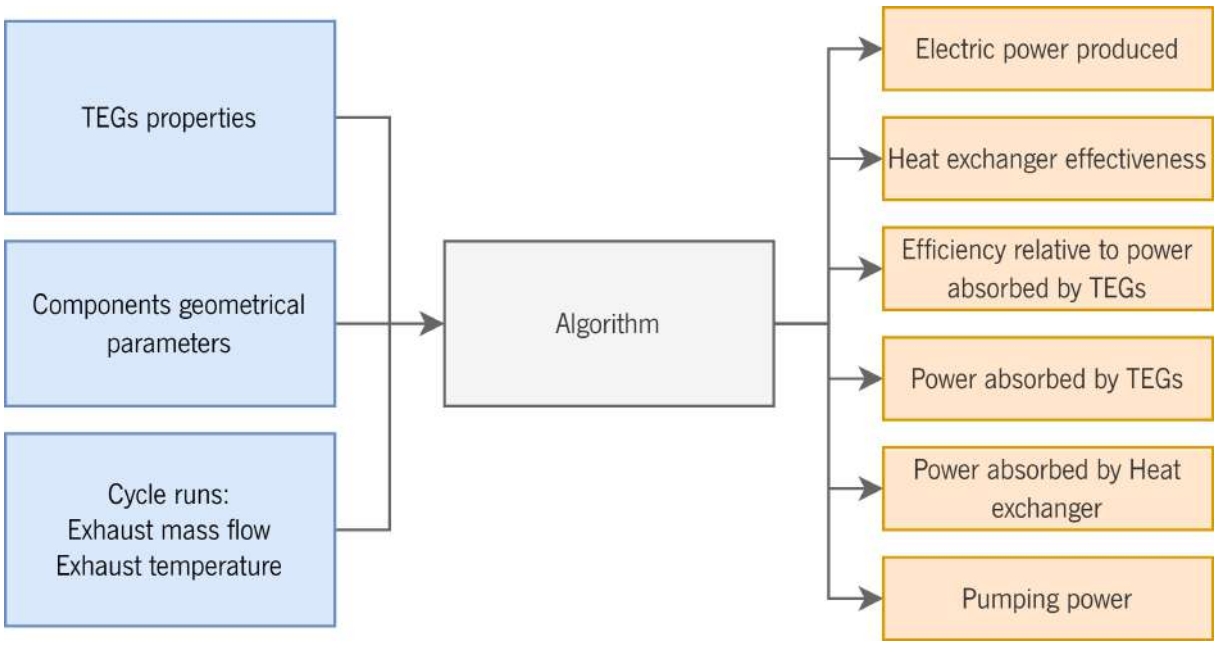

Figure 51: Matlab outputs

5.3.2 System Size Definition

With the algorithm above mentioned it is possible to scale the model for the HDV needs. By changing the number of CPs or dividing the exhaust mass flow by the scale value, it is possible to select the length of the system by choosing the number of coolers in the flow direction. Figure 46 shows the configurations tested, with two and three cooler length. Figure 52 shows the configurations tested, with two and three cooler length. The program only simulates a system with a fixed number of coolers along the width (four). However, to simulate a system with, say, a width of 8 coolers, symmetry considerations are used. A system with half the size (width of 4 coolers) is simulated, with also half of the exhaust flow rate. Then, the power results are all multiplied by two. Figure 52 hows the two geometries compared, both with 8 coolers in width. Each CP has two TEGs by length, increasing the number of CP can increase the electrical production, but because the length of the system is higher, the exhaust gas needs more pumping power to overcome the pressure, also if the HE is too long the distance that the vapour and the condensated will have to travel inside the VCs might become excessive. On the other hand, having a system which is very wide, will decrease pressure drop but it will divide the flow too much, causing thermal dilution under low loads and defeating the reason for the thermal control and the heat spreading. After several simulations, it was discovered that pressure drop would be excessive for systems with lengths longer than three coolers, therefore, two set-ups were considered favourable, depicted in Figure 52. Note that, since the thermal analysis is one-dimensional the thermal resistances are the same regarding the orientation of the system, this enables stacking the models. One of the chosen designs is composed of three CPs in length and with 4+4 blocks in width , Figure 52a. The other is similar but with only two coolers along its length, Figure 52b.

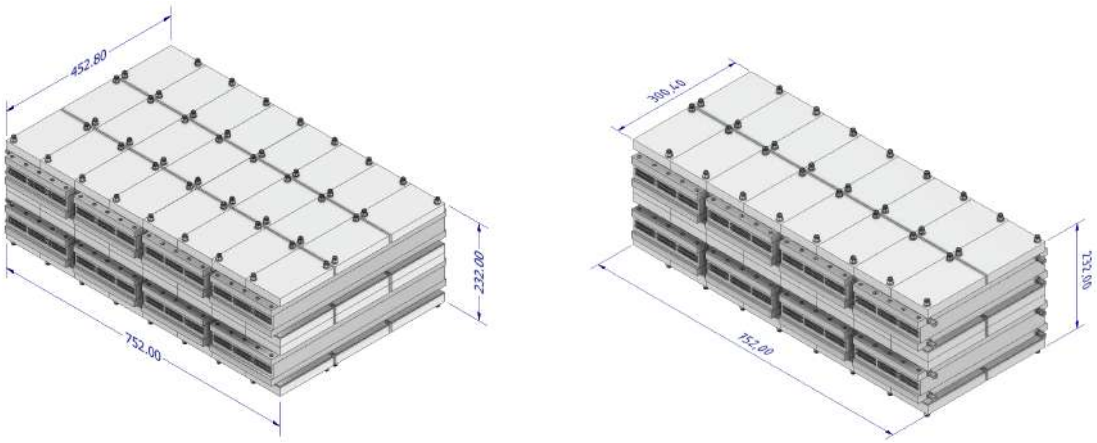

(a) 3 CPs model (b) 2 CPs model

Figure 52: Two different system designs evaluated

5.3.2.1 Results analysis

To choose the most suitable design, the two models were simulated in the algorithm with the Long Haul cycle run, since it has a longer course enabling a more valuable analysis. General outputs regarding the HE and TEGs effectiveness, pumping losses or production of electrical energy are gathered in Table 16.

Table 16: Global results from simulation with Long Haul cycle run on 25.5 t load

Model	**3 CPs**	**2 CPs**	
Parameter	**Value**		**Unit**
Weight	158	104	kg
Total electrical energy	10.6	10.07	MJ
Total Exhaust energy available	345	345	MJ
System average thermoeletric efficiency, η	2.9%	2.8%	
Average HE effectiveness , η_{HE}	93%	85%	
Average TEG conversion efficiency, η_{TEG}	3.1%	3.3%	
Total Exhaust energy absorbed by TEGs	317	284	MJ
Total Exhaust energy absorbed by HE	317	284	MJ
Total energy lost by engine backpressure: w/o bypass	1.64	1.19	MJ
Global efficiency relative to the available heat	3.1%	2.9%	
Global efficiency relative to the heat absorbed by HE	3.3%	3.5%	
Global efficiency relative to the heat absorbed by TEGs	3.3%	3.5%	
Global effectiveness (fraction absorbed by HE)	92%	82%	
Global effectiveness (fraction absorbed by TEGs)	92%	82%	
Maximum electric power	**5.26**	**4.74**	**kW**
Average electric power	**2.40**	**2.28**	**kW**
Maximum exhaust thermal power	166	166	kW
Average exhaust thermal power	78.1	78.1	kW
Maximum exhaust power absorbed by TEGs	136	111	kW
Maximum exhaust power absorbed by HE	136	112	kW
Average pumping loss (w/o bypass)	0.37	0.27	kW
Maximum pumping loss (w/o bypass)	1.76	1.27	kW
Electric production kWh/100 km	2.95	2.8	kWh/100km
Electric production kJ/km	10.6	10.7	kJ/km

As expected, the model with more TEGs rows has a higher average electric power production however, the pumping loss is also higher due to the longer path the exhaust gases have to flow through. Regarding the relation between the available thermal load and the produced electrical energy, both designs have similar performances. In terms of efficiency, the HE with a longer length can absorb more thermal load, due to the higher heat transfer area, nevertheless, in the 2 CPs model, the TEGs are more efficient in generating electricity from heat. This is justified by the fact that in the longer model less heat is reaching the two additional lines of TEGs producing less electrical energy. Although the first four TEG lines of both models have very similar electrical outputs, as is shown in Figure 53 and Figure 54, at the TEGs third line

the exhaust gas arrives with much lower temperatures. By adding two more TEG lines the TEGs efficiency is reduced since these modules have low electricity production due to the poor heat rate arriving at them.

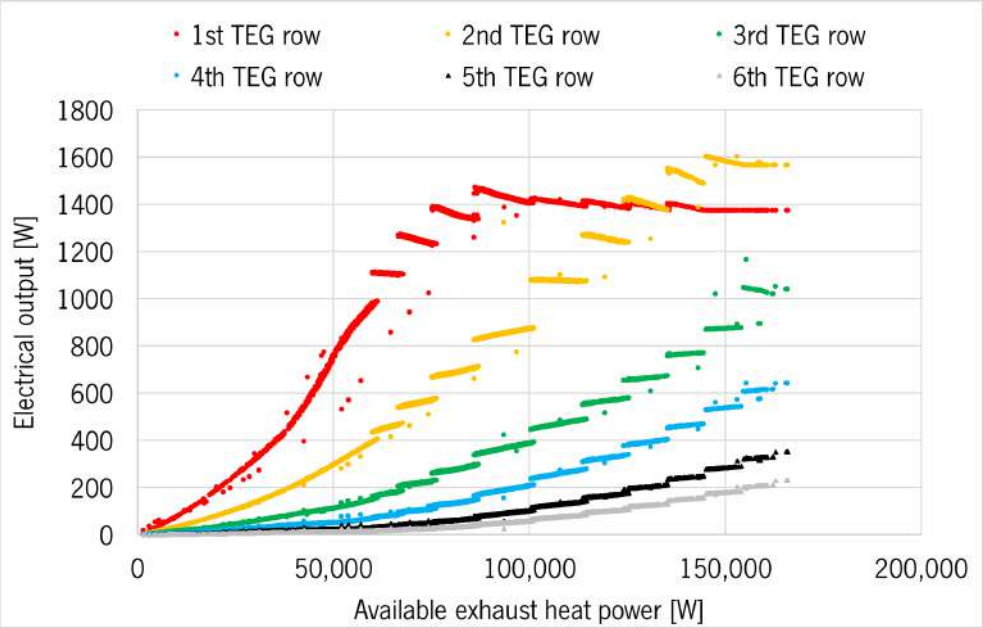

Figure 53: 3 CPs model electrical output per row of TEG

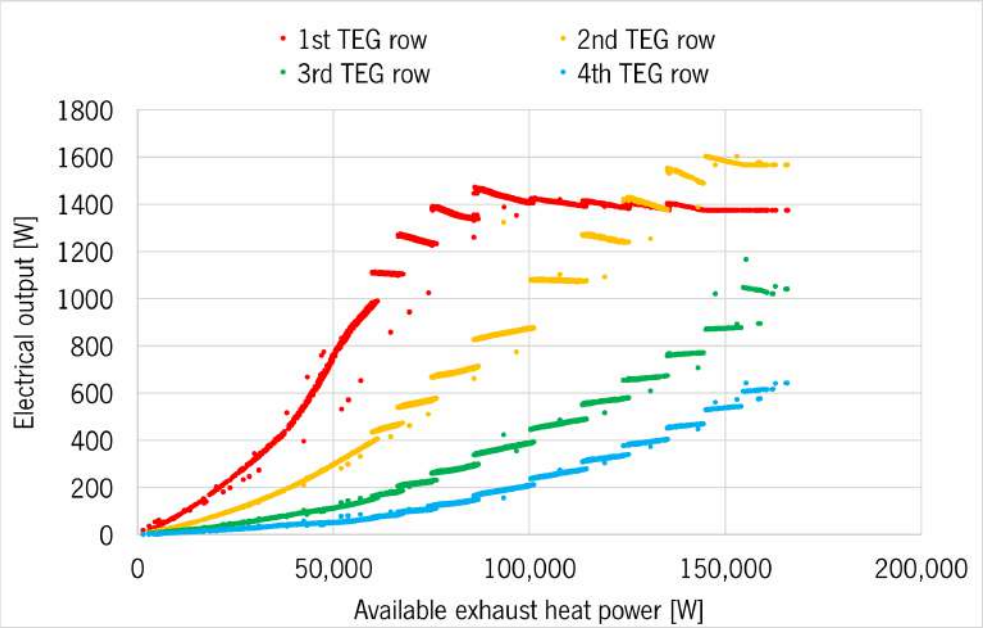

Figure 54: 2 CPs model electrical output per row of TEGs

One decisive feature to take into consideration in the model is its compactness. The 3 CPs model is near 1.5 times longer and heavier than the 2 CPs model. In HD applications heavy components mean less payload to comply with the maximum GVWR. Thus, a bigger model would not be commercially advantageous. Also, a small-scale model is easily included in the exhaust HD systems. Thus, the 2 CPs model is selected for the continuity of this study.

Chapter 6

Results and Discussion

On account of the simulation environments and algorithm previously described, it is now possible to fully analyse the main outputs under the selected operating conditions. These operating conditions include the assigned cycle runs data regarding the exhaust gases, described in Chapter 4 and the HE components and model design, defined in Chapter 3. The simulations were performed for a system with a total of 128 commercial TEGs, GM250-127-28-10 ([5]), which withstand with a maximum temperature of 250°C. The exhaust gases flow through the WFs providing a heart source to the system. The temperature control is ensured by the variable conductance VCs machined into the aluminum block. This system follows the stacked setup presented in Figure 52b and was simulated under two cycle runs, Long Haul and WHVC.

6.1 Temperature and Heat Distribution

The thermal control is ensured by the VCs. As mentioned above, these devices spread the excess heat from the hotter regions of the HE to colder sections, where the deficit thermal load would otherwise be insufficient to allow the TEGs to operate near the maximum allowed temperature. The heat accumulation was computed based on the sum of the excess or deficit of heat along each slice of the system. To illustrate this process, two cycle points under the fully loaded WHVC cycle with low and high exhaust thermal load are highlighted in Figure 55, where the thermal behaviour is illustrated from the inlet to the outlet of the HE. Figure 55a demonstrates the exhaust gases, TEGs faces and cooling water temperatures distribution along the HE, while Figure 55b presents the heat fluxes behaviour. By analysing the low thermal load graphics it is clear that the VCs act as adiabatic bodies since the exhaust gas and TEGs hot face temperatures are very close and do not come near to the maximum TEGs working temperature, thus the heat flux is fully absorbed by the HE. In this cycle point, the TEGs do not work at their optimal temperature (250°C), as no

heat was absorbed or accumulated by the system in order to compensate this lack of thermal power. As expected, due to the low thermal load, the cooling water hardly changes its temperature.

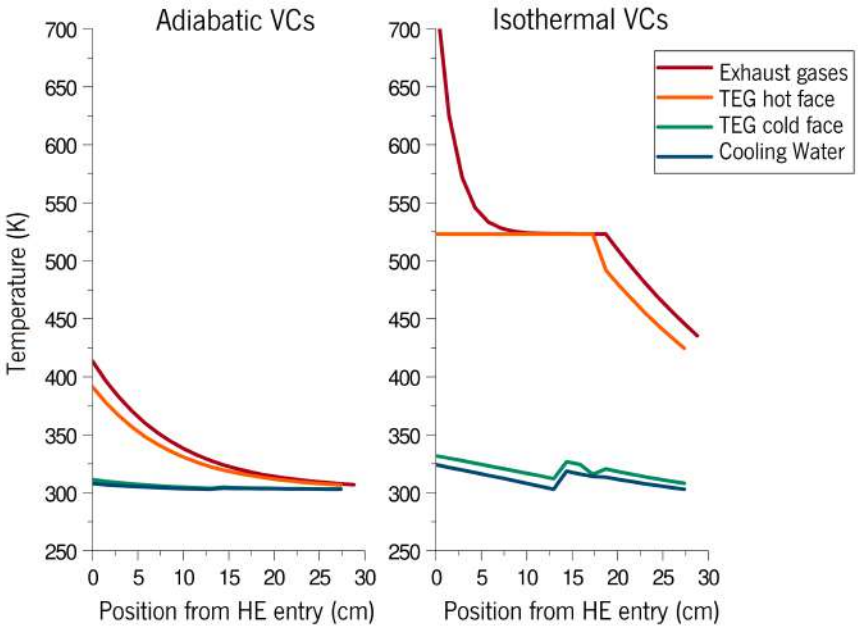

(a) Temperature profiles

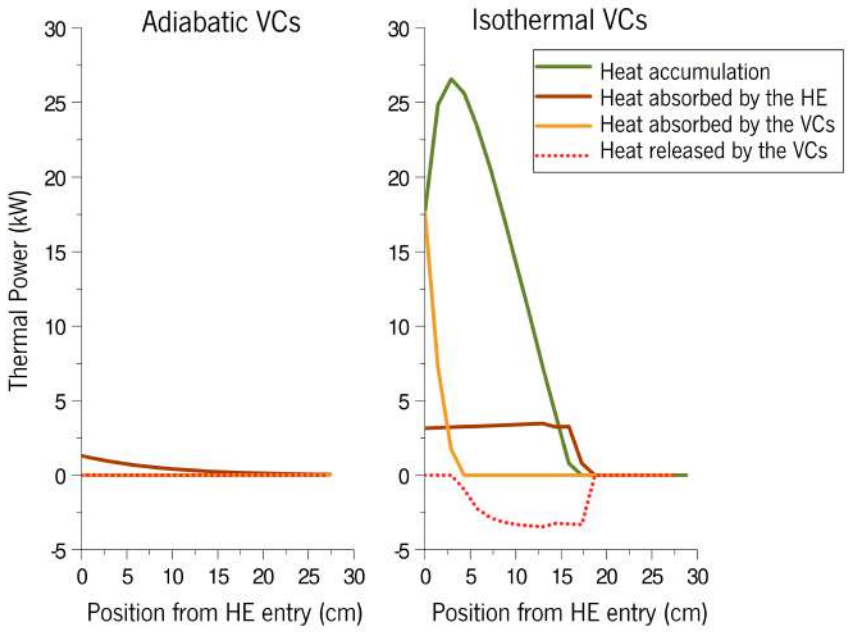

(b) Thermal power profiles

Figure 55: Temperature profiles and thermal power variation along the HE length for WHVC cycle run under two cycle points: 187s (low thermal load) and 1296s (high thermal load)

In the high thermal load cycle point, instance 1296s, the VCs are active along the first 17 cm of the HE. Initially, the VCs are absorbing the excess heat (0 - 5cm), which is then released in the following active VCs section (between 5 and 17 cm), visualized in Figure 55b. By absorbing the heat, the VCs are preventing the TEGs hot face from overheating, while releasing the absorbed heat in the following colder area, which without the VCs would be under heating, and therefore with TEGs working at their non-optimal temperature. This thermal control results in the temperature profile presented in Figure 55a. By absorbing the excess thermal load, the exhaust gas temperature is reduced to the TEGs optimal temperature, which is kept due to the release of the excess heat flux along the deficit area. However, a temperature drop is observed in the TEGs hot face (from 17 cm until the end of the HE) because the deficit region consumed all the heat released from the VCs, which are no longer spreading any thermal load and therefore, adiabatic.

6.1.1 Power distribution along TEG rows

The heat from the exhaust gases flowing inside the WFs is absorbed by the HE. When the thermal level absorbed by the HE is lower than the maximum operating temperature of the TEGs, all the heat will reach the TEGs by conduction across the HE, since the VCs are not active. Otherwise, the VCs start absorbing the excess heat by vaporization, preventing the rise of the temperature above the established limit. The generated vapour occupies a portion of the VCs towards the cooler regions. This heat spreading is done through a longitudinal direction. The accumulated vapour inside the VCs condensates in the cooler regions, heating them. This thermal control results in different thermal loads achieving the TEGs without overheating them, thus varying the thermal output along the TEG rows. The graphics from Figure 56 to Figure 59 show the thermal power distribution along the TEG rows. The stabilization of the electrical outputs, mostly on the first and second TEG rows, reflects the moment when the VCs are absorbing thermal power and releasing it, as the TEGs hot face is kept constant. The second TEGs row achieves higher electrical outputs since the VCs are realising most of the heat in this area. In the following rows, the VCs have drained all the excess heat, therefore the TEGs are not working near their maximum operating temperature. Essentially, the next row will increase its power generation rate, when the previous one achieves its maximum performance.

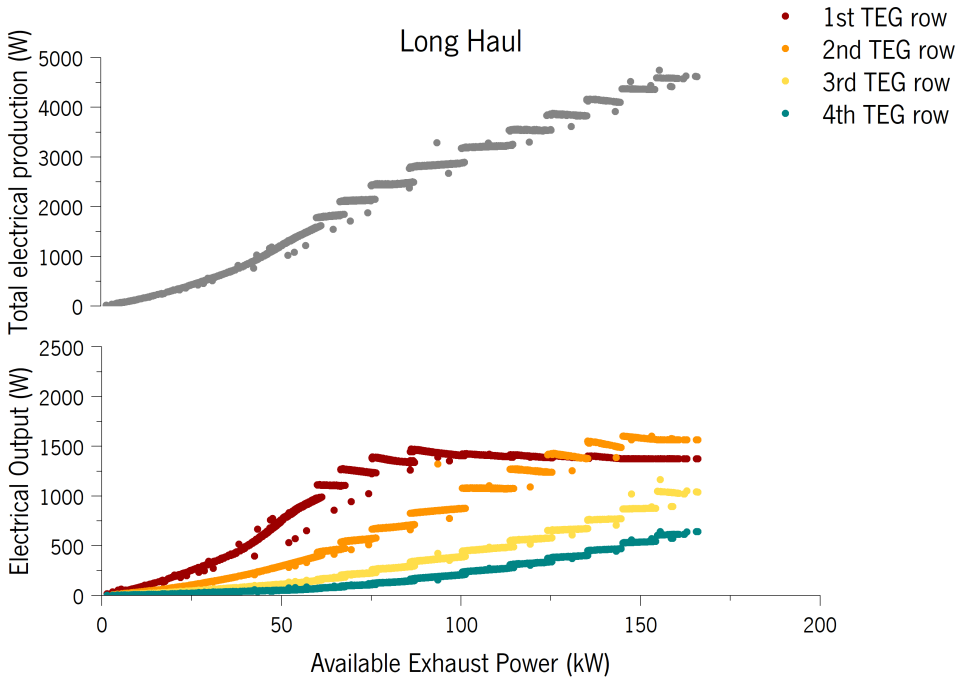

Figure 56: Power distribution along the system modules for Long Haul driving cycle with 25.5 t

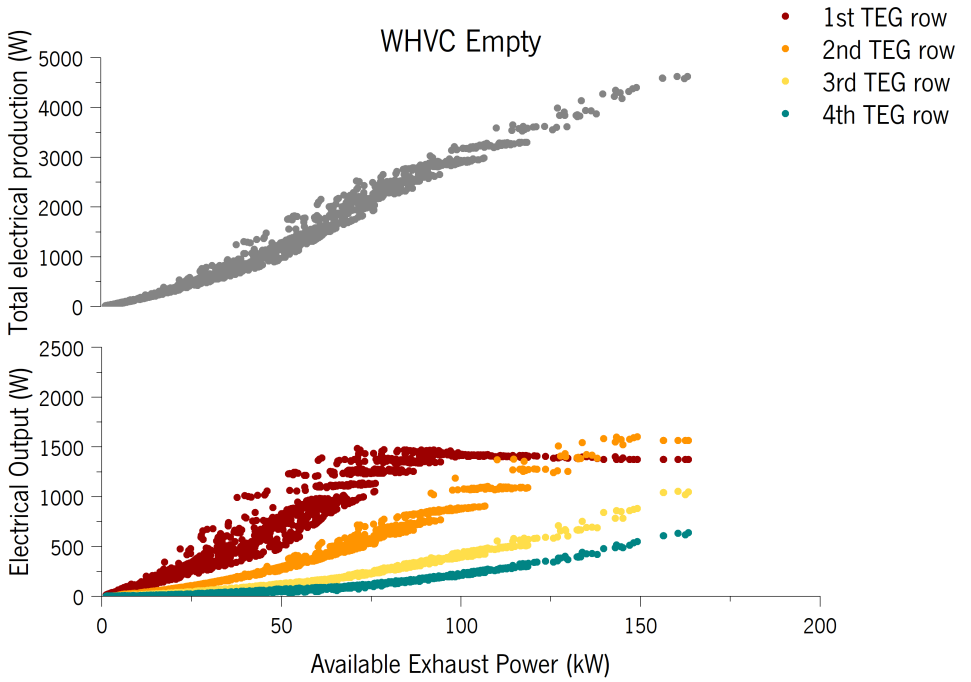

Figure 57: Power distribution along the system modules for WHVC driving cycle with 7.5 t

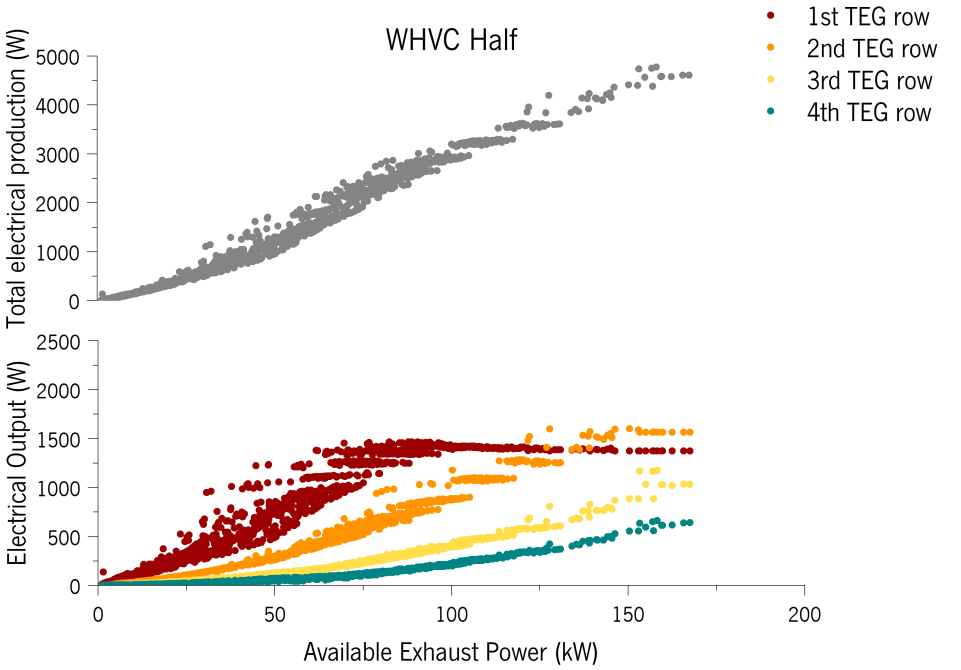

Figure 58: Power distribution along the system modules for WHVC driving cycle with 12.75 t

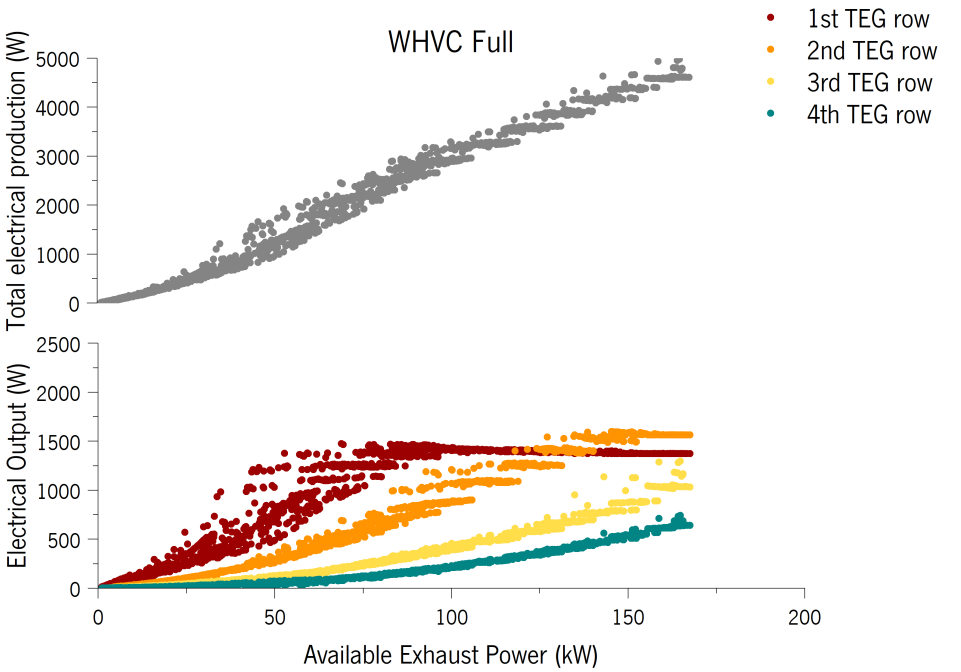

Figure 59: Power distribution along the system modules for WHVC driving cycle with 25.5 t

6.2 Electrical Production

A possible evaluation of the system performance is the analysis of the electrical generation and the thermal power absorbed by the HE, during the driving cycles. Figures 60 to 63 represent the power produced by the TEGs along time and compared against the absorbed exhaust power by the HE and the available exhaust power in each driving cycle. As expected, the higher the available thermal power, the higher the electrical production, regardless of the variable thermal load. This proves not only the efficient thermal control of the HE but also the ability of electricity generation under different thermal loads.

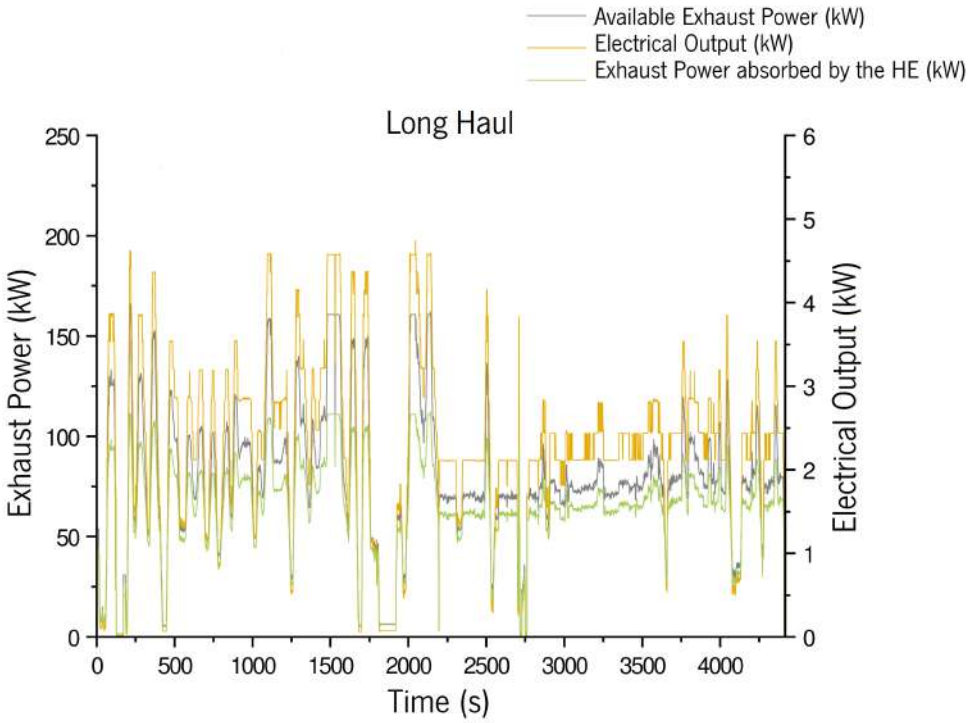

Figure 60: Results of the TEGs generated power, absorbed exhaust power and the available exhaust power for Long Haul driving cycle with 25.5 t

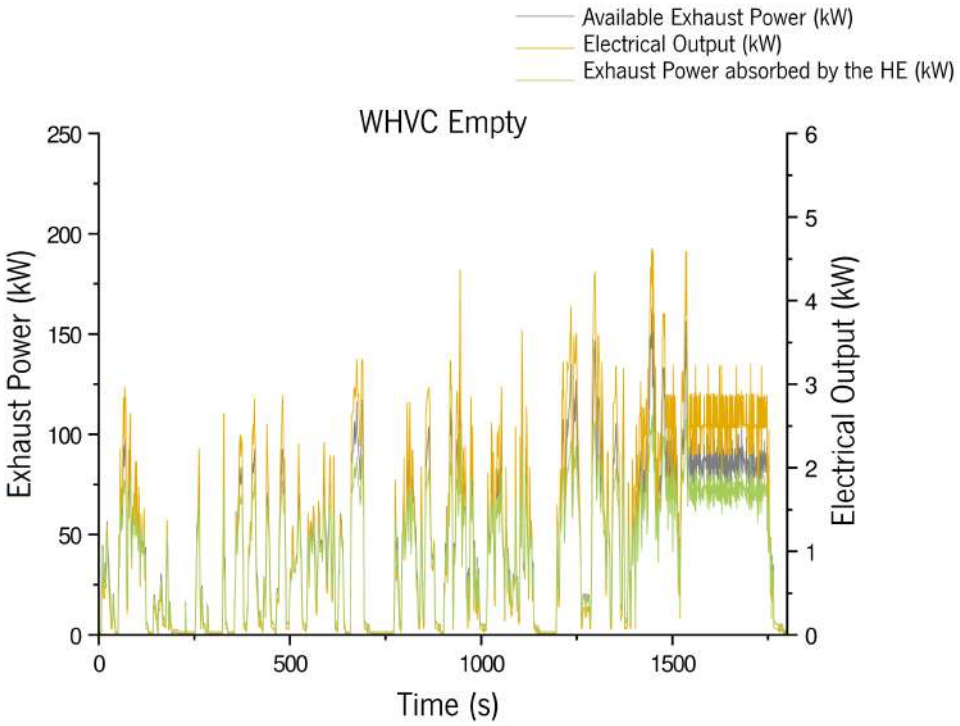

Figure 61: Results of the TEGs generated power, absorbed exhaust power and the available exhaust power for WHVC driving cycle with 7.5 t

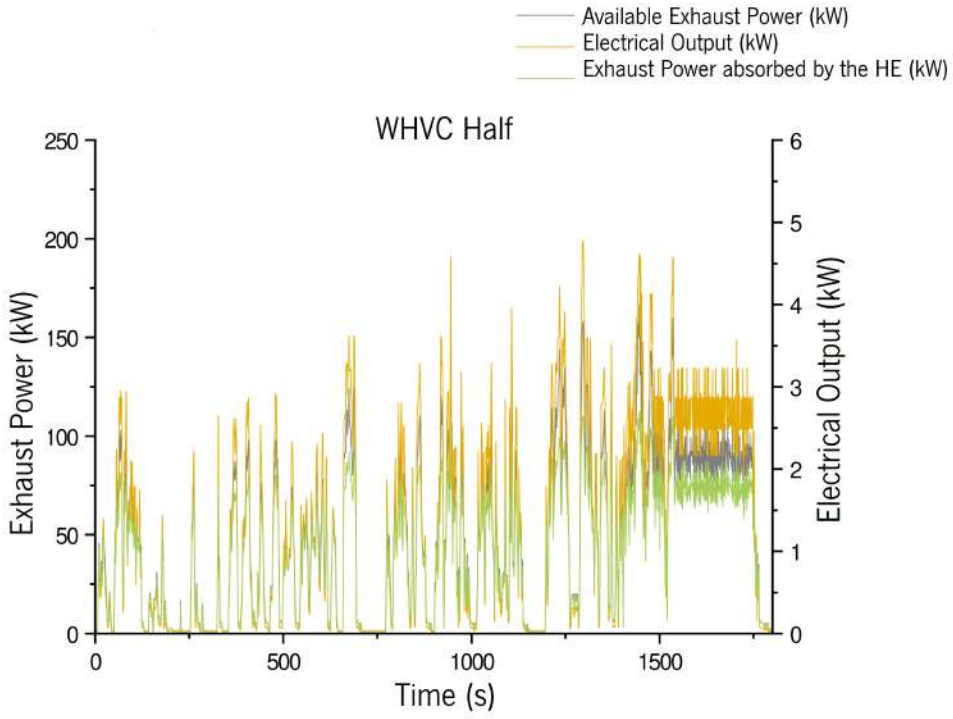

Figure 62: Results of the TEGs generated power, absorbed exhaust power and the available exhaust power for WHVC driving cycle with 12.75 t

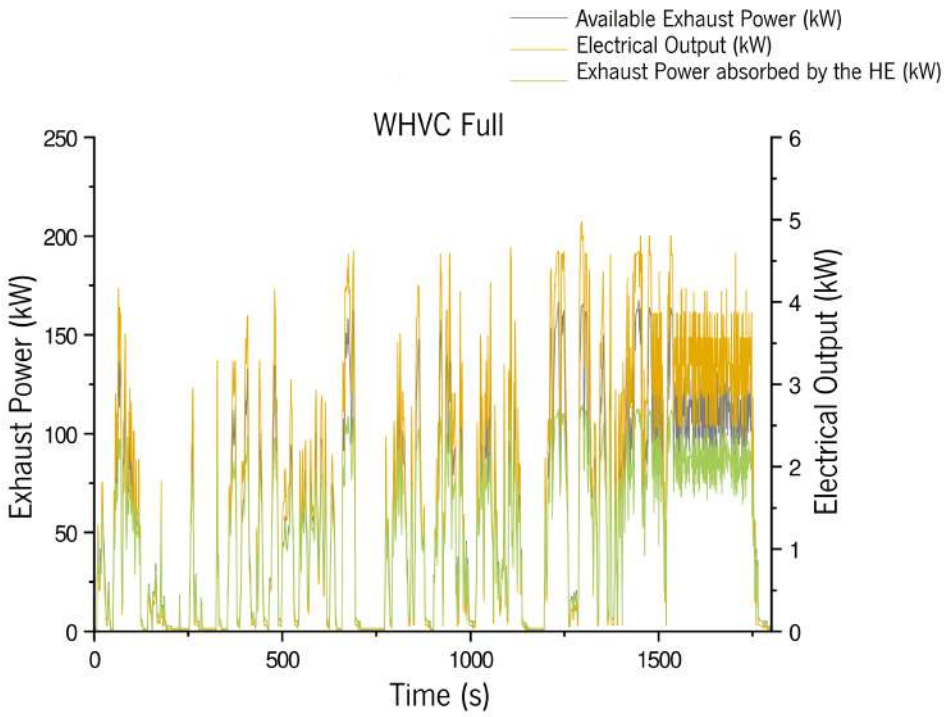

Figure 63: Results of the TEGs generated power, absorbed exhaust power and the available exhaust power for WHVC driving cycle with 25.5 t

In Figure 64 are gathered the resulting maximum and average electrical outputs. It is clear that the vehicle load influences the electrical production since more power is needed and therefore more available power in the exhaust gases, thus a maximum of 4622 W, 4773 W and 4975 W and an average of 1242 W, 1304 W and 1629 W of generated electricity were achieved in the WHVC cycle run with empty, half and full load, respectively. In the course of the Long Haul cycle run, the HDV has to overcome higher inclinations during a longer path (100 km) than the WHVC (20 km), resulting in a higher available thermal power, thus higher average electrical power. The maximum electrical power outputs achieved in each cycle run are similar. This means that the incoming heat from the exhaust gases was sufficient to be spread along the whole length of the generator, resulting in a uniform temperature in the TEGs hot face close to their maximum operating temperature and the VCs boiling temperature (250°C) [11].

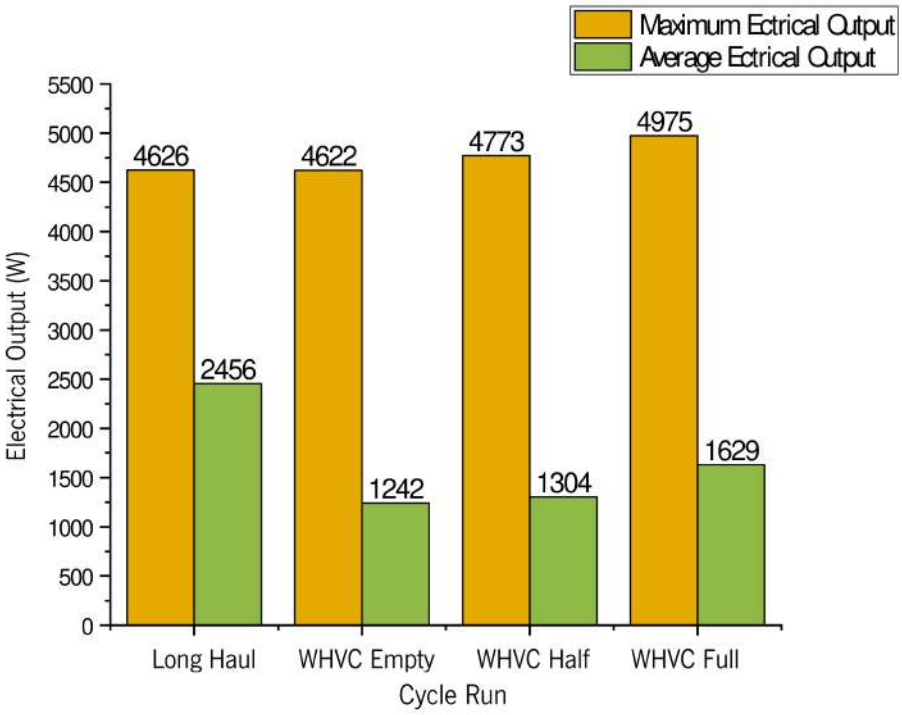

Figure 64: Average and maximum electrical output per cycle run

6.3 Conversion Efficiency and Pressure Drop

Important aspects to also take into consideration are the conversion efficiencies and the pumping power needed to overcome the pressure drop caused by the HE. In the graphics from Figure 65 to Figure 68 each dot represents one time step of the given cycle run in function of the available exhaust power. Regarding the power conversion efficiencies, two efficiencies were analysed: the efficiency as function of the heat crossing the TEGs modules, presented by red boxes, and the efficiency as function of the total available exhaust power, light green dots. The pumping power is given by the grey boxes. The electrical output is presented as well, in light orange dots.The observed breaks correspond to the TEG rows being activated by the increasing available power along the VCs. In all simulations, the efficiency relative to the power absorbed by the TEGs is proportional to the available exhaust power, as it increases with it up to about 4.4 %, resulting in maximum electrical outputs presented in Figure 64. Regarding the conversion efficiency relative to the available exhaust power, it is clear the visualization of its decrease under high power circumstances. This behaviour is justified by the fact that the system is in a state where the electrical production is only possible through more heat, this leads to the stabilization of the efficiency curve. One major influence to the engine mechanical efficiency is the additional back-pressure caused by the HE system. In the simulation model, a bypass valve was considered upstream of the HE. This valve is opened when the HE can no longer absorb more heat, thus by opening the valve the exhaust gas flows though an alternative path, preventing additional loads of back-pressure [11]. For the WHVC with full, half and empty loads, An average of 236 W, 151 W

and 137 W of back-pressure were measured in the WHVC with full, half and empty loads, respectively, and for the Long Haul cycle run, 236 W, this physical meaning of this value is the power that the engine loses because the exhaust stroke will need more mechanical work to overcome the higher outlet pressure.

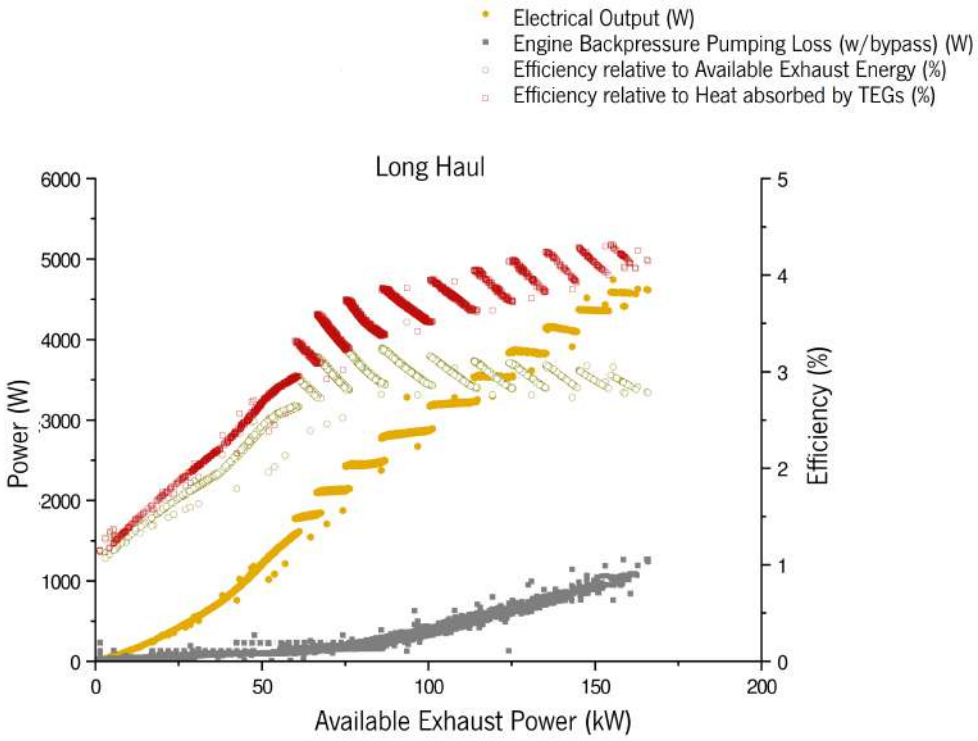

Figure 65: Results of the overall conversion efficiencies, generated power and pressure drop for the Long Haul driving cycle with 25.5 t

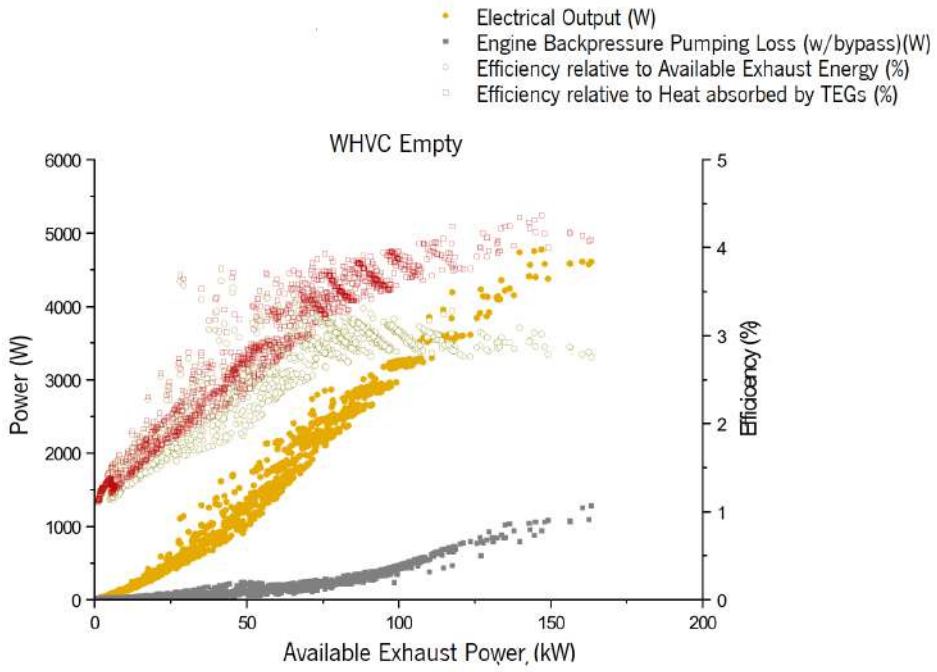

Figure 66: Results of the overall conversion efficiencies, generated power and pressure drop for the WHVC driving cycle with 7.5 t

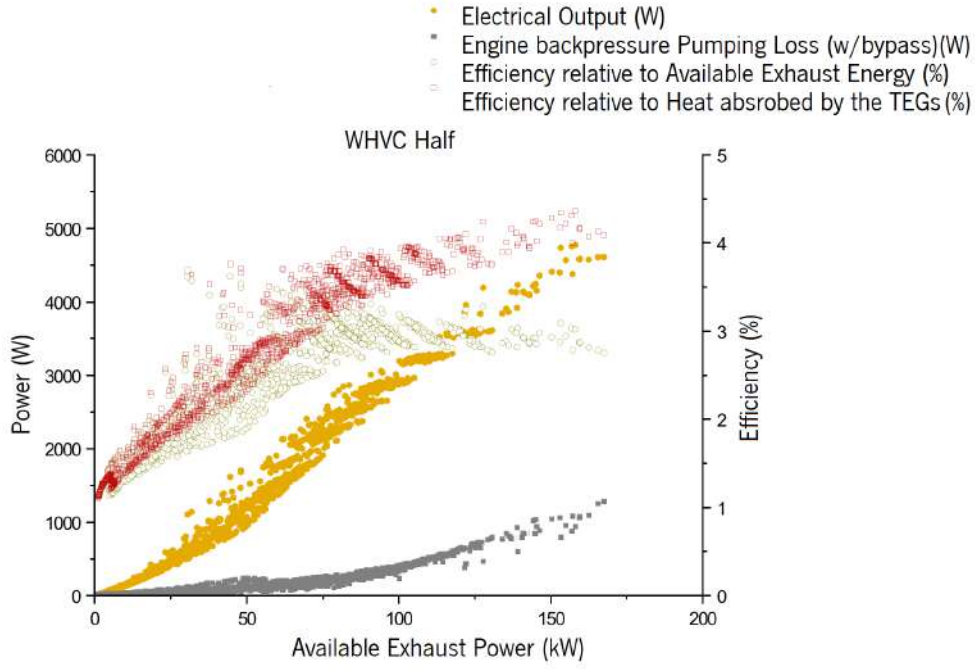

Figure 67: Results of the overall conversion efficiencies, generated power and pressure drop for the WHVC driving cycle with 12.75 t

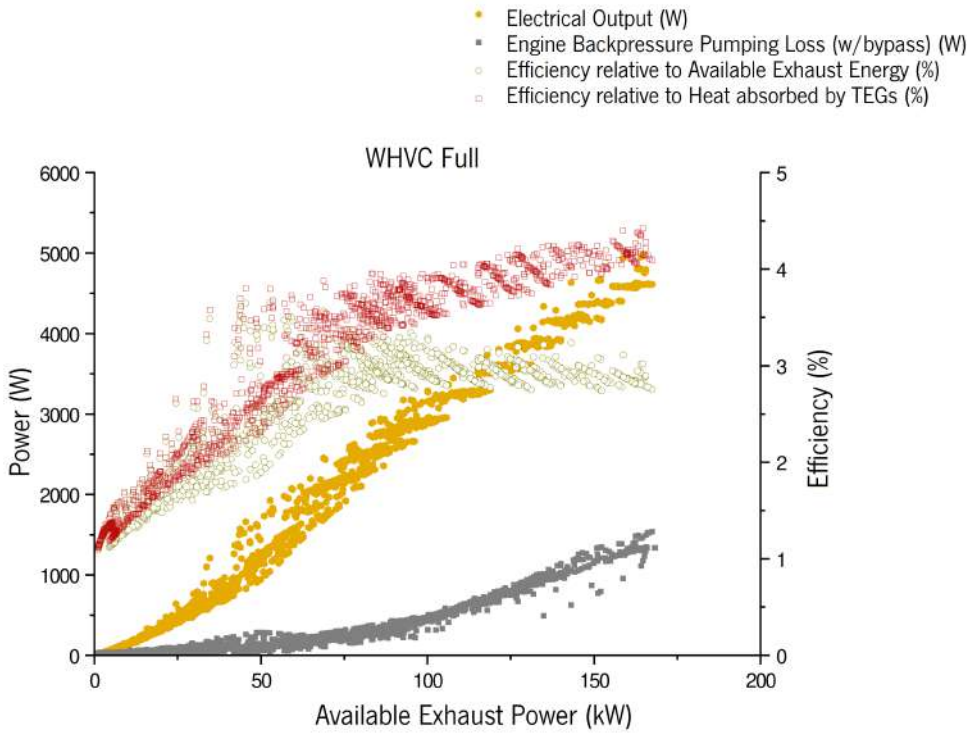

Figure 68: Results of the overall conversion efficiencies, generated power and pressure drop for the WHVC driving cycle with 25.5 t

6.4 Fuel and CO2 Savings

The vehicle alternator and battery support all the electrical load of the HDVs. The increasing electrical components present in the modern commercial transportation, such as the emissions control system, gauges, air conditioner, headlights, tail lights, cab marker lights, fog lights and van or trailer lights, are accountable for decreasing the fuel efficiency. Most commercial HDVs alternators have near 2.52 kW of electrical loads when operating, which for an alternator, such as the 36SI HD Alternator ([65]), with an efficiency of 68% results in a total of 3.7 kW of mechanical power consumption, representing more than 12 kW of fuel power in an engine with an average mechanical efficiency of 30%. In Table 17 are presented the fundamental savings obtained by applying the TEG system assuming the mentioned alternator with 68% efficiency for both cycle runs, Long Haul and WHVC with different loads. It was considered that the alternator was being fully used along the entire cycle runs. Along the Long Haul cycle, the system can almost produce enough an average electric power to fully compensate the alternator power needs by producing near 2.5 kW, resulting in a fuel savings of 1.07 L/100 km and reducing the CO_2 emissions by 28.75 g/km. In respect to the WHVC cycle run, the electrical production does not completely meet the alternator requirements, specially in the cycle with the lightest weight, with an average of 1.2 KW in contrast to the necessary 2.5kW. However, this cycle run has fuel savings rates near to the Long Haul ones. This is justified due the lower WHVC engine efficiencies, on which the savings in the mechanical

power requirements cause proportionally higher fuel savings.

Table 17: Average and on maximum engine power Savings from applying the developed TEG system within the several cycle runs

	AVERAGE VALUES				MAXIMUM ENGINE POWER			
	Long Haul	**WHVC 7.5 t**	**WHVC 12.75 t**	**WHVC 25.5 t**	**Long Haul**	**WHVC 7.5 t**	**WHVC 12.75 t**	**WHVC 25.5 t**
Driving cycle data								
Distance [km]	100	20	20	20	-	-	-	-
Engine efficiency [%]	34%	28%	29%	30%	38%	39%	39%	41%
Required Mechanical Power [kW]	173	102	108	141	382	378	378	384
Using the TEG system								
Electric energy produced [kw]	2.4	1.24	1.3	1.63	3.83	3.93	4.24	4.77
Energy produced [kJ/km]	101	112	117	146.73	-	-	-	-
Required Mechanical Power [kW]	169	100	106	138	375	371	371	377
Fuel savings [L/100km]	1.14	1.33	1.37	1.64	0.0004	0.002	0.002	0.002
Fuel savings [%]	2.31%	1.96%	1.85%	2.12%	1.83%	1.85%	1.85%	1.82%
CO2 emissions savings [g/km]	30.45	35.57	36.68	43.92	0.01	0.06	0.06	0.06

By comparing the simulation outputs with state-of-the-art results from literature, it is possible to better analyse the study performance. As mentioned above, Heber et al. [41] simulated and tested the efficiency of a waste heat recovery system through the generation of the thermal power from the exhaust gas into electricity using TEGs in an HDV powered by natural gas. In this novel, the maximum fuel savings for a WHVC cycle run with the HDV on full load were 2.3%, corresponding to a reduction in CO_2 emissions of 24.6 g/km, while the system was generating 1424W. The fuel savings and the electrical output present similar values to the ones simulated in the present study, except in the Long Haul which has a higher average electrical production, while the CO_2 emissions in [41] present a significantly lower decrease since more CO_2 is released during the Diesel combustion.

Chapter 7

Conclusion

The goal of this project was to simulate a typical commercial HDV along with two cycle runs and the adaptation of a waste heat recovery system with thermal control, designed by LaMoTA research group described in [11], to be applied in a heavy-duty vehicle (HDV). The purpose of the system is to convert the part of the heat lost through the exhaust gases into electricity, thus, according to the HDV simulation results regarding the exhaust mass flow and exhaust temperature rates, the waste heat recovery system was developed.

The HDV simulation was done through AVL CRUISE and BOOST software. With these tools an HDV with a 16 L, 515 hp Diesel engine was simulated within two cycle runs, World Harmonized Vehicle Cycle (WHVC) and the Long Haul cycle run (an AVL CRUISE template cycle). For the HDV simulation, engine information was collected from literature and applied in the software. Aspects about the vehicle weight load, dimensions, and the existent resistances were also taken into consideration. The simulations were processed along with two cycle runs. The WHVC was simulated with three curb weight loads, 25.5 t(WHVC Full), 12.75 t (WHVC Half) and 7.5 t (WHVC Empty). The main results from these simulations are the exhaust gas mass flow rate and the exhaust gas temperature. As expected, the higher the weight load higher were the engine needs and the exhaust gases thermal power. The Long Haul cycle run was simulated with the HDV on its maximum weight. As this cycle has not only a longer distance but also higher inclinations, greater available exhaust powers were observed. Thus, the average available exhaust powers were 59.64 kW, 48.91 KW, 46.9 kW for the WHVC Full, Half and Empty, respectively, and 81.42 kW for the Long Haul. In previous LaMoTA projects, data from the exhaust gas was obtained through Matlab algorithms for specific cycle runs. The integration of the HDV simulation in AVL CRUISE made it possible to obtain information about not only the exhaust gases but all the vehicle components, particularly regarding

the engine, along different cycle runs with different constraints at the desired cycle points. Thus, providing more valid and realistic results.

Regarding the waste heat recovery system, the model has to be capable of converting the thermal load from the exhaust gas into electricity, thus reducing the fuel consumption. In the proposed concept the exhaust gases flow through the system via wavy fins (WFs) plates. The heat conversion into electricity is enabled by thermoelectric modules (TEGs) (GM250-127-28-10 were used ([5])), which for a proper operation need to work nearest to their maximum supported temperature of 250°C in the hot face. Since the thermal load from the exhaust gases can either exceed or be above the optimal temperature, the system must feature a thermal control quality, which is granted by the application of vapour chambers (VCs) with variable conductance. Additionally, the TEGs need to have their cold face coldest as possible, hence the cooling is compromised by cooling plates (CPs). This concept system model was created in CAD tools (Inventor and Autocad). The system thermal evaluation was processed in a 2D heat transfer COMSOL simulation (two models were analysed: one with six plates of WFs, other with nine WFs plates), from where the system thermal resistances were obtained and used in a 1D model. This 1D model is a Matlab algorithm that predicts the system thermoelectric and thermal behaviour and pressure drops associated with the model. This algorithm has as input not only all the components (WF, TEGs, VCs and CP) properties but also the HDV simulation results of the exhaust gases in each point of the simulated cycle runs. Thus the algorithm outputs are provided along the cycle runs points. From the 1D model is possible to evaluate a suitable geometric setup and the system size definition. Here, two designs were calculated, one with three CPs in length other with two CPs in length. From the 2D heat transfer COMSOL simulation was concluded that the six plates layout had lower thermal resistance, thus was chosen for the system. Through the 1D model with two CPs in length was identified has with the lowest pressure drop and higher TEGs efficiency, and thus selected for the continuity of the project. The final model resulted in a 128 TEGs model with a total weight of 103.66 Kg with 300.4 X 750 X 232 mm (length x width x height).

The accomplished project results of the developed TEG system regarding the electricity production, fuel savings and corresponding CO_2 emission savings were overall satisfactory, especially when compared with existing results in literature. Average electric power production of 1.63 kW, 1.3 kW, 1.24 kW were achieved for the WHVC Full, Half and Empty, respectively, and 2.4 kW for the Long Haul cycle run. The maximum electrical powers were similar in the four cases since the same modules were used: 4.98 kW , 4.77 kW, 4.62 kW for WHVC Full, Half and Empty, respectively, and 4.63 kW for the Long Haul cycle run, meaning that at these points of the cycle the TEGs were operating at their optimal working temperature, 250°C. Average fuel consumption savings of about 2% and CO_2 emissions savings of around 37 g/km were determined in all simulations. Is possible to conclude the system has a good potential for waste recovery applications in HDV, especially when submitted to long vehicle use. This positive performance

of the system is thanks to the ability of the system to maximize heat absorption, while still keeping the modules close to their optimal temperature while preventing them from overheating or from excessive thermal dilution.

7.1 Future Work

One goal of this project was to prove the waste recovery system concept can be applied to HDVs and to provide a preliminary study of the maximum possible power that can be recovered from the exhaust gases, however, no optimization of the shape of the system was done, but it will be possible to develop a system with a geometry that is much lighter and compact. It is suggested geometric optimization, namely by reducing aluminium thicknesses in the block and by using lightweight cooling plates. Further study regarding system dimensioning is advisable. Between the VCs and the TEGs lies a thick block of aluminium which is increasing the system thermal resistance and weight. This layer can be reduced if respecting the necessary space for the heat transfer to occur and the minimum dimensions for structural and construction purposes. The CPs water pumping power was not considered in this study. It is suggested that detailed pumping power calculations are done and the optimization of the CP geometry and water flow rate be optimized. The influence of the mass of the system was also not analyzed because the mass of the system proposed has not been optimized. It is proposed that a mass optimization and a calculation of its influence on results may be done. A simulation with a stronger integration of AVL Boost into AVL Cruise is also advisable for a better assessment of the influence of the generator on engine performance. The use of Wavy Fin profiles with a wider section area could be explored, because the profile used seems to induce too much pressure drop for the flow typology of Diesel engines (lower temperature, a higher flow rate of gases because of the lean mixtures used, when compared with gasoline and natural gas engines). The use of better TEGs (in terms of performance and cost) is also suggested. LaMoTA team has developed affordable TE materials recently. These could enable cheap generators. Finally, the same CP dissipating heat from the cold TEG face in the top of one heat exchanger model could be dissipating the heat of the TEG paced in the bottom of the heat exchange staked above, thus eliminating 8 CPs.

Bibliography

[1] V. V. Georgatzi, Y. Stamboulis, and A. Vetsikas. “Examining the determinants of CO2 emissions caused by the transport sector: Empirical evidence from 12 European countries.” In: *Economic Analysis and Policy* 65 (Mar. 2020), pp. 11–20. doi: 10.1016/j.eap.2019.11.003. url: https://doi.org/10.1016/j.eap.2019.11.003.

[2] J. Krause, C. Thiel, D. Tsokolis, Z. Samaras, C. Rota, A. Ward, P. Prenninger, T. Coosemans, S. Neugebauer, and W. Verhoeve. “EU road vehicle energy consumption and CO2 emissions by 2050 – Expert-based scenarios.” In: *Energy Policy* 138.December 2019 (2020), p. 111224. issn: 0301-4215. doi: 10.1016/j.enpol.2019.111224. url: https://doi.org/10.1016/j.enpol.2019.111224.

[3] C. Baptiste and P. Khadija. *MEPs approve new CO2 emissions limits for trucks*. 2019. url: https://www.europarl.europa.eu/news/en/press-room/20190412IPR39009/meps-approve-new-co2-emissions-limits-for-trucks.

[4] *Overview of electricity production and use in Europe*. 2018. url: https://www.eea.europa.eu/media/infographics#c5=&b_start=0 (visited on 10/29/2020).

[5] A. E. T. Limited. *GM250-127-28-10 Thermoelectric Generator Module*. 2017.

[6] R. Rodriguez, S. Member, M. Preindl, S. Member, J. S. Cotton, and A. Emadi. “Review and Trends of Thermoelectric Generator Heat Recovery in Automotive Applications.” PP (2019), p. 1.

[7] *CO2 emissions from cars: facts and figures (infographics)*. 2019. url: https://www.europarl.europa.eu/co2-emissions-from-cars-facts-and-figures-infographics (visited on 10/29/2020).

[8] K. Holmberg, P. Andersson, N. O. Nylund, K. Mäkelä, and A. Erdemir. “Global energy consumption due to friction in trucks and buses.” In: *Tribology International* 78 (2014), pp. 94–114. doi: 10.1016/j.triboint.2014.05.004.

[9] J. R. Armstead and S. A. Miers. “Review of Waste Heat Recovery Mechanisms for Internal Combustion Engines.” In: *Journal of Thermal Science and Engineering Applications* 6.1 (Oct. 2013). 014001. issn: 1948-5085. doi: 10.1115/1.4024882. eprint: https://asmedigitalcollection.

asme.org/thermalscienceapplication/article-pdf/6/1/014001/6333268/tsea_006_01_014001.pdf. url: https://doi.org/10.1115/1.4024882.

[10] L. Heber and J. Schwab. "Modelling of a thermoelectric generator for heavy-duty natural gas vehicles: Techno-economic approach and experimental investigation." *Applied Thermal Engineering* 174 (2020).

[11] N. Pacheco, F. Brito, R. Vieira, J. Martins, H. Barbosa, and L. Gonçalves. "Compact automotive thermoelectric generator with embedded heat pipes for thermal control." In: *Energy*. 2020. doi: 10.1016/j.energy.2020.117.

[12] M. D. Sandip S. kale, V. W. Bhatkar. "Performance Evaluation of Plate-Fin-And Tube Heat Exchanger with Wavy Fins- A Review." In: *Journal of Engineering Research and Applications* 4.9 (2014), pp. 154–158.

[13] M. C. Tsai, S. W. Kang, and K. Vieira De Paiva. "Experimental studies of thermal resistance in a vapor chamber heat spreader." In: *Applied Thermal Engineering* 56 (2013). issn: 13594311. doi: 10.1016/j.applthermaleng.2013.02.034. url: http://dx.doi.org/10.1016/j.applthermaleng.2013.02.034.

[14] X. Cheng, G. Yang, and J. Wu. "Recent advances in the optimization of evaporator wicks of vapor chambers: From mechanism to fabrication technologiesautocaravana." In: *Applied Thermal Engineering* 188.October 2020 (2021), p. 116611. issn: 13594311. doi: 10.1016/j.applthermaleng.2021.116611. url: https://doi.org/10.1016/j.applthermaleng.2021.116611.

[15] E. G. Giakoumis. *Driving and Engine Cycles*. Springer US, 2017. isbn: 9783319490335.

[16] DieselNet. *Emission Test Cycles*. url: https://dieselnet.com/standards/cycles/whtc.php (visited on 06/09/2021).

[17] V. Viswanathan. "Performance Metrics Required of Next- Generation Batteries to Make a Practical Electric Semi Truck." In: (2017). doi: 10.1021/acsenergylett.7b00432.

[18] U.S. Department of Energy. "Vehicle Weight Classes & Categories." url: https://afdc.energy.gov/data/10380 (visited on 05/20/2021).

[19] P. Europeu. *DIRETIVA (UE) 2015/719*. 2015.

[20] J. Martins. *Motores de Combustão Interna*. Quarta Edi. Publindústria, 2013, p. 512.

[21] D. Yanakiev and I. Kanellakopoulos. "Engine and Transmission Modeling for Heavy-Duty Vehicles." In: *Electrical Engineering* May (1995).

[22] Ultimatespecs. *Ford Focus 3 1.6 TDCi 95HP Trend Specs*. url: https://www.ultimatespecs.com/car-specs/Ford/24700/Ford-Focus-3-(EU-Market)-16-TDCi-95HP-Auto-Start-Stop-Trend.html (visited on 06/08/2021).

[23] D. D. G. Brand. *DETROIT DD13 Engine specifications*. June. 2016, p. 2018.

[24] K. Tanabe, K. Susumu, and N. Shinjii. "Effect of Fuel Injection Rate Control on Reduction of Emissions and Fuel Consumption in a Heavy Duty DI Diesel Engine." *SAE* 2005 ().

[25] A. Mulemane, J.-s. Han, P.-h. Lu, S.-j. Yoon, and M.-c. Lai. "Modeling Dynamic Behavior of Diesel Fuel Injection Systems." In: 2004.724 (2018).

[26] P. Braun, J. Gebhard, F. M. Matysik, and H. P. Rabl. "Potential Technical Approaches for Improving Low-Temperature NOx Conversion of Exhaust Aftertreatment Systems." In: *Chemie-Ingenieur-Technik* 90.6 (2018), pp. 762–773. issn: 15222640. doi: 10.1002/cite.201700122.

[27] A. Russell and W. S. Epling. "Diesel oxidation catalysts." In: *Catalysis Reviews - Science and Engineering* 53.4 (2011), pp. 337–423. issn: 01614940. doi: 10.1080/01614940.2011.596429.

[28] H. Jääskeläinen and M. K. Khair. "Exhaust Gas Recirculation." *DieselNet Technology Guide* (2020). doi: 10.1007/bf03224626.

[29] H. Nguyen-Schäfer. "Turbocharging concepts." In: *Springer Tracts in Mechanical Engineering* 22 (2015), pp. 1–20. issn: 21959870. doi: 10.1007/978-3-319-17644-4_1.

[30] G. Holger and J. Zagone. "Commercial Vehicle Turbocharging Technologies for CO2 Targets from 2025 Onward." In: *Springer Fachmedien Wiesbaden: ATZheavy duty worldwide* 12.Electronic ISSN: 2524-8774 (2019). doi: 10.1007/s41321-019-0034-6.

[31] A. M. Andwari, A. Pesyridis, V. Esfahanian, A. Salavati-Zadeh, and A. Hajialimohammadi. "Modelling and evaluation of waste heat recovery systems in the case of a heavy-duty diesel engine." In: *Energies* 12.7 (2019). issn: 19961073. doi: 10.3390/en12071397.

[32] M. He, E. Wang, Y. Zhang, W. Zhang, F. Zhang, and C. Zhao. "Performance analysis of a multilayer thermoelectric generator for exhaust heat recovery of a heavy-duty diesel engine." In: *Applied Energy* 274.May (2020), p. 115298. issn: 0306-2619. doi: 10.1016/j.apenergy.2020.115298. url: https://doi.org/10.1016/j.apenergy.2020.115298.

[33] D. Rowe. *Thermoelectrics Handbook: Macro to Nano*. Ed. by C. Press. 1st Editio. 2006. isbn: 9781315220390.

[34] L. Heber and J. Schwab. "Energy and Thermal Management, Air-Conditioning, and Waste Heat Utilization." In: *Energy and Thermal Management, Air-Conditioning, and Waste Heat Utilization* July (2019). doi: 10.1007/978-3-030-00819-2.

[35] S. Kwon, Y.-g. Kim, S. Lee, and J. C. Kim. "Measurement of the figure of merit of a thermoelectric material." In: (2012).

[36] F. P. Brito, R. Vieira, J. Martins, L. M. Goncalves, A. P. Goncalves, R. Coelho, E. B. Lopes, E. Symeou, and T. Kyratsi. "Analysis of thermoelectric generator incorporating n-magnesium silicide and p-tetrahedrite materials." *Energy Conversion and Management* 236.May (2021). issn: 01968904. doi: 10.1016/j.enconman.2021.114003.

[37] "Solid state generators and energy harvesters for waste heat recovery and thermal energy harvesting." In: *Thermal Science and Engineering Progress* 9.January (2019). issn: 24519049. doi: 10.1016/j.tsep.2018.11.011. url: https://doi.org/10.1016/j.tsep.2018.11.011.

[38] J. Fairbanks. "Thermoelectric Applications in Vehicles Status." *U.S. Department of Energy Washington, D.C., U.S.A.* 58 (2008).

[39] E. F. Thacher, B. T. Helenbrook, M. A. Karri, and C. J. Richter. "Testing of an automobile exhaust thermoelectric generator in a light truck." *. Proceedings of the Institution of Mechanical Engineers, Part D: Journal of Automobile Engineering* 221.1 (2007), pp. 95–107. issn: 09544070. doi: 10.1243/09544070JAUT051.

[40] J. Liebl, S. Neugebauer, A. Eder, M. Linde, B. Mazar, and W. Stutz. *The thermoelectric generator from BMW is making use of waste heat*. 2009. doi: 10.1007/bf03226939.

[41] K. Y. Heber, Lars, J. Schwab, T. Knobelspies, Dr. M. Grill. *HD-TEG: Potential for increasing the efficiency of heavy duty vehicles through the use of a new type of waste heat recovery system (thermoelectrics)*. Tech. rep. 2020, p. 72.

[42] J. Martins, F. P. Brito, L. Gonçalves, J. Antunes, and R. Romeu. "Heat-Pipe Assisted Thermoelectric Generators for Exhaust Gas Applications." In: *Proceedings of the ASME 2010 International Mechanical Engineering Congress & Exposition* (2010).

[43] J. Martins, L. M. Goncalves, J. Antunes, and F. P. Brito. "Thermoelectric Exhaust Energy Recovery with Temperature Control through Heat Pipes." *SAE 2011 World Congress and Exhibition* (2011), pp. 1–19. doi: 10.4271/2011-01-0315.

[44] F. P. Brito, J. Martins, L. M. Goncalves, and R. Sousa. "Temperature controlled exhaust heat thermoelectric generation." *SAE Technical Papers* (2012). issn: 26883627. doi: 10.4271/2012-01-1214.

[45] F. P. Brito, J Martins, L. M. Goncalves, D Sousa, and N Antunes. "Influence of Heat Pipe Operating Temperature on Exhaust Heat Thermoelectric Generation." In: 6.2 (2013). doi: 10.4271/2013-01-0559.

[46] N. Kedam, U. Dmitry A, B. Evgeniy V, and G. Alexey A. "Heat transfer factor j and friction factor f correlations for offset strip fin and wavy fin of compact plate-fin heat-exchangers." In: *Case Studies in Thermal Engineering* 28.August (2021), p. 101552. issn: 2214157X. doi: 10.1016/j.csite.2021.101552. url: https://doi.org/10.1016/j.csite.2021.101552.

[47] Y. Çengel. *Heat Transfer: A Practical Approach*. McGraw-Hill series in mechanical engineering. McGraw-Hill, 2003. isbn: 9780072458930. url: https://books.google.pt/books?id=nrbfpSZTwskC.

[48] B. Zohuri. *Compact Heat Exchanges: Selection, Application, Design and Evaluation*. Apr. 2016. isbn: 978-3319298344.

[49] S Ezzitouni, L Sánchez, and O Armas. "Global energy balance in a diesel engine with a thermoelectric generator." In: *Applied Energy* 269.May (2020), p. 115139. issn: 0306-2619. doi: 10.1016/j.apenergy.2020.115139. url: https://doi.org/10.1016/j.apenergy.2020.115139.

[50] ETSU and WS Atkins Consultants. *Compact Heat Exchangers - Guidance for Engineers*. 2000.

[51] J. Bell. *Maintaining a Plate Heat Exchanger*. url: https://www.process-heating.com/articles/86243-maintaining-a-plate-heat-exchanger (visited on 09/06/2021).

[52] J. P. H. Exchanger. *Brazed Plate Heat Exchanger Feature*. url: https://www.jiawei-phe.com/Brazed-Plate-Heat-Exchanger.html (visited on 09/06/2021).

[53] L. B. Erbay. *Compact heat exchangers*. January. 2013, p. 570. isbn: 978-3-319-29834-4. arXiv: arXiv:1011.1669v3.

[54] R. Le Pierres, D. Southall, and S. Osborne. "Impact of mechanical design issues on printed circuit heat exchangers." In: *Proceedings of SCO2 power cycle symposium* (2011).

[55] C. Z. Z. Y. Dong Junqi Chen Jiangping and Z. Wenfeng. "Heat transfer and pressure drop correlations for the wavy fin and flat tube heat exchangers." In: *Applied Thermal Engineering* 27.11 (2007), pp. 2066–2073. issn: 1359-4311. doi: https://doi.org/10.1016/j.applthermaleng.2006.11.012. url: https://www.sciencedirect.com/science/article/pii/S1359431106004121.

[56] F. manufacturer. *Advanced Fin UK*. url: http://advancedfinuk.com/wavy.htm (visited on 09/06/2021).

[57] P. DUNN and D. REAY. *Heat Pipes*. 4th. Pergamon, 1994, p. 358.

[58] "A Review of Vapor Chambers." In: *Heat Transfer Engineering* 40.19 (2019), pp. 1551–1573. issn: 15210537. url: https://doi.org/10.1080/01457632.2018.1480868.

[59] J. Velardo, A. Date, R. Singh, J. Nihill, A. Date, T. L. Phan, and M. Takahashi. "Experimental investigation of a vapour chamber heat spreader with hybrid wick structure." *International Journal of Thermal Sciences* 140.February (2019), pp. 28–35. issn: 12900729. doi: 10.1016/j.ijthermalsci.2019.02.009. url: https://doi.org/10.1016/j.ijthermalsci.2019.02.009.

[60] Y.-C. Li and S.-C. Wong. “Effects of vapor duct thickness on the capillary blocking and thermal performance of ultra-thin vapor chambers under natural convection cooling.” In: *Applied Thermal Engineering* 195 (2021), p. 117148. issn: 1359-4311. doi: https://doi.org/10.1016/j.applthermaleng.2021.117148. url: https://www.sciencedirect.com/science/article/pii/S1359431121005871.

[61] M. Wang, W. Cui, and Y. Hou. “Thermal spreading resistance of grooved vapor chamber heat spreader.” In: *Applied Thermal Engineering* 153 (2019), pp. 361–368. issn: 1359-4311. doi: https://doi.org/10.1016/j.applthermaleng.2019.03.025. url: https://www.sciencedirect.com/science/article/pii/S1359431118348488.

[62] Y. Li, Z. Li, W. Zhou, Z. Zeng, Y. Yan, and B. Li. “Experimental investigation of vapor chambers with different wick structures at various parameters.” In: *Experimental Thermal and Fluid Science* 77 (2016), pp. 132–143. issn: 0894-1777. doi: https://doi.org/10.1016/j.expthermflusci.2016.04.017. url: https://www.sciencedirect.com/science/article/pii/S0894177716300930.

[63] Q. Xin. *Diesel Engine System Design*. 1st. Woodhead Publishing, 2011, p. 1088. isbn: 978-1-84569-715-0. doi: 10.1533/9780857090836.

[64] Fischerelektronik. *Standard extruded heatsinks*. url: https://www.fischerelektronik.de/web_fischer/en_GB/heatsinks/A01/Standard\%20extruded\%20heatsinks/PG/SK624/search.xhtml.

[65] BorgWarner. *Alternator 36SI ™ Heavy Duty Alternator*. Delco Remy, 2000.

[66] A. I. Zografos, W. A. Martin, and J. E. Sunderland. “Equations of properties as a function of temperature for seven fluids.” *Computer Methods in Applied Mechanics and Engineering* 61.2 (1987). issn: 00457825. doi: 10.1016/0045-7825(87)90003-X.

Annex I

Useful Fluid Properties Equations

Since most of the fluid properties are temperature dependent, values that are usually stored in long tables, for an accurate thermal simulation, equations that grant precise values for a designated temperature simplify the computational model construction. The following equations display the thermodynamics properties and were gathered from [66].

I.1 Water properties

Property equations for liquid water, temperature range 273.2 K-600 K:

- Density [kg/m^3]

$$\rho_{water} = -3.0115 \times 10^{-6} T^3 + 9.6272 \times 10^{-4} T^2 - 0.11052T + 1022.4 \quad (52)$$

- Dynamic viscosity [Pa.s]

$$\mu_{water} = 3.8208 \times 10^2 (T - 25.33)^{-1} \quad (53)$$

- Specific heat [kJ/kgK]

$$Cp_{water} = 1.7850 \times 10^{-7} T^3 - 1.9149 \times 10^{-4} T^2 + 6.7953 \times 10^2 T - 3.7559 \quad (54)$$

- Thermal conductivity [W/mK]

$$k_{water} = 4.2365 \times 10^{-9} T^3 - 1.1440 \times 10^{-5} T^2 + 7.1959 \times 10^{-3} T - 0.63262 \quad (55)$$

I.2 Air properties

Property equations for air, temperature range 100 K-3000 K:

- Density [kg/]

$$\rho_{air} = -345.57(T - 2.688)^{-1} \tag{56}$$

- Dynamic viscosity [Pa.s]

$$\mu_{air} = 2.5914 \times 10^{15} T^3 - 1.4346 \times 10^{-11} T^2 + 5.0523 \times 10^{-8} T + 4.1130 \times 10^{-6} \tag{57}$$

- Specific heat capacity [kJ/kgK]

$$\begin{aligned} Cp_{air} &= 1.3864 \times 10^{-13} T^4 - 6.4747 \times 10^{-10} T^3 \\ &+ 1.0234 \times 10^{-6} T^2 - 4.3282 \times 10^{-4} T + 1.0613 \end{aligned} \tag{58}$$

Annex II

Heavy-Duty Simulation

The present annex describes how the HD engine was specified in the CRUISE software. All data points were carefully collected from the engine map and entered into the CRUISE software.

II.1 New version

From the User Area, presented in Figure 69, the Commercial Model was selected from the available projects. The Class 05 version was selected because of its setup: a truck with a three axle trailer.

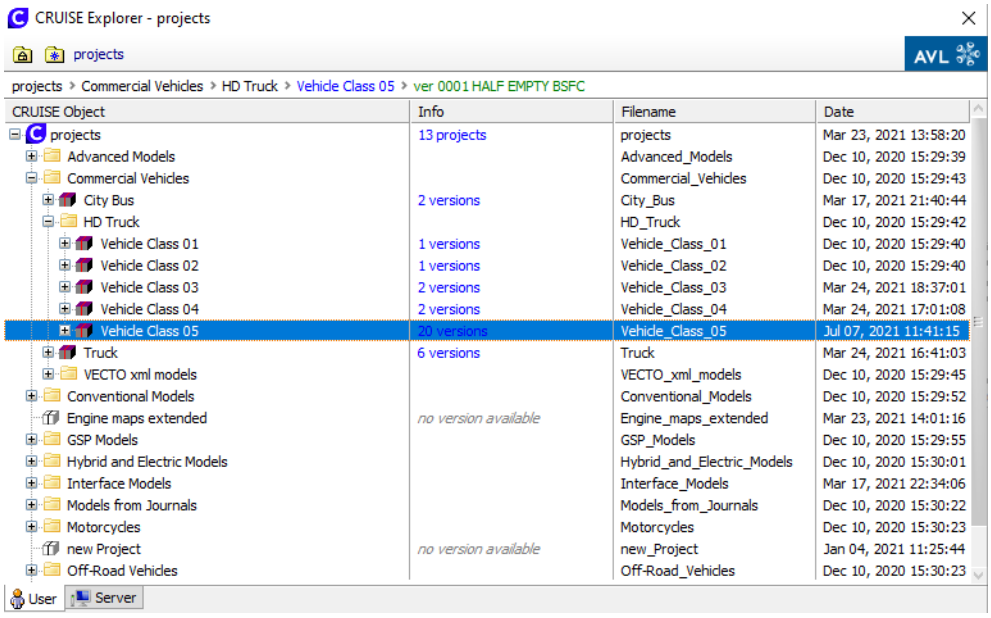

Figure 69: CRUISE User Area with the available templates

II.2 Components Input Data

Figure 28 represent the complete model used for the simulation. The Engine Truck settings were adjusted to an engine based on literature and the AVL Exhaust System component was added.

II.2.1 Engine

The primary information regarding the engine geometry presented on table 6 were placed on the window pictured in Figure 70.

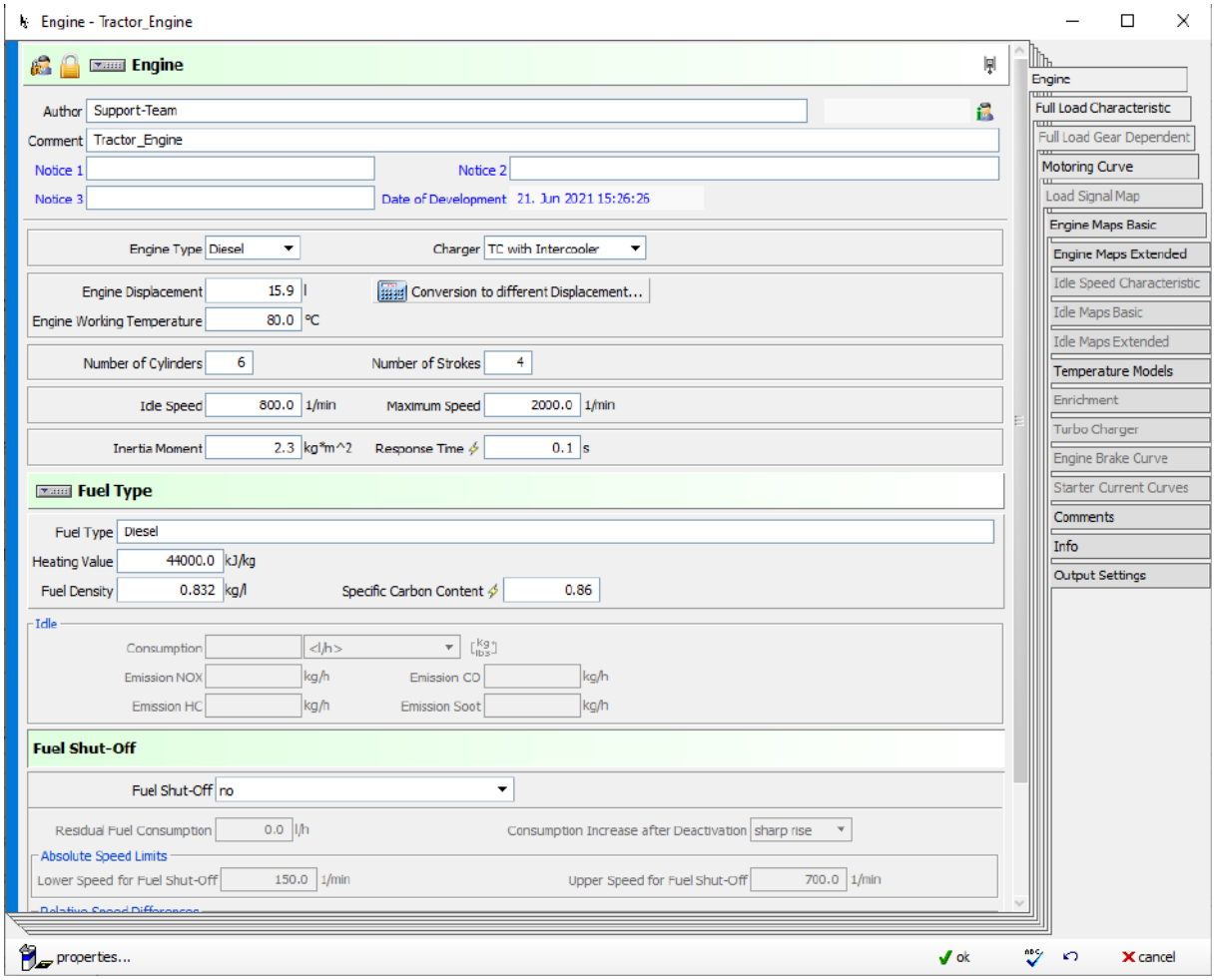

Figure 70: CRUISE Engine settings definition

II.2.1.1 Engine Full Load Characteristic

On the Full Load Characteristic section, the data points regarding the maximum torque and respective engine speed were collected from Figure 29 BSFC map and placed on the table illustrated in Figure 71. The values are discriminated on Table 18.

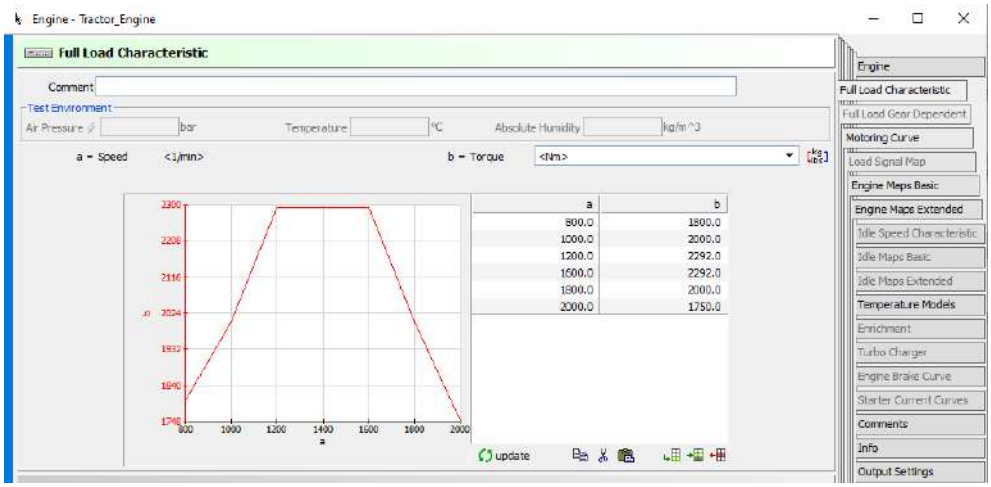

Figure 71: CRUISE Engine Full Load Characteristic

Table 18: HD Engine Full Load Characteristic values

Engine Full Load Characteristic	
Speed (rpm)	**Torque (N.m)**
800	1800
1000	2000
1200	2292
1600	2292
1800	2000
2000	1750

II.2.1.2 Fuel Consumption Characteristic

The Engine Maps Basic, enables the introduction of the Fuel Consumption Map described in Figure 72. The data points in 19 were calculated from the engine performance.

Table 19: HD Engine Fuel Consumption Map values

Engine Fuel Consumption Map					
Speed (rpm)	**Torque (N.m)**	**Mass Flow (kg/s)**	**Speed (rpm)**	**Torque (N.m)**	**Mass Flow (kg/s)**
800	100	0.001	1400	500	0.006
800	250	0.002	1400	750	0.007
800	500	0.003	1400	1000	0.009
800	750	0.004	1400	1250	0.012
800	1000	0.005	1400	1500	0.013
800	1500	0.007	1400	1750	0.015
800	1650	0.008	1400	2292	0.019
1000	100	0.001	1600	100	0.002
1000	250	0.002	1600	250	0.004
1000	500	0.003	1600	500	0.007
1000	750	0.005	1600	1000	0.011
1000	1000	0.006	1600	1500	0.015
1000	1250	0.008	1600	2000	0.019
1000	1500	0.009	1600	2200	0.021
1000	1600	0.010	1600	2292	0.021
1000	2000	0.012	1800	100	0.002
1200	100	0.001	1800	250	0.004
1200	250	0.003	1800	500	0.007
1200	500	0.004	1800	750	0.009
1200	900	0.007	1800	1000	0.012
1200	1000	0.008	1800	1250	0.015
1200	1200	0.009	1800	1500	0.018
1200	1500	0.011	1800	1750	0.020
1200	2000	0.014	1800	2000	0.022
1200	2100	0.014	2000	100	0.002
1200	2292	0.014	2000	250	0.005
1400	100	0.001	2000	500	0.008
1400	250	0.003	2000	1000	0.013
1400	500	0.006	2000	1500	0.020
			2000	1750	0.023

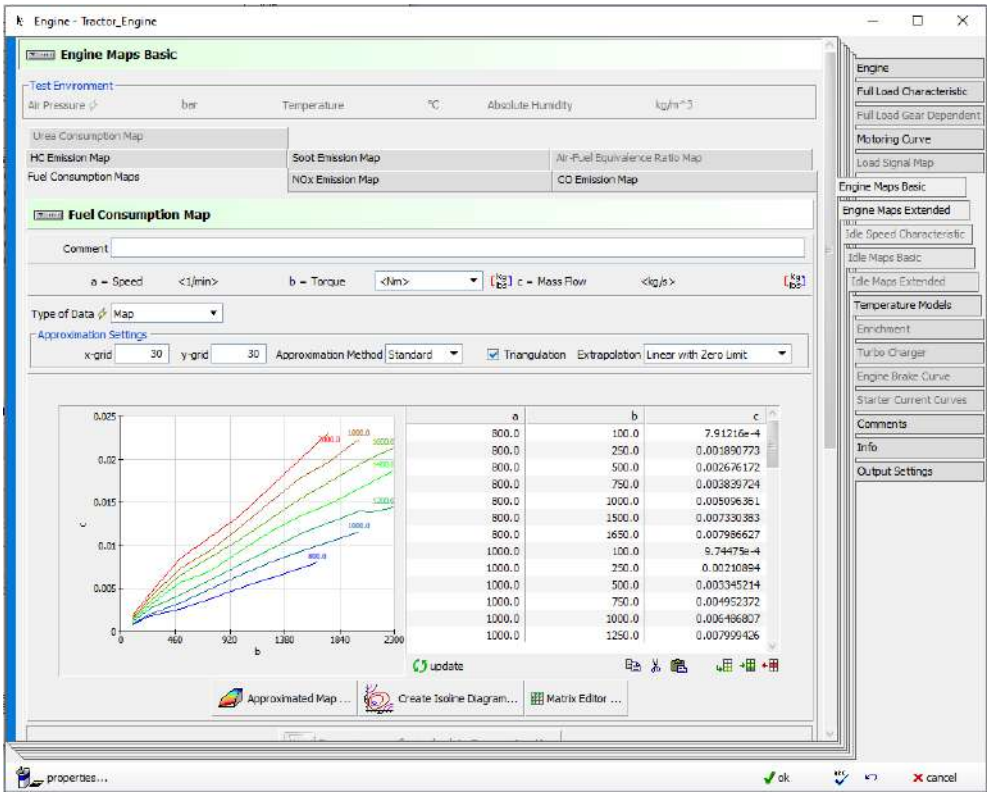

Figure 72: CRUISE Engine Maps Basic - Fuel Consumption Map

II.2.1.3 Exhaust Mass Flow and Temperature Maps

The Engine Maps Extended is a supplementary section and was be enabled by changing the properties of the engine. In the "Intended for Calculation to"section "Performance, Consumption, Emission, CO2-Emission"was selected. This section enables the iterations regarding the exhaust gases. In the Exhaust Mass Flow Map, Figure 73, the values in Table 20 were introduced and in the Temperature Map, Figure 74, the ones from Table 21.

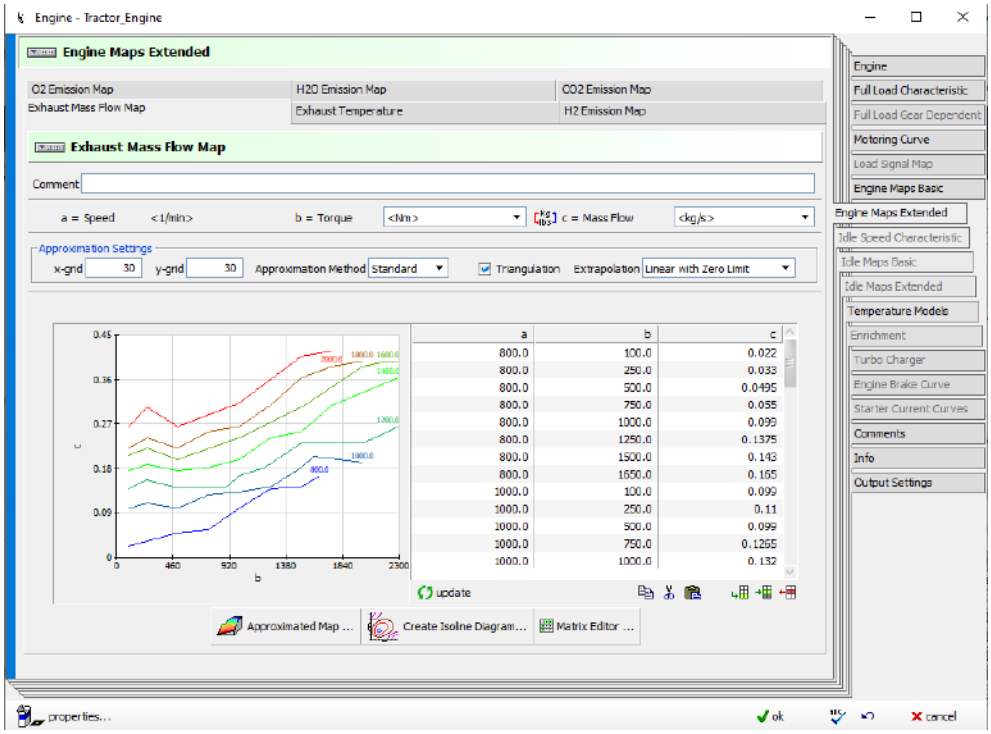

Figure 73: CRUISE Engine Maps Extend - Exhaust Mass Flow Map

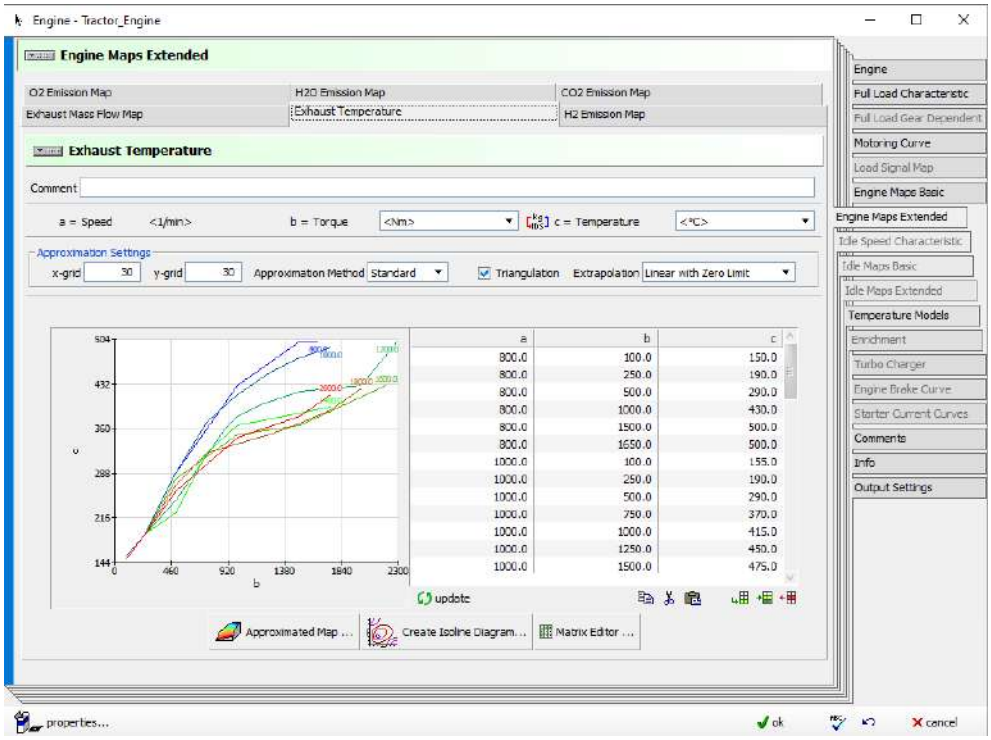

Figure 74: CRUISE Engine Maps Extend - Exhaust Temperature Map

Table 20: HD Engine Exhaust Mass Flow values

Exhaust Mass Flow					
Speed (rpm)	**Torque (N.m)**	**Mass Flow (kg/s)**	**Speed (rpm)**	**Torque (N.m)**	**Mass Flow (kg/s)**
800	100	0.022	1400	500	0.176
800	250	0.033	1400	750	0.182
800	500	0.050	1400	1000	0.198
800	750	0.055	1400	1250	0.242
800	1000	0.099	1400	1500	0.253
800	1250	0.138	1400	1750	0.308
800	1500	0.143	1400	2292	0.363
800	1650	0.165	1600	100	0.206
1000	100	0.099	1600	250	0.220
1000	250	0.110	1600	500	0.198
1000	500	0.099	1600	1000	0.242
1000	750	0.127	1600	1500	0.303
1000	1000	0.132	1600	2000	0.385
1000	1250	0.143	1600	2200	0.396
1000	1500	0.182	1600	2292	0.396
1000	1600	0.204	1800	100	0.220
1000	2000	0.193	1800	250	0.242
1200	100	0.138	1800	500	0.220
1200	250	0.156	1800	750	0.253
1200	500	0.141	1800	1000	0.264
1200	900	0.143	1800	1250	0.308
1200	1000	0.165	1800	1500	0.363
1200	1200	0.182	1800	1750	0.385
1200	1500	0.231	1800	2000	0.396
1200	2000	0.231	2000	100	0.264
1200	2100	0.242	2000	250	0.303
1200	2292	0.264	2000	500	0.264
1400	100	0.176	2000	1000	0.311
1400	250	0.187	2000	1500	0.407
			2000	1750	0.418

Table 21: HD Exhaust Gas Temperature Values

Exhaust Gas Temperature					
Speed (rpm)	**Torque (N.m)**	**Temperature (°C)**	**Speed (rpm)**	**Torque (N.m)**	**Temperature (°C)**
800	250	190	1400	750	320
800	500	290	1400	1000	365
800	1000	430	1400	1250	375
800	1500	500	1400	1500	385
800	1650	500	1400	1750	395
1000	100	155	1600	100	150
1000	250	190	1600	250	190
1000	500	290	1600	500	280
1000	750	370	1600	1000	350
1000	1000	415	1600	1500	365
1000	1250	450	1600	2200	430
1000	1500	475	1800	100	150
1000	1750	490	1800	250	190
1200	100	150	1800	500	270
1200	250	190	1800	750	320
1200	500	245	1800	1000	335
1200	900	360	1800	1250	350
1200	1000	380	1800	1500	369
1200	1200	400	1800	1750	390
1200	1500	420	1800	2000	425
1200	2000	430	2000	100	150
1200	2292	500	2000	250	190
1400	100	150	2000	500	260
1400	250	190	2000	1000	345
1400	500	225	2000	1500	380
			2000	1750	415

II.2.2 AVL Exhaust System

The AVL Exhaust System component enables a coupling with the BOOST Aftertreatment model with CRUISE. The aftertreatment Model File (*.atm), Figure 30, can be started from CRUISE in the form of a coupled calculation. Is important to select the desire exhaust system, highlighted in Figure 75 by changing the properties. Also, two connections are important, an exhaust connection between the engine and an informal connection between the monitor for controlling purposes.

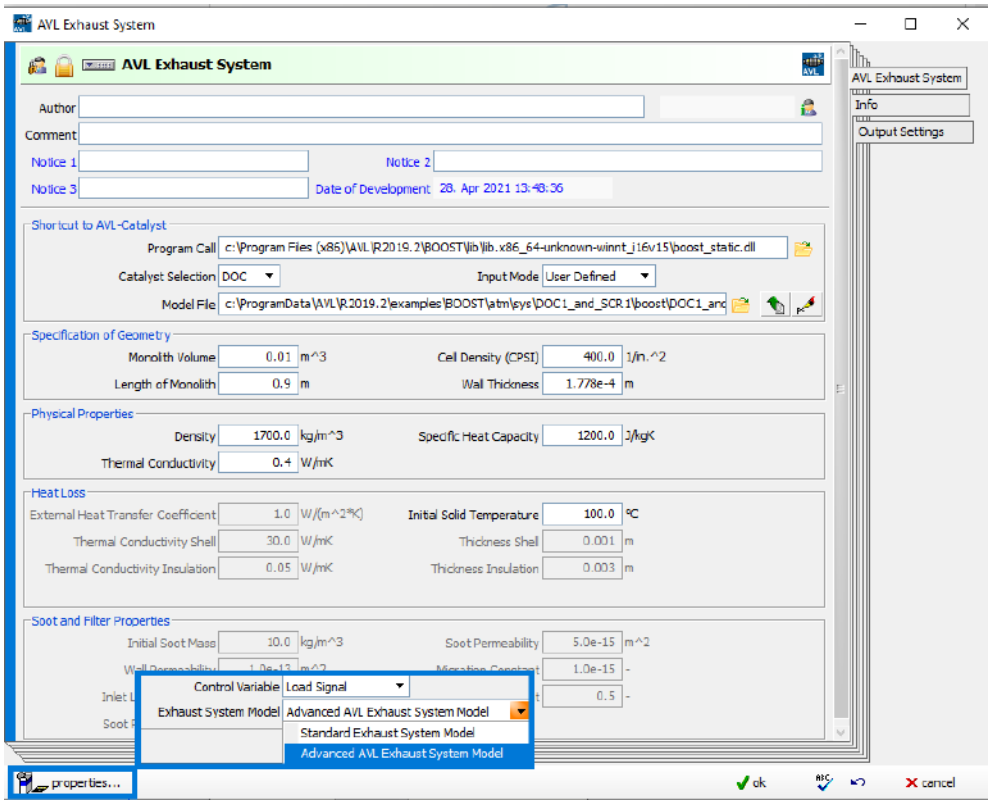

Figure 75: CRUISE AVL Exhaust System settings

II.3 Project Data

II.3.0.1 Settings

In the setting section, to the format of the components results a MAT "Char/Double format"was added so that was possible to analyze the results in Matlab.

II.3.0.2 Task Folder

To analyze the WHVC cycle run with empty, half, and full load and a long haul cycle run with full load four task folders were created, Figure 76. The long haul was available within the driving cycles layouts in the AVL server but the WHVC had to be introduced manually. The task folder settings are presented in Table 22.

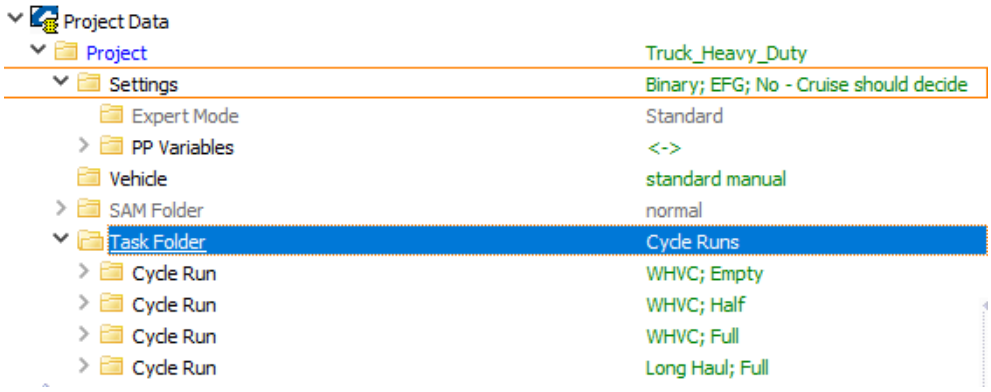

Figure 76: CRUISE Simulation Task Folders

Table 22: Task Folders definitions

General	
Simulation	VSS Implicit Euler
Driving Resistance	Physical
Shifting	
Gear Selection	According to Speed
Initial Values	Hot start - transient
Load State	
WHVC Full	Full
WHVC Half	Half
WHVC Empty	Empty
Long Haul Full	Full

II.4 Run Calculation and Result Analysis

Once the simulation parameters are all defined, the simulation is done in the Calculation Center by clicking on "Start Calculation". In Figure 77 is illustrated the monitor available during the computation, on which is possible no see the described variables in real-time. These variables feedback was set by informal connections from the component which provide the information to the monitor. For example, the engine delivers output information about the exhaust temperature to the monitor. The results are available in the Result Manager area either in table format or graphically. The MAT files are stored in the defined path and were used for the data processing.The results are available in the Result Manager area either in table format or graphically.

Figure 77: CRUISE Calculation Center window

The mat files are stored in a defined path and were used for data processing. Each component has a mat file, so, a Matlab algorithm was written to gather the important outputs from the several mat files from the CRUISE simulation and calculate or change the units to get the desire outputs presented in Figure 78. Also, because Cruise gives outputs after every 0.15 seconds it was necessary to select only the outputs after 1 second using a Matlab function that brings only the outputs from integral numbers of time.

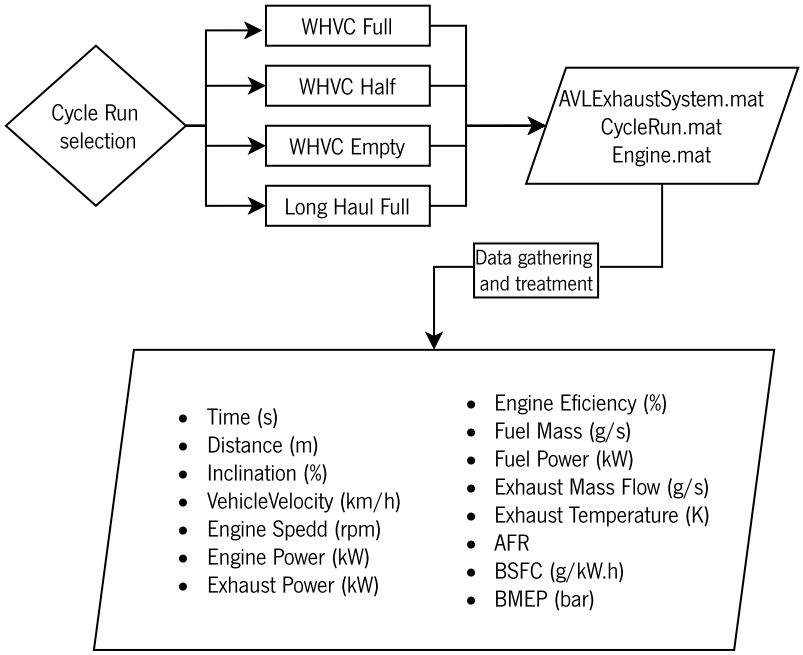

Figure 78: Matlab algorithm scheme used for the analysis of CRUISE results

Annex III

Heavy Duty Simulation Results

III.1 WHVC

III.1.1 Full Load

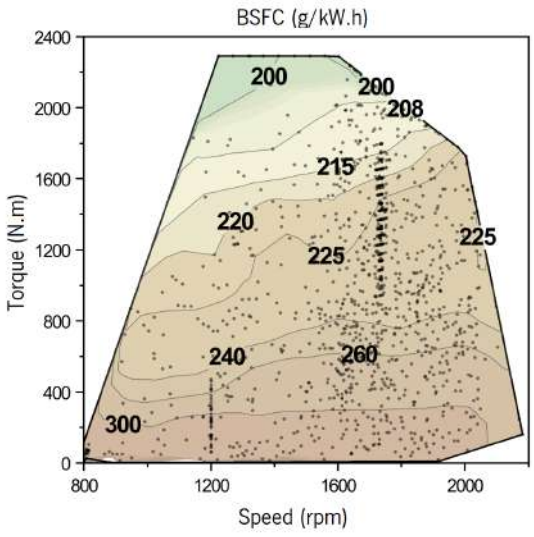

(a) BSFC

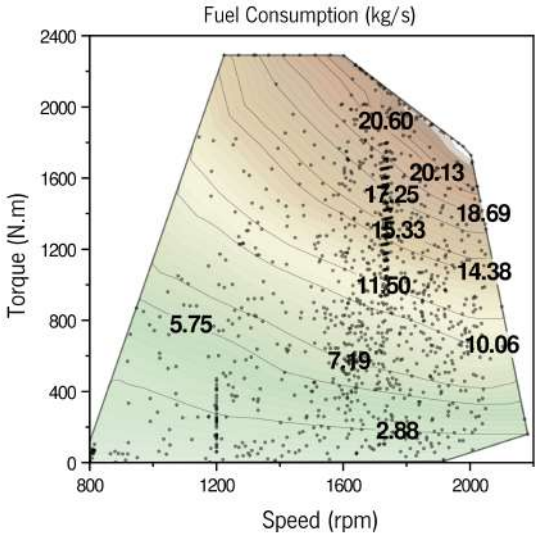

(b) Fuel consumption map

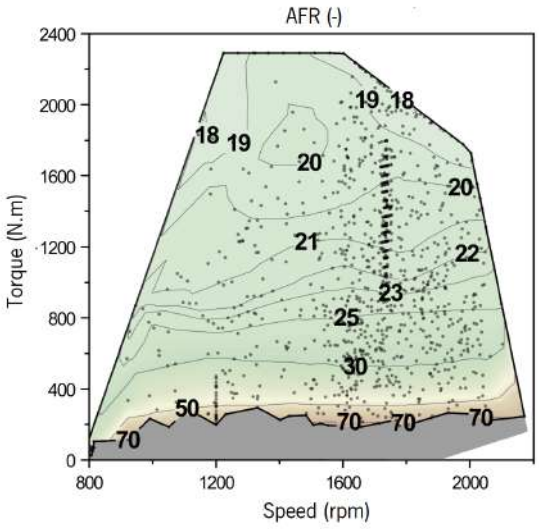

(a) AFR

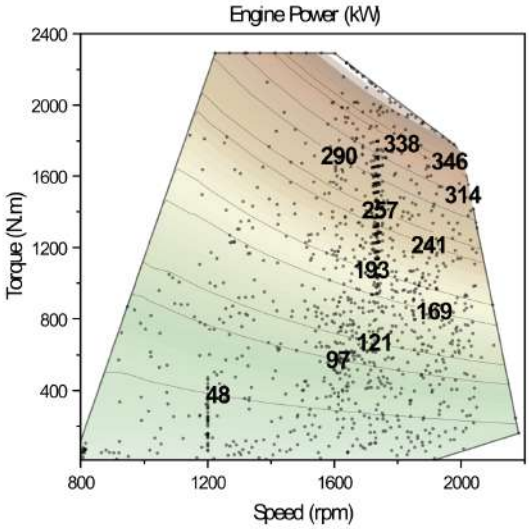

(b) Engine power

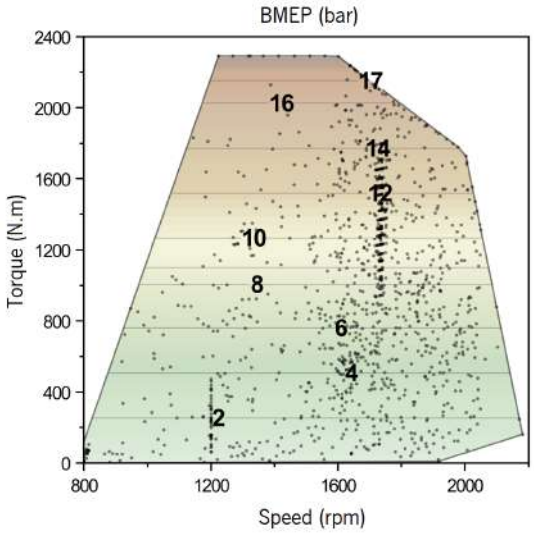

(c) BMEP

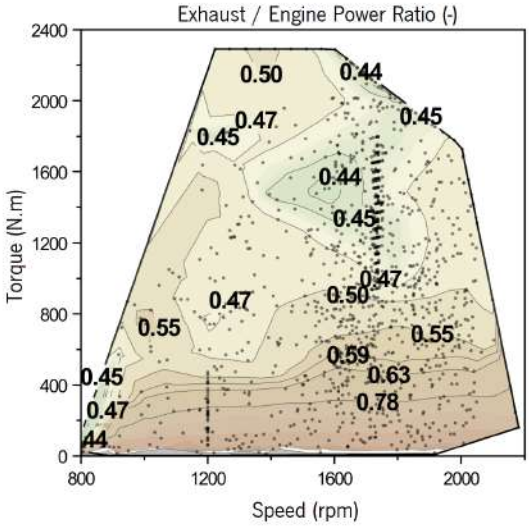

(d) Exhaust power and engine power ratio

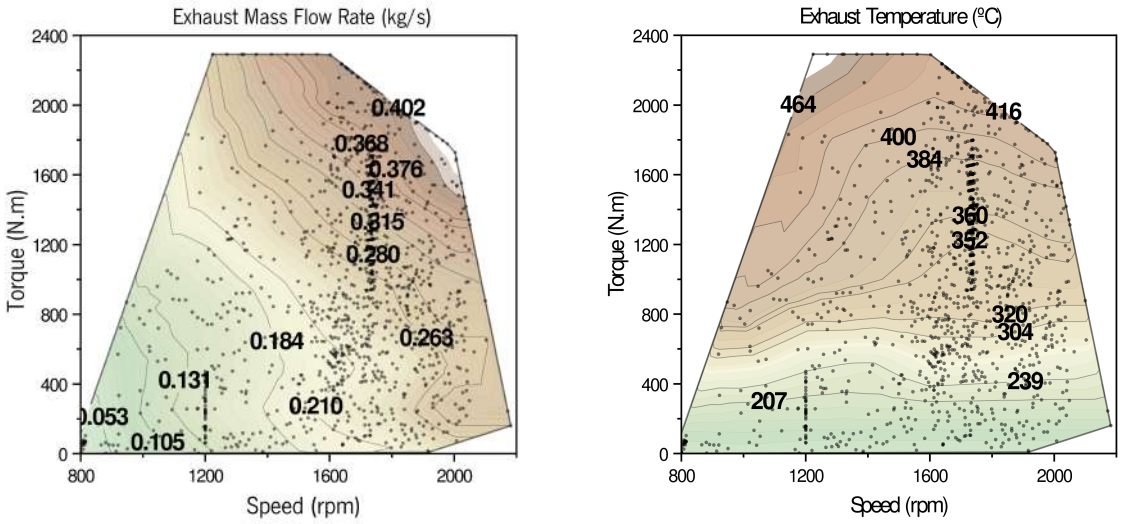

(a) Exhaust gas mass flow in the aftertreatment outlet (b) Exhaust gas temperature in the aftertreatment outlet

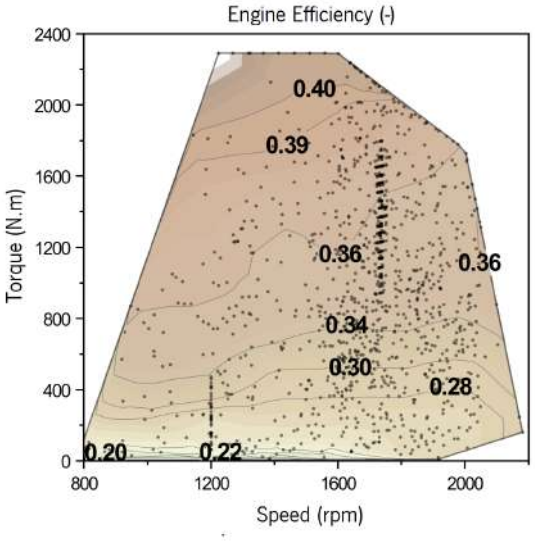

(c) Engine efficiency

Figure 79: HDV simulation results for WHVC driving cycle with 25 t

III.1.2 Half Load

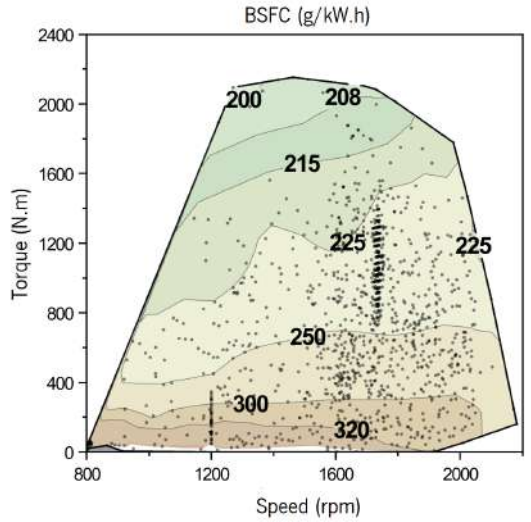

(a) BSFC

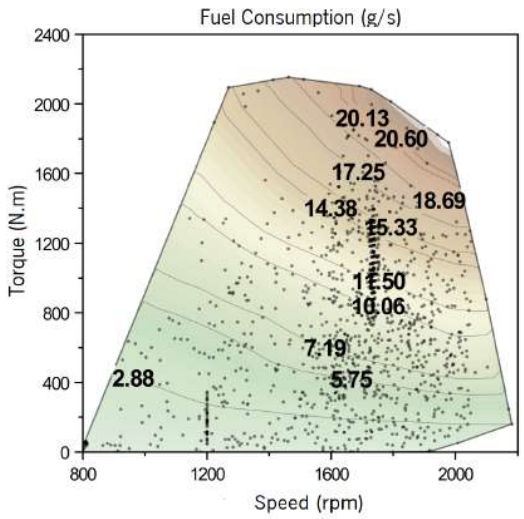

(b) Fuel consumption

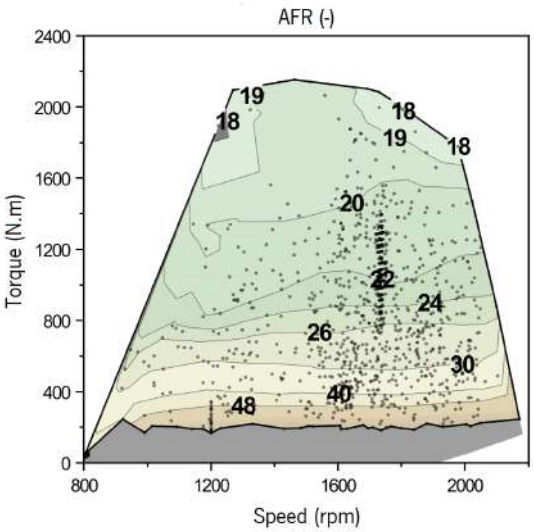

(c) AFR

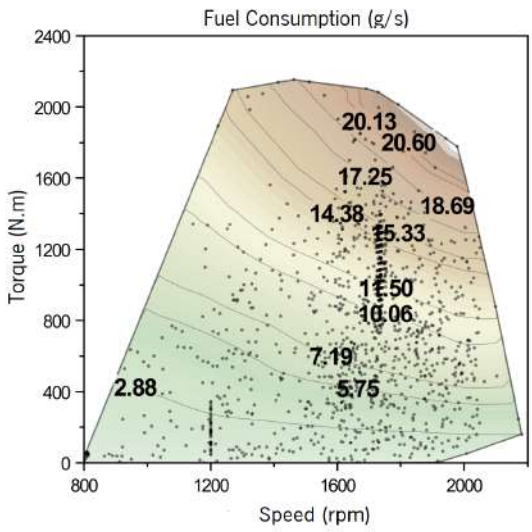

(d) Engine power

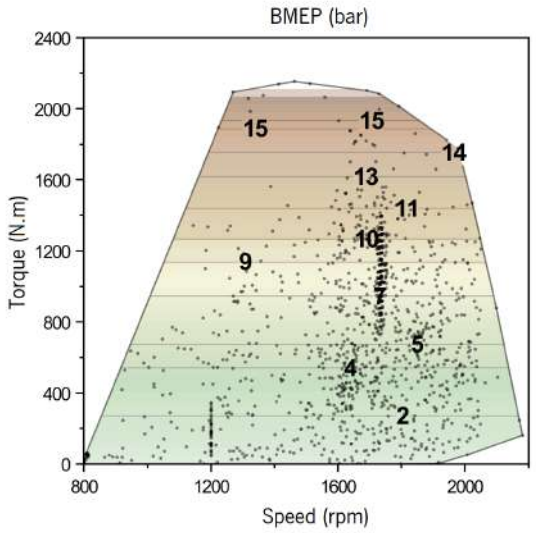

(a) BMEP

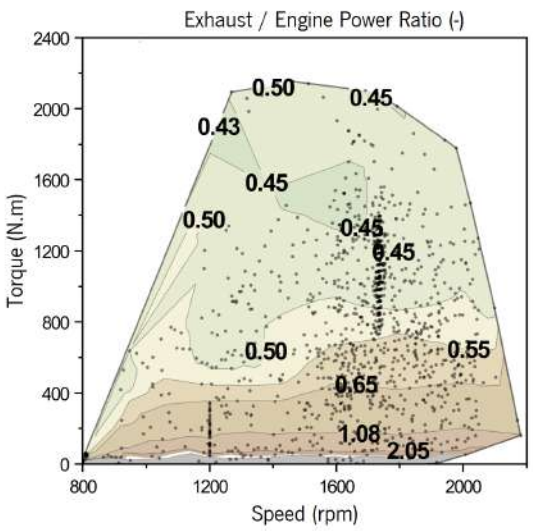

(b) Exhaust power and engine power ratio

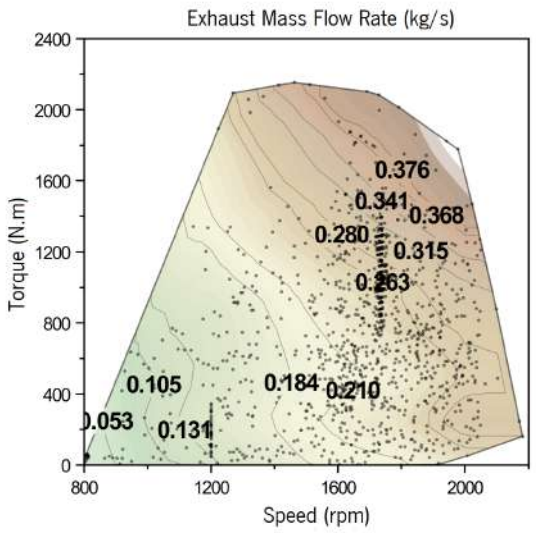

(c) Exhaust mass in the aftertreatment outlet

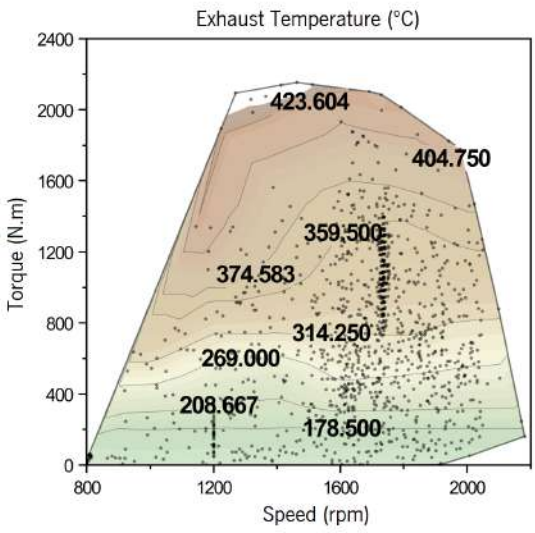

(d) Exhaust temperature in the aftertreatment outlet

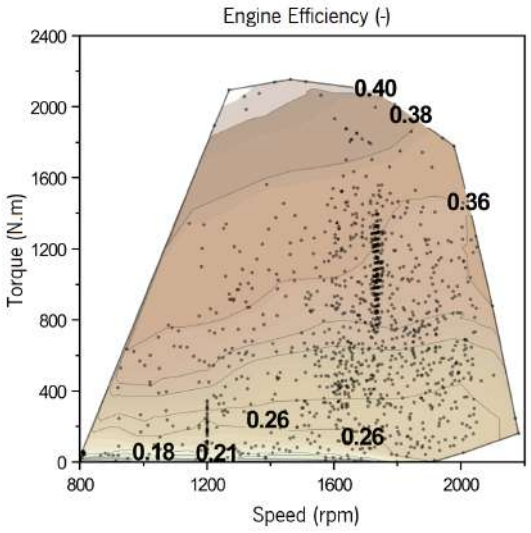

(a) Engine efficiency

Figure 80: HDV simulation results for WHVC driving cycle with 12.5 t

III.1.3 EMPTY Load

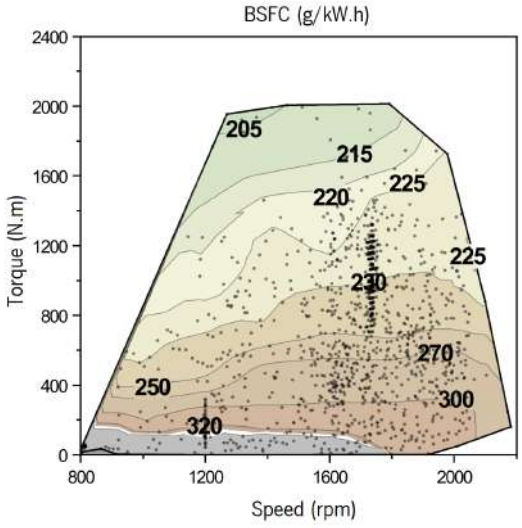

(a) BSFC

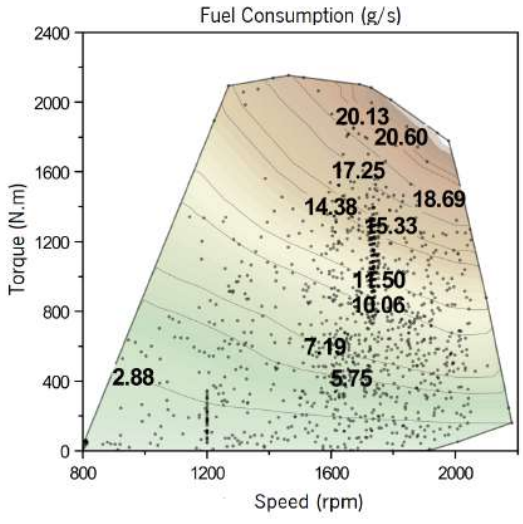

(b) Fuel consumption

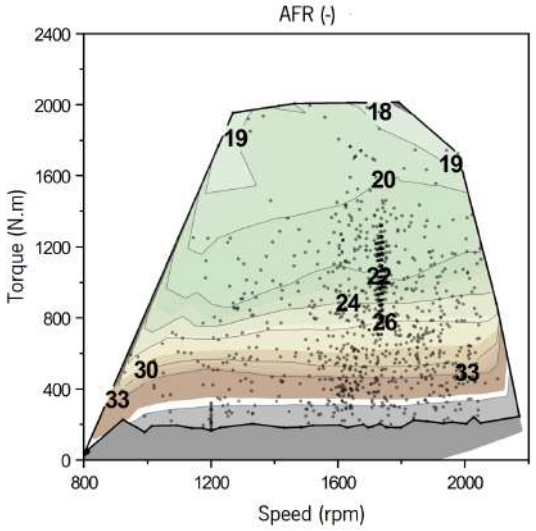

(a) AFR

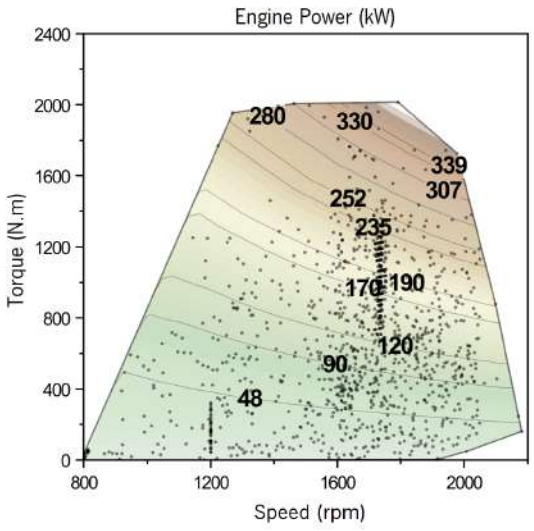

(b) Engine power

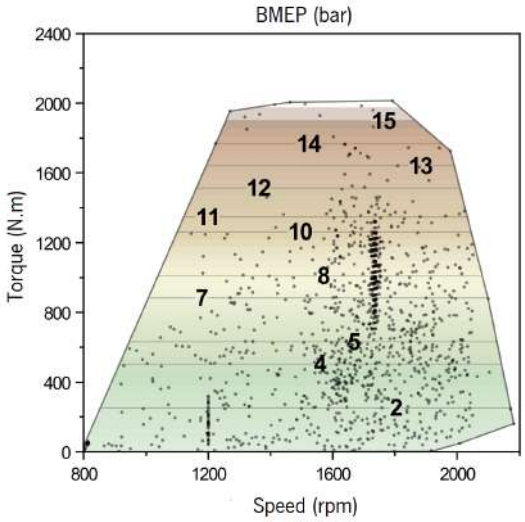

(c) BMEP

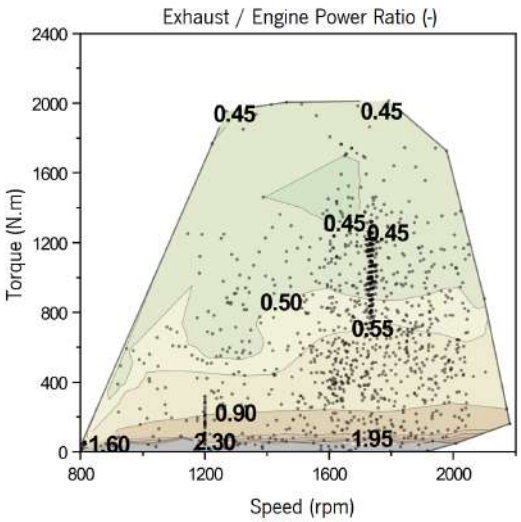

(d) Exhaust power and engine power ratio

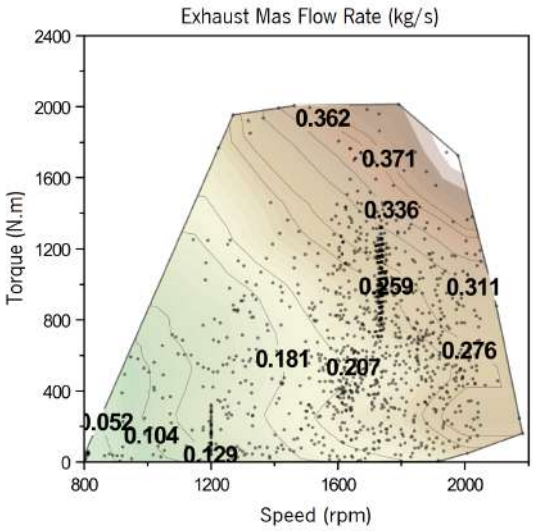

(a) Exhaust mass in the aftertreatment outlet

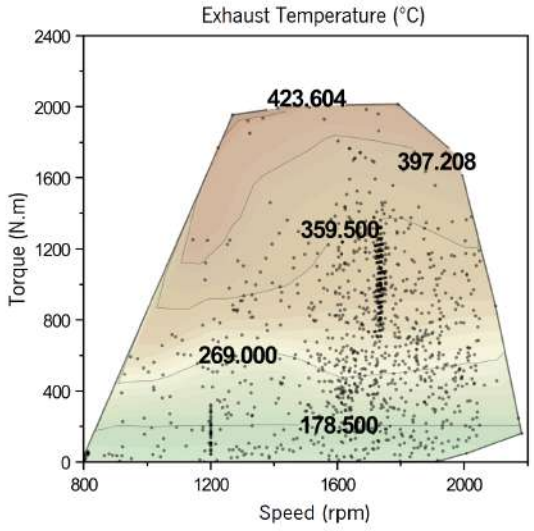

(b) Exhaust temperature in the aftertreatment outlet

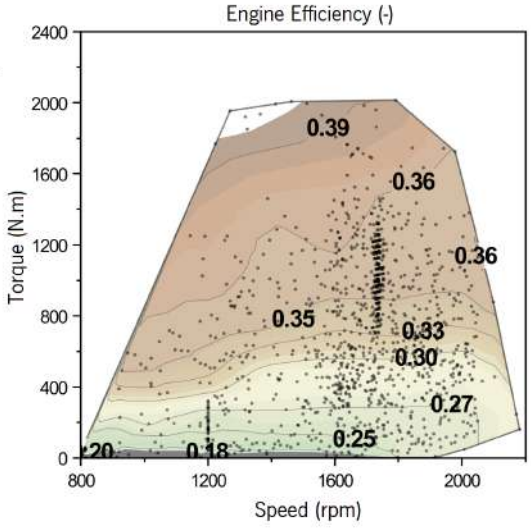

(c) Engine efficiency

Figure 81: HDV simulation results for WHVC driving cycle with 7.5 t

III.2 Long Haul

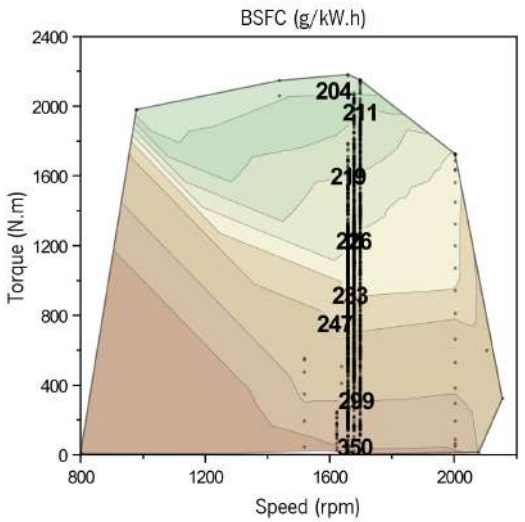

(a) BSFC

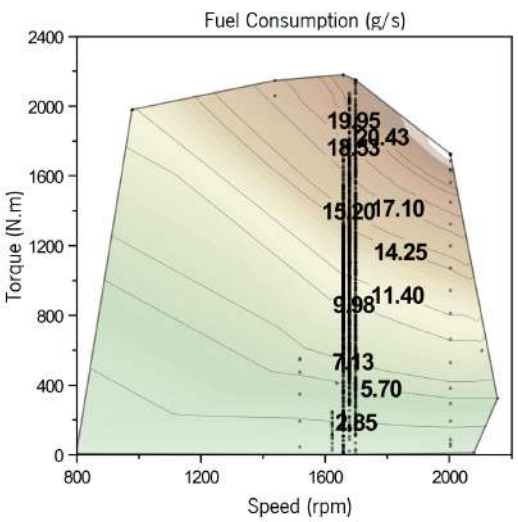

(b) Fuel consumption

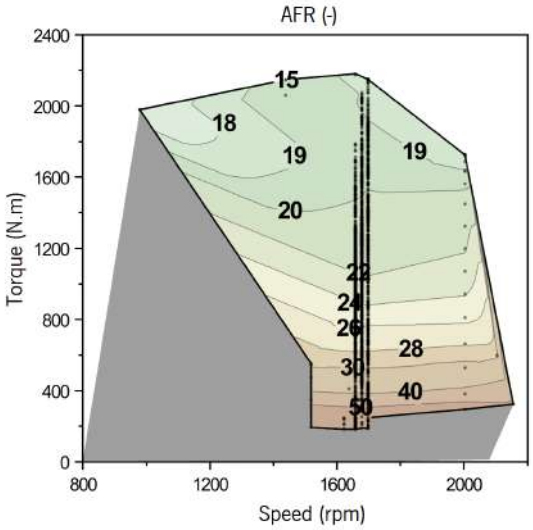

(c) AFR

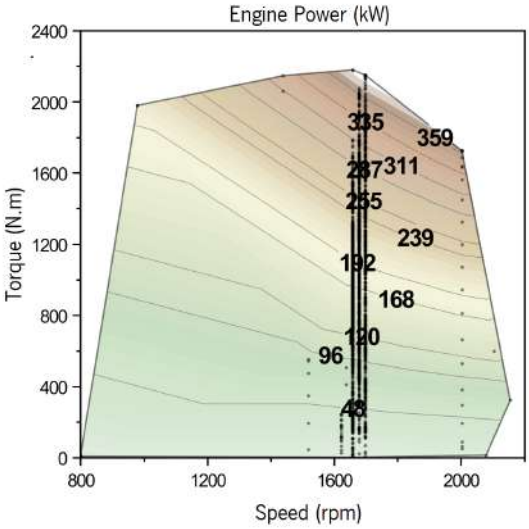

(d) Engine power

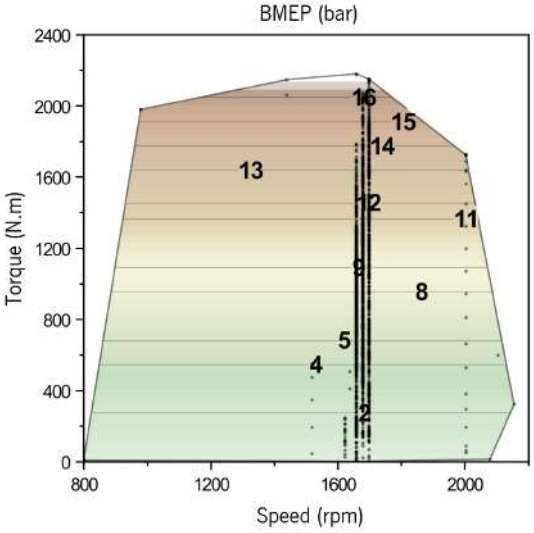

(a) BMEP

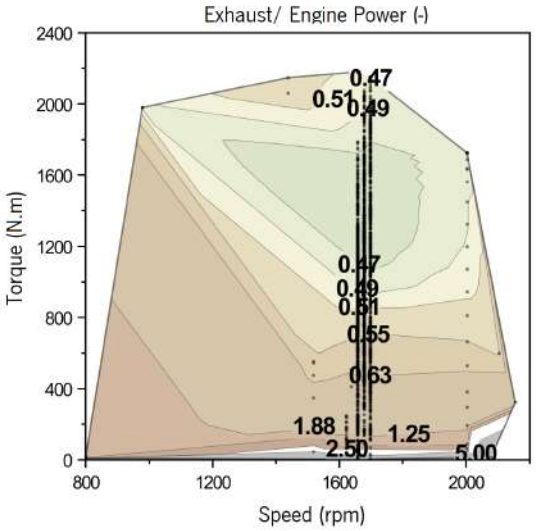

(b) Exhaust power and engine power ratio

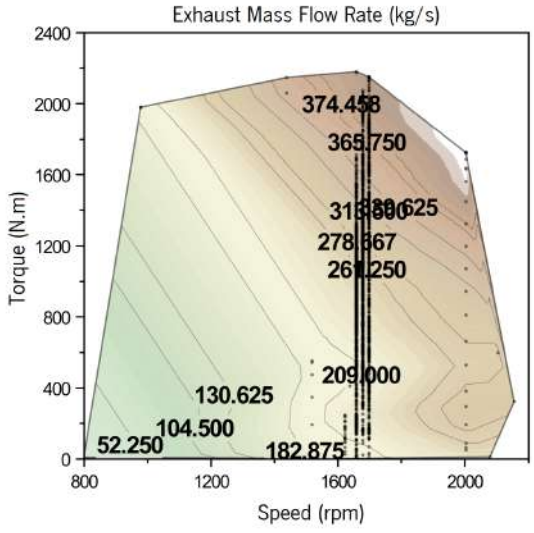

(c) Exhaust mass in the aftertreatment outlet

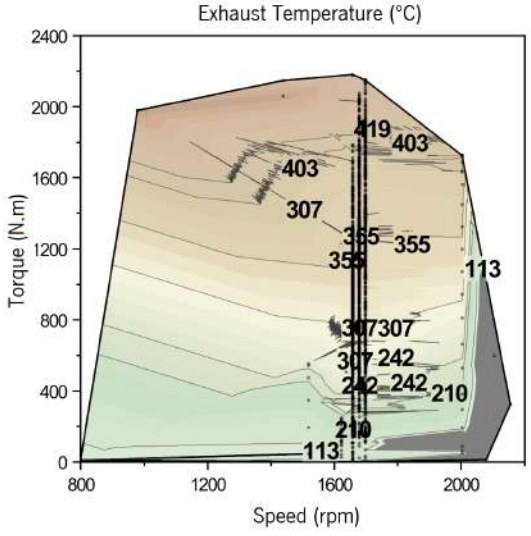

(d) Exhaust temperature in the aftertreatment outlet

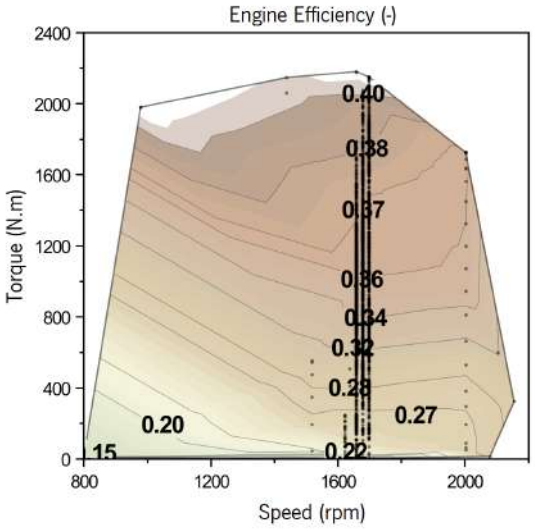

(a) Engine efficiency

Figure 82: HDV simulation results for Long Haul driving cycle with 25 t

Annex IV

COMSOL Simulation

In the present annex are present the surfaces selected in COMSOL for the thermal resistance calculation

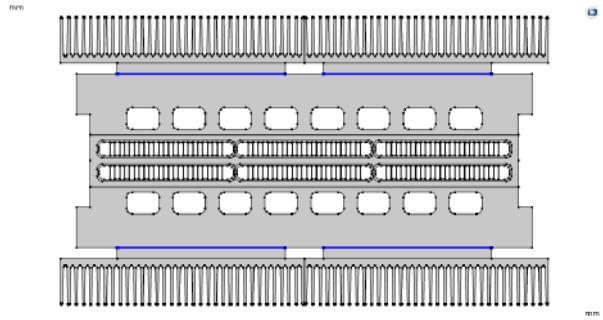

(a) TEG hot face

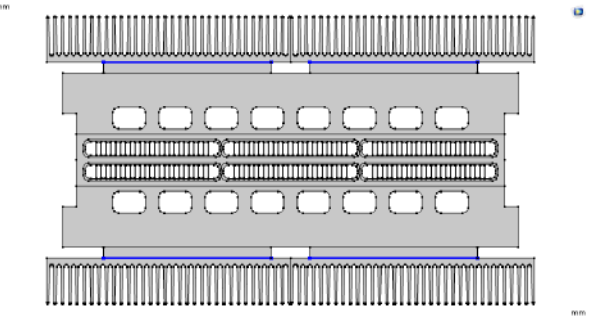

(b) TEG cold face

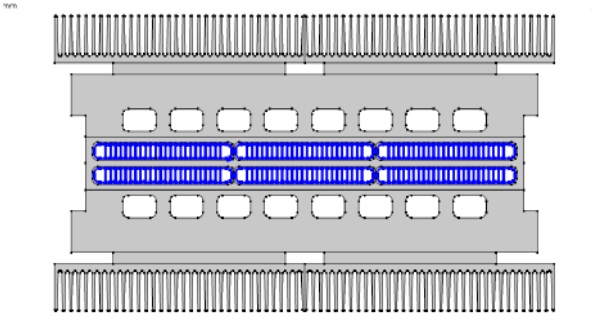

(c) WF surface

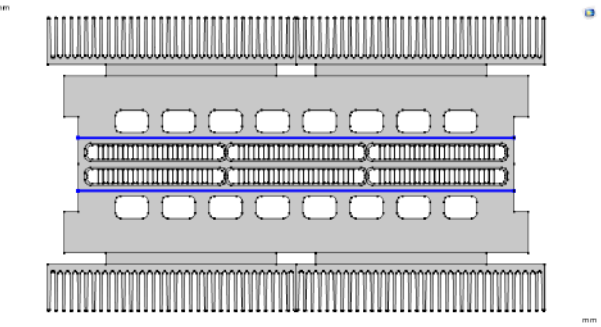

(d) Division between WFs and VCs

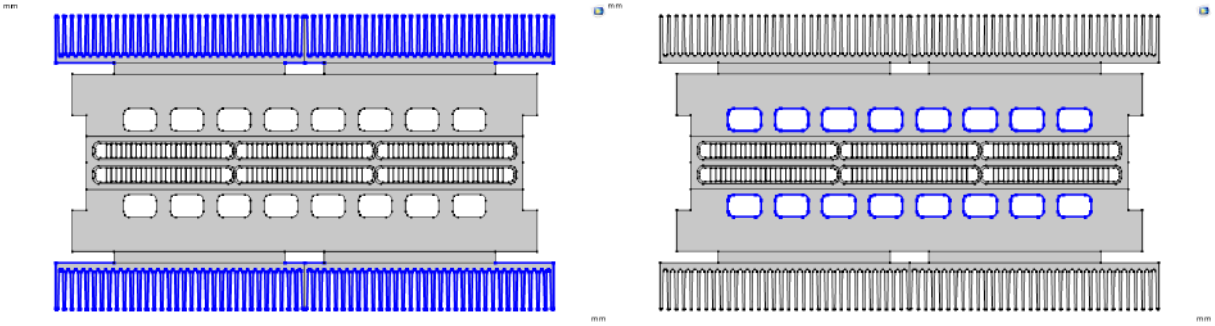

(a) CPs surface (b) VC surface

Figure 83: Selected surfaces for temperature and heat flux gathering in COMSOL simulation